EVALUATING CLAY MINERALOGY AS A THERMAL MATURITY INDICATOR FOR UPPER DEVONIAN BLACK AND GREY SHALES AND SILTSTONES WITHIN THE OHIO APPALACHIAN BASIN

A Thesis

Presented to

The Graduate Faculty of The University of Akron

In Partial Fulfillment

of the Requirements for the Degree

Master of Science

Zachary M. Strong

December, 2015

EVALUATING CLAY MINERALOGY AS A THERMAL MATURITY INDICATOR FOR UPPER DEVONIAN BLACK AND GREY SHALES AND SILTSTONES WITHIN THE OHIO APPALACHIAN BASIN

Zachary M. Strong

Thesis

Approved:	Accepted:
_____	_____
Advisor Dr. Ira D. Sasowsky	Interim Dean of the College Dr. John C. Green
_____	_____
Faculty Reader Dr. John A. Peck	Dean of the Graduate School Dr. Chand K. Midha
_____	_____
Faculty Reader Dr. James McManus	Date
_____	
Department Chair Dr. James McManus	

ABSTRACT

The clay mineralogy of the Upper Devonian age Chagrin and Huron Shale Members of the Ohio Shale was analyzed over in eastern Ohio to evaluate the usefulness of comparing the ratio between illite and smectite within mixed layer clay minerals to estimate thermal maturity. The process by which smectite diagenetically converts over time to illite via burial diagenesis has been rigorously studied in the past because of its relationship with thermal maturity. While simply understanding the thermal maturity of target formations is important, studies of illitization with depth can also give insight to hydrocarbon generation windows. This relationship allows for a prediction to be made on the stages of hydrocarbon generation that have occurred in a target formation based on the ratio of illite to smectite and the Reichweite ordering within the mixed layer clay.

Eighty-four samples were taken across an 8 county study area from the top and center of the Chagrin Shale Member and the center of the Huron Shale Member. X-ray diffraction (XRD) analysis was carried out on both bulk powder and clay fraction powder samples to gain an understanding of both clay and nonclay minerals present in each sample. Clay fraction samples were analyzed in the air-dried state, after treatment with ethylene glycol, and after heating to 550º for 30 minutes, to identify all clays present. The Kübler index, the measure of full width at half maximum (FWHM), of the 10 Å illite peak in the air-dried state was also recorded using XRD analysis for each sample. This was done to help identify the presence of mixed layer clays containing only a small expandable component. Environmental Scanning Electron Microscope (ESEM) imaging

was carried out to evaluate clay authigenesis with depth, and total organic carbon (TOC) was measured via elemental combustion in a CHN analyzer.

XRD analysis revealed that illite is the dominant clay mineral in all of the samples analyzed in the study and, on average, illite increased in abundance with depth. Reichweite ordering values within mixed layer clays, as interpreted from changes between diffraction patterns in the air-dried state and after treatment with ethylene glycol, were R3 ordered on average. Furthermore, the Kübler indices of the illite peak for all but two samples analyzed lie between 0.4 and 0.65, which corresponds to thermal conditions promoting hydrocarbon generation. ESEM images confirm the increase in authigenic illite with depth. However, this finding is more qualitative than quantitative because of the small size of clay mineral growth in shale pore spaces. The general increase of illite abundance with depth, the level of Reichweite ordering within the mixed layer clays encountered, and the Kübler indices measured from the illite peak, lead to the conclusion that evaluation of clay mineralogy to estimate thermal maturity is more accurate than vitrinite reflectance in the Upper Devonian shales of Ohio. Vitrinite reflectance can be suppresseed by high abundances of alginitic organic matter (Laughrey, 2012). It is also reccommended that the immaure/oil window boundary from previous studies (Milici and Swezey, 2006; Rowan, 2006) be moved far enough west to include the study area.

ACKNOWLEDGEMENTS

First off, I would like to thank my mother for her initial support to attend graduate school and her continued support throughout the duration of my time at The University of Akron; I would not be where I am today without her guidance and encouragement. I would like to thank my thesis advisor, Dr. Ira Sasowsky, for the hard and time consuming work put in to help me reach this point throughout the entire duration of the project. Furthermore, I extend my gratitude to my committee members, Dr. James McManus and Dr. John Peck, who were not only useful in editing, but also for bouncing ideas off of and answering any question that I had.

I would like to extend a thank you to Matthew Weinreich for his initial input of ideas for a project and addition of parameters to analyze to ensure a strong thesis. The input I received from Matthew is ultimately how I came to choosing this specific project.

An extreme amount of gratitude is extended to Aaron Evelsizor at the H.R. Collins lab for his always quick response to questions about samples available for viewing and for having all samples pulled from the shelves and ready for inspection upon my arrival. Furthermore, the study could not have been completed without the well logs graciously provided by the Ohio Geological Survey.

The completion of this project would not have been possible without the input from Dr. Warren Huff of the University of Cincinnati, who was nearly always available for email contact regarding questions about the interpretation of X-ray diffraction data and clay mineralogy as a whole. Dr. Anabelle Foos also provided useful information about clay mineralogy that helped the project run its course. I also am thankful to Hongji Yuan

for providing the ClayStrat + software. Although this program was not used for final analyses, it was very helpful to gain insight on changes that occur in diffraction patterns due to changes in clay mineralogy.

My deepest gratitude goes to Tom Quick, who always takes it upon himself to ensure that all equipment is working properly and will go above and beyond to make sure the data needed for your project is taken in a timely and accurate fashion. Annie Hartwell was immensely helpful with running the CHN analyzer, the Coulometer, and also by teaching techniques used to organize and visualize my data. Elaine Butcher also cannot go without mentioning, as she keeps everything in order, seems to have the answers to all questions, and always made sure I was scheduled for classes when I would get distracted by my thesis work. Her guidance and experience in the geosciences department is one of the reasons I am currently sitting here typing my final project (on time).

Finally, I would like to thank all of my peers for their support in my journey through graduate school. Many late nights, beers, and heated rants were had with a number of people in order to keep from going insane and to have someone to remind you that the end is in sight even when it seems your goals are unobtainable. Graduate students Stephanie Mitchell, Chris Biro, Carl Medvid, Charles Spurr, Natalie Murray, and Paul Krasner are worthy of special mentioning as not only colleagues, but as friends.

TABLE OF CONTENTS

Page

LIST OF FIGURES

LIST OF TABLES

CHAPTER I

INTRODUCTION

The Appalachian Basin in Ohio contains several packages of Devonian-age black and grey shales and siltstones with the potential to produce gas on a commercial scale (Milici and Swezey, 2006). The ability for shale to generate hydrocarbons is controlled by many factors, with one major component being thermal maturity (Pollastro, 1993; Johns, 1979). Although a shale formation may contain all of the material ingredients for hydrocarbon generation, the lack of appropriate thermal conditions can result in the absence of gas and oil.

Several methods are used to evaluate thermal maturity in black shale and siltstone formations. These include vitrinite reflectance, conodont and pollen coloration, and clay mineralogy (Dewing and Sanei, 2009). While vitrinite reflectance is considered a standard method for estimating thermal maturity, it can give low thermal maturity estimates for Devonian black shale units in northwestern Pennsylvania and in other major shale plays worldwide (Laughrey 2012; Raymond and Murchison, 1991). This phenomenon, known as vitrinite suppression, is related to the amount of alginites present in the source rock compared to the amount of homogeneous vitrinite A (Raymond and Murchison, 1991). This suppression in the reflectance of vitrain has been attributed to the absorption of aliphatic-rich fluids that originate from the exinitic minerals present (Raymond and Murchison, 1991). Although models for the correction of vitrinite reflection exist (Lo, 1993), they require the precise measurements of several parameters. Clay mineralogy

can potentially be used to identify zones fit for oil generation, due to the coincidence of increased illite/smectite ordering near the onset of peak oil generation (Jiang, 2012).

The present study investigated clay mineralogy and its correlation to oil generation zones in Upper Devonian age black and grey shales and interbedded siltstones across Ohio's Appalachian Basin, to give insight to the expected phase of hydrocarbons present at a given locality. Such knowledge will also aid in understanding the evolution of reservoir quality and the possibility of prior migration due to diagenetic changes (Jiang, 2012).

While the Upper Devonian strata have been studied rigorously in the past as potential hydrocarbon source rocks (Gray et al., 1982), these tight shales were initially deemed uneconomical as reservoirs. Recent advances in tight shale hydrocarbon extraction have sparked the exploration of new plays worldwide (Chengzao et al., 2012; Kargbo et al., 2010; Kuuskraa et al., 1998), and have transformed many strata from simply being source rocks to being potential reservoir rocks. Due to rising oil prices, exploration and completion of wells able to produce oil instead of solely gas are being targeted. Since the phase of hydrocarbons present in the subsurface is primarily controlled by the thermal maturity of in-place organic material, a detailed study of these parameters will greatly enhance our understanding of the expected hydrocarbons in the formation. Confirming the correlation between clay mineral transformations and the oil generation zone, along with alternate methods of measuring thermal maturity, will ultimately add confidence to Upper Devonian black shale commercialization.

1.1 Hypothesis

This study tests the hypothesis that the thermal maturity of Upper Devonian black and grey shales and siltstones can be determined by observing the ratio between Illite/

Smectite within mixed layer clay grains. As depth, and therefore subsurface temperature, increases, illite/smectite (I/S) mixed layer grains go through measurable transitions that directly relate to kerogen maturation zones (Pollastro, 1993). These changes include a transition from a smectite dominated mixed layer I/S clay to an illite dominated grain, which will be discussed in more detail in the background section. Time is not considered a factor in the mixed layer transitions, which corresponds to the time independence of kerogen maturation during oil generation. This quality makes the correlation between clay mineral composition and hydrocarbon generation easier due to the lack of many independent variables.

The hypothesis will be evaluated by comparison with already existing geothermometer interpretations via alternate methods, including the use of burial and thermal history models created by Rowan (2006).

1.2 Application of Clay Mineralogy as a Paleothermometer

Clay mineralogy has been applied to evaluate (I/S) layering and its use as a paleothermometer (Figure 1.1) in Miocene to Mississippian aged U.S. Gulf Coast sediments (Pollastro, 1993). However, the I/S ratio in Upper Devonian strata in the Appalachian Basin has not been extensively researched. The common clay minerals associated with the Upper Devonian strata include illite, chlorite, interstratified illite/ smectite, and small amounts of kaolinite and mixed layer illite/chlorite (Hosterman and Whitlow, 1981). Illite [Fixed Cations $(K, NH_4)_{0.89}Al_{1.85}Fe^{3+}_{0.05}Mg_{0.10}Si_{3.20}Al_{0.80}O_{10}(OH_2)$] is a dioctahedral clay mineral that is compositionally close to muscovite, with increased amounts of Si, Mg, and H_2O, but decreased amounts of Al and interlayer K (Moore and Reynolds, 1997). Smectite clays [$R_{0.33}^{+}(Al_{1.67}Mg_{0.33})Si_4O_{10}(OH_2)$] refer to the entire group of clay minerals, both dioctahedral and trioctaedral, that have the ability to expand

A)

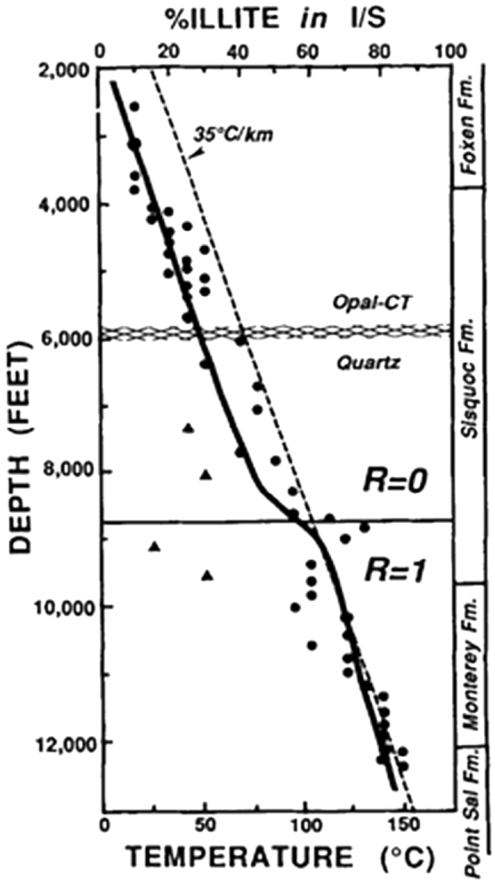

B)

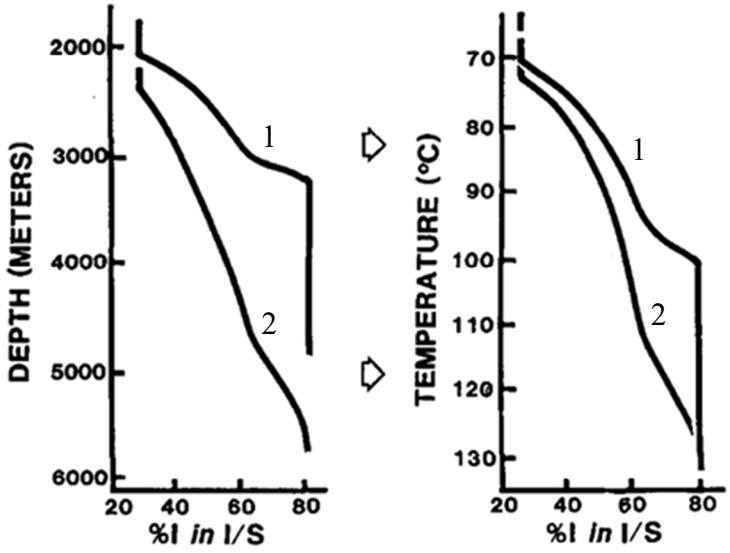

Figure 1.1. Graphs showing relation of percent illite in mixed layer clays to burial depth (Figure from Pollastro, 1993). A) Percent illite plotted against depth for the Foxen, Sisquoc and Monterey, and Point Sal Formations in the Santa Maria Basin of California. B) Variability in % illite with depth for samples from 1) Oligocene and 2) Miocene aged deposits in the Gulf of Mexico.

and contract their crystal structure while maintaining two-dimensional integrity by the process of interlayer cation exchange (Moore and Reynolds, 1997). The R value in the smectite formula represents an exchangeable cation, either Na or Ca, in the interlayer space (Moore and Reynolds, 1997). Illite is non expandable, and is therefore easily distinguished between smectite by performing X-ray diffraction analysis of samples in the air-dried state and after saturation with ethylene glycol (Moore and Reynolds, 1997).

While the occurrence of the smectite to illite transition and its relation to thermal conditions has been well documented (Jiang, 2012; Pollastro, 1993; Burtner and Warner, 1986), the reaction mechanism is poorly understood (Bethke and Altaner, 1986). Lynch et al., (1997) performed geochemical studies over intervals in the Frio shales where the smectite to illite reaction occured to gain understanding the illitization process. From the geochemical analysis, the following reaction was given: 10.93 I/S (20%I) + 0.91 discrete illite + 2.75 kaolinite + 0.86 potassium feldspar + 1.46 plagioclase feldspar + 2.11 Al_2O_3 + 2.66 $K_2O \rightarrow$ 12.59 I/S (85%I) + 0.27 chlorite + 3.16 quartz + 1.98 albite + 4.70 SiO_2 (Lynch et al., 1997).

The main postulated mechanisms within a MacEwan Crystallite (Figure 1.2a) in which smectite transforms into illite (Figure 1.2b) are solid-state transformation and the process of dissolution and recrystallization (Altaner and Ylagan, 1997; Bethke and Altaner, 1986). Altaner and Ylagan (1997) show evidence supporting both mechanisms of transformation depending on the lithology, with the solid-state transformation model (SST) representing shale environments and the dissolution and recrystallization model (DC) representing hydrothermal and sandstone environments. Solid-state transformation is supported by the idea that energy barriers within the crystal would not be overcome in sub-metamorphic temperatures. Evidence for SST in shale environments comes from the observation of similarly sized I/S plates throughout a large range of bentonite samples with differing illitic content (Altaner and Ylagan, 1997). Additionally, SST is supported

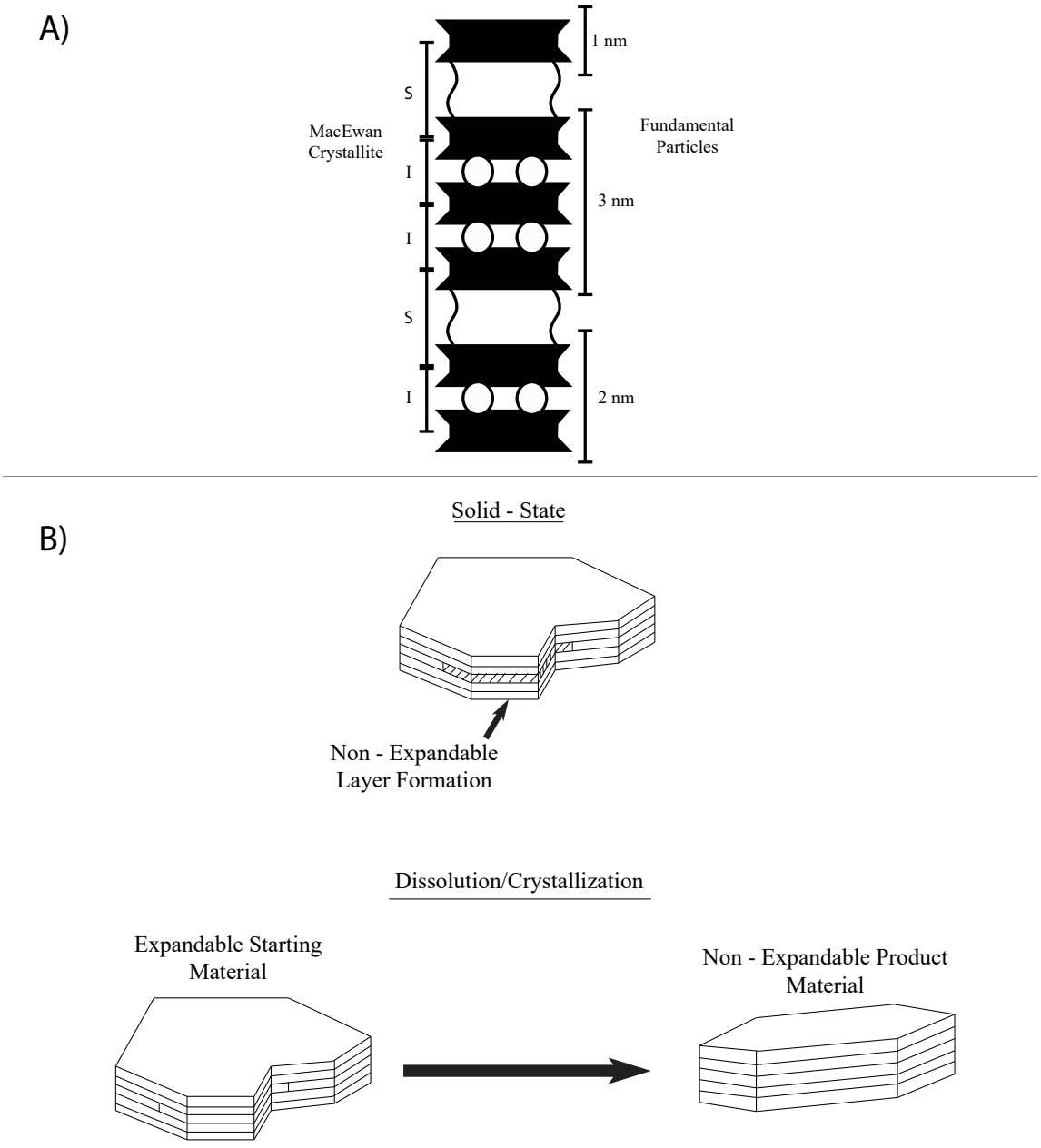

Figure 1.2. Illustration showing methods of illitization. A) Mixed-layer I/S crystal as both a MacEwan Crystallite and an assemblage of fundamental particles. Anvils represent 2:1 silicate layers, circles represent K cations in illitic interlayers, and wavy lines represent water in between the expandable layers of smectite. Modified from Altaner and Bethke (1988). B) Two different methods of illitization thought to occur in nature. Modified from Altaner and Ylagan (1997).

by observing gradual changes in oxygen isotopes incorporated from surrounding pore waters and retention of original Ar in the crystal's structure, which can then be dated using K/Ar dating methods. The dissolution recrystallization model is supported by observation of abrupt changes in oxygen isotopes due to incorporation of oxygen isotopes from pore water held in deeply buried sediments and loss of Ar in the dissolution process (Bethke and Altaner, 1986). Furthermore, DC transformation results in abrupt structural and textural changes as illitization proceeds, documented by the TEM observation of spiral growing I/S crystals from hydrothermal environments (Altaner and Ylagan, 1997). In order to further test the solid-state transformation mechanism, synthetic X-ray diffraction patterns of I/S crystal structures computed by the Monte Carlo Model were compared to real diffraction patterns from interstratified I/S crystals with good agreement (Bethke and Altaner, 1986).

Chemical and mineralogical analysis of Devonian age black shales from the Appalachian Basin (Leventhal and Hosterman, 1982) revealed that I/S interlayered clays account for 20-30% of the total clay material present within the formations. Huang et al. (1993) completed laboratory geochemical testing to quantify the influence of potassium cation concentrations in solution on smectite-illite conversions. They concluded that increased amounts of K^+ led to higher rates of conversion, and it has been postulated that the interaction between smectite and K^+ atoms leads to the creation of illite layers (Huang et al. 1993).

Pollastro (1993) studied I/S layering for its use as a geothermometer and to better understand its relationship to hydrocarbon generation in deposits ranging from Mississippian to Miocene age. Reichweite notation is a method of classifying the ordering of illite and smectite layers within a MacEwan Crystallite (Altaner and Bethke, 1988). This value is interpreted from changes in peak location between 5º and 8.5º 2Θ that occur after treatment with ethylene glycol (Moore and Reynolds, 1997). A

Rechweite Notation (R) of 0 is signified by a strong 17 Å reflection occuring near 5.2º 2Θ, and points towards random ordering. In randomly ordered mixed layer clays, both illite and smectite layers can be neighbors to either another illite or smectite layer. With increasing illite content, crystals become R1 ordered and produce a peak near 6.5º 2Θ. No smectite layers can be neighbors with another smectite layer in R1 ordered crystals and are separated by at least one illite layer (Moore and Reynolds, 1997). R2 and R3 are referred to as long-range ordered crystal structures which occur from a further increase in illite content and require at least two and three illite layers, respectively, to occur between each smectite layer (Altaner and Bethke, 1988). These long-range ordered crystals produce peaks between 7º and 8º 2Θ, which migrate towards the pure illite peak near 9º 2Θ with increasing illitization (Moore and Reynolds, 1997). Analysis of glycolated XRD mounts shows that I/S levels of ordering, characterized by Reichweite notation (R), increase from 0 to 1 at around 100 degrees C, which is the lower limit of the oil generation window (Pollastro, 1993). Additionally, I/S R values reach 3 at about 175-180 degrees Celsius, the upper bounds of the oil generation window (Figure 1.3). Figure 1.4 displays the ordering of illite and smectite layers within a mixed layer crystal along with the Reichweite values and percentages of illite layers present. Some representative XRD patterns for mixed – layer I/S containing different percentages of illite and different levels or ordering (R) are shown in figure 1.5.

Burtner and Warner (1986) reported sharply defined initial smectite conversion with increasing depth, and therefore temperature, along with an abrupt change to a 4:1 illite to smectite ratio at higher depth/temperatures in Cretaceous age shales of the Rocky Mountains. Transition from primarily smectite to 20% smectite (increased illitization) was also noted to occur around 100 degrees C. These results concur with those of Foscolos et al. (1976), which show greater than 50% illitization occurring in the early mesodiagenesis phase of kerogen, the stage at which hydrocarbon production also

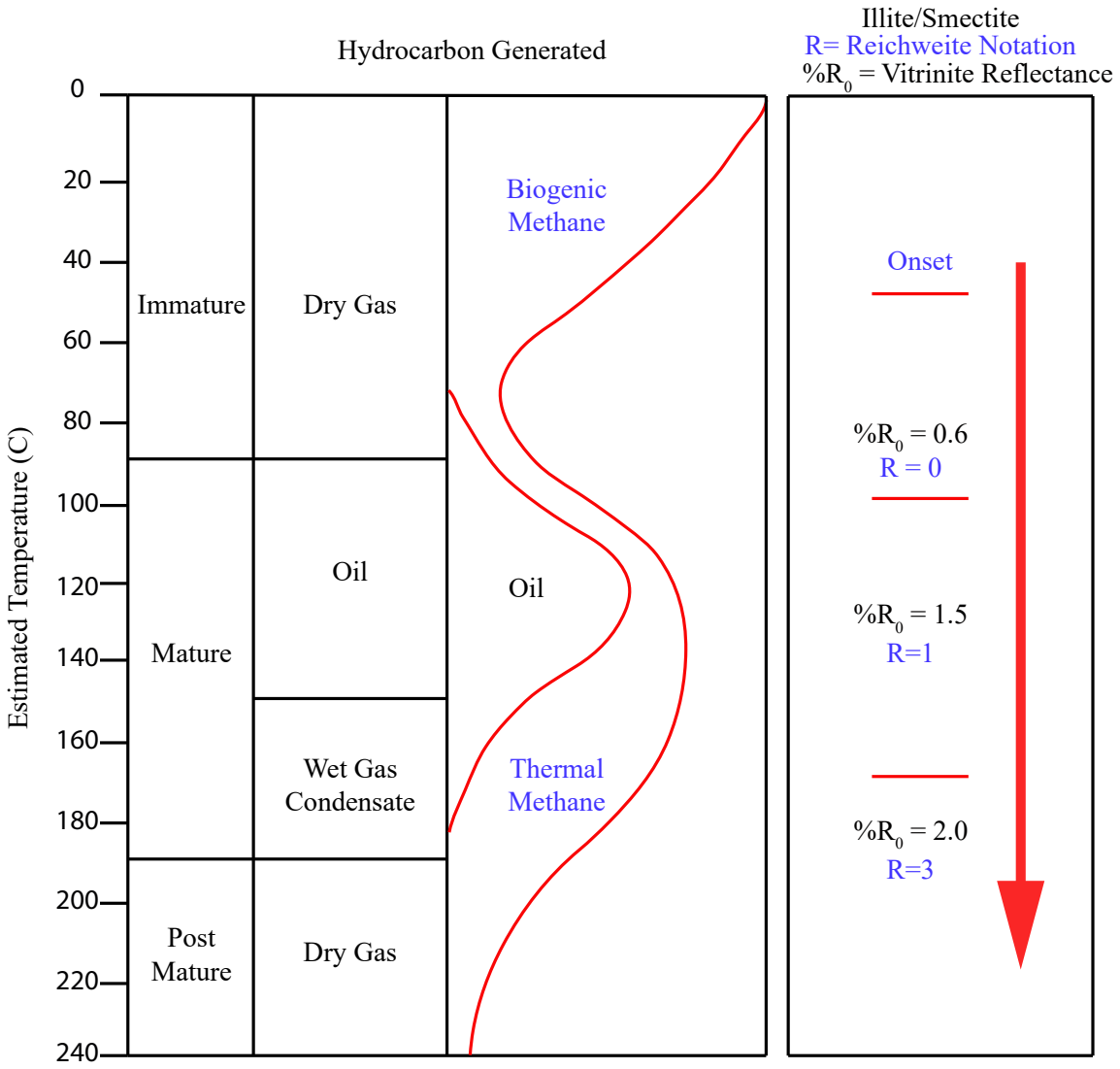

Figure 1.3. Illustration showing the relation between ordering in mixed layer I/S and the different stages of kerogen maturation. Modified from Pollastro (1993).

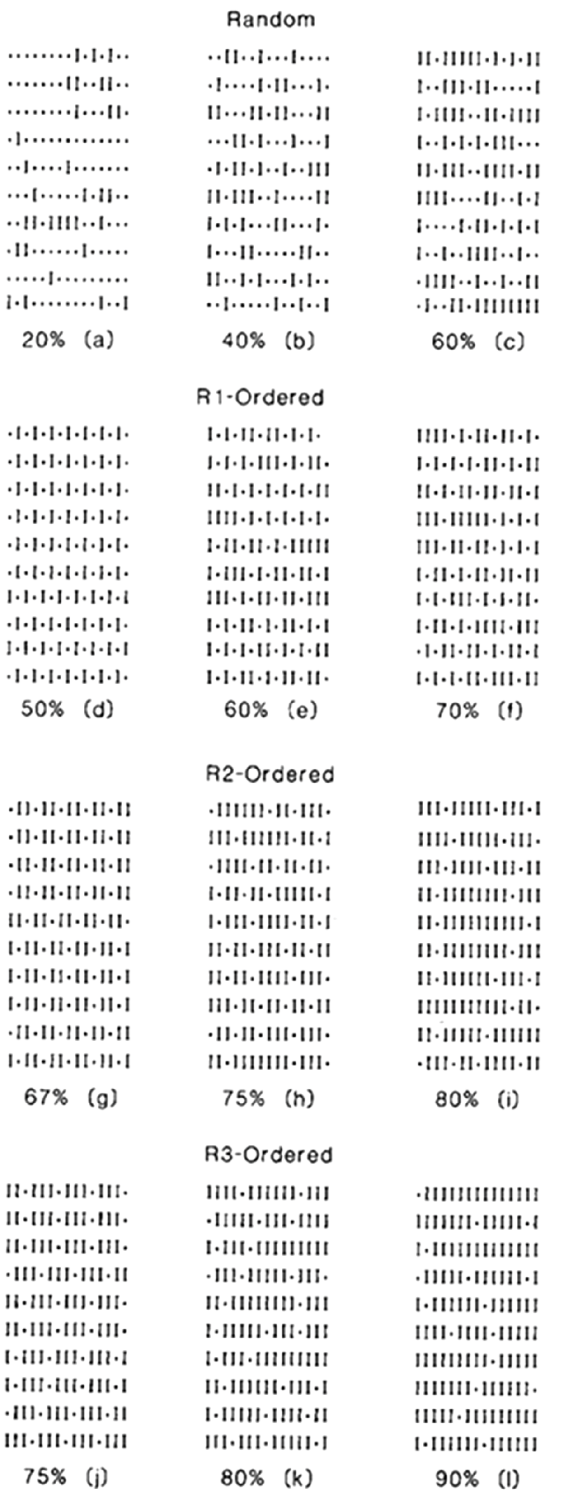

Figure 1.4. Illustration demonstrating the ordering of illites and smectites that can occur at the different Reichweite values. "I" represents illite layers and "·" represents smectite layers. Possible ordering of illite and smectite layers for each case presented is read horizontally (Figure from Altaner and Bethke, 1988).

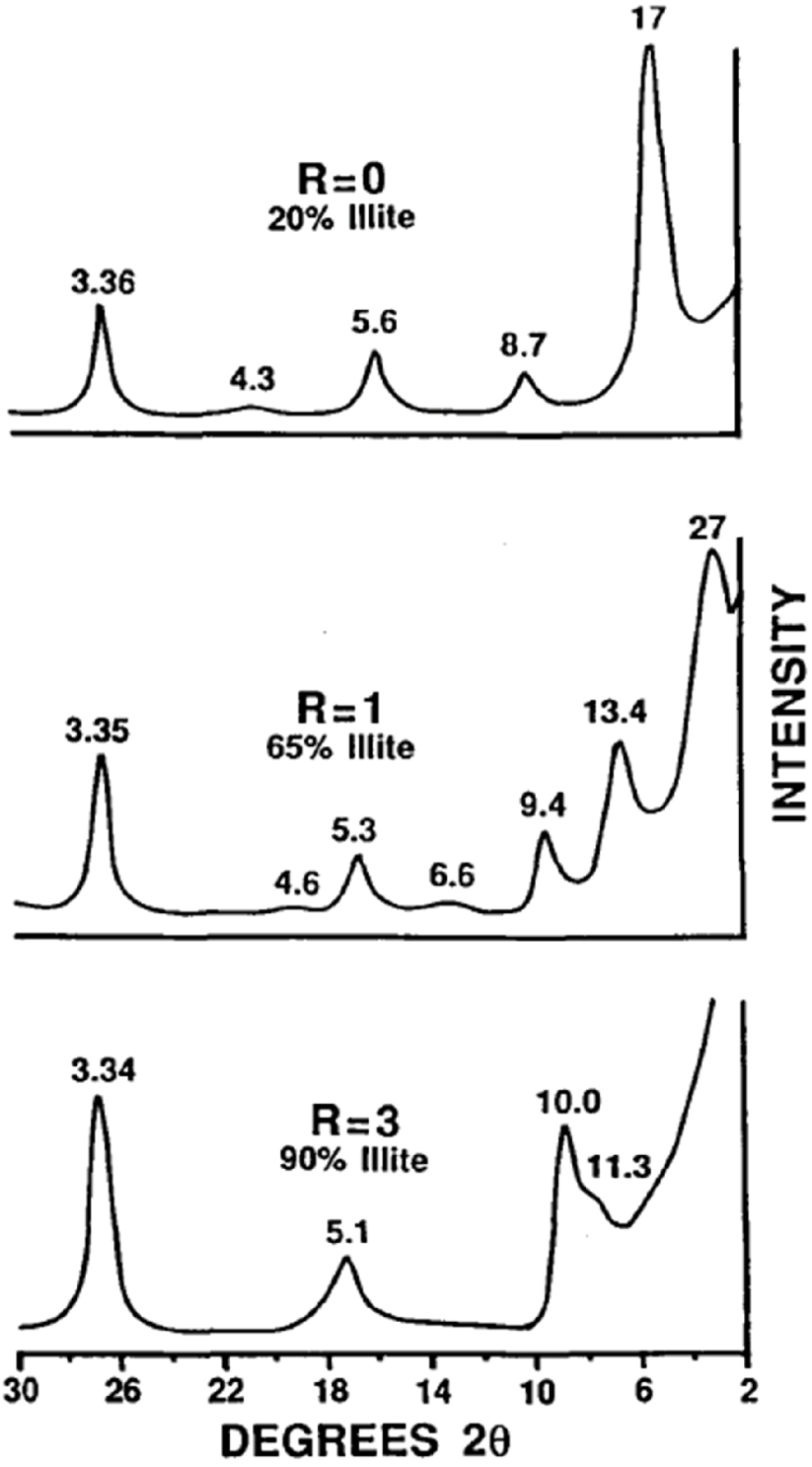

Figure 1.5. Examples of diffraction patterns of mixed layer I/S with different percentages of illite and R values. R values relate to the ordering of individual illite and smectite layers within the mixed layer material. Numbers located above peaks show d-spacing in angstroms (Figure from Pollastro, 1993).

commences. High I/S ratios, around 75% illite, characterize the shift from the upper boundary of the oil generation zone to the formation of dry gas (Foscolos et at. 1976).

1.3 Geologic Setting of Study Area

The Upper Devonian shales in Ohio lie primarily within the Appalachian Basin, but are also present to the west of the Cincinnati Arch. The history of the Appalachian Basin began with the late Precambrian rifting of Grenville basement rocks along the eastern continental margin, leading to the formation of a stable carbonate bank until the Early Ordovician (Quinlan and Beaumont, 1984). The subsequent Taconic Orogeny resulted in the uplift of continental strata into a large mountain range, known as the Appalachian Mountains, which stretched across the majority of what is known today as the east coast of the United States (Faill, 1997). The formation of this mountain chain effectively separated the Laurentian craton from the Theic Sea, halting growth of the large carbonate platform once situated on the Laurentian shelf (Faill, 1997). Uplift due to compressional forces along with the thrusting of micro continents Brandywine and Baltimore onto the Laurentian shelf both combined to transform the previously existing carbonate shelf into what is today the Appalachian Basin (Faill, 1997). The continued uplift greatly increased sedimentation rates, effectively increasing the sediment load in the basin. The formation of the Cincinnati Arch coupled with increased subsidence due to both sediment loading and tectonic forces are the main events responsible for the creation of the new basin (Faill, 1997).

The tectonic structures created during the Taconic Orogeny, including the Appalachian Mountains and sediments deposited in the Appalachian Basin, had been mostly eroded by the Devonian Period as uplift continued (Faill, 1997). During the Devonian Period, two separate tectonic events, the Acadian and Antler orogenies, played

a role in the deposition of sediments within the basin. During the early Devonian Period, the onset of the Acadian orogeny resulted in nearly the same conditions as the previously discussed Taconic orogeny. Uplift of the new Acadian mountain range paired with a rapid transgressive phase led to an increased sediment supply to the basin, resulting in sediment loading (Faill 1997; Lash and Engelder, 2011). This sediment loading and additional thrust loading resulted in a deep anoxic basin that allowed for the deposition of the Upper Devonian black shales.

The main focus of this study will be the Ohio Shale, a known hydrocarbon production target in the Appalachian Basin (Figure 1.6). Marginally commercial quantities of hydrocarbons have been produced from these strata for over 100 years (Broadhead et al., 1982). The Ohio Shale is a wedge shaped deposit, which thickens to the east (Schwietering, 1979), and is composed of the Huron Shale Member, Chagrin Shale Member, and Cleveland Shale Member, in order of decreasing age. Due to the wedge shape, the thicknesses of each of the three members vary across the state. Estimated thickness for the Cleveland Shale Member underneath Cleveland, Ohio, where it is thickest, varies between 20 and 50 feet[1], and the member pinches out in eastern Ohio near the study area (Schwietering, 1979). The Chagrin Shale Member has a maximum thickness of 1200 feet, which thins to merely feet in the western counties of Erie and Huron, and thickens to the east into Pennsylvania (Schwietering, 1979). Lastly, the thickness of the Huron Shale Member averages 410 feet in the center of the basin and thins to the east across the Ohio-Pennsylvanian border to accommodate for the thickening Chagrin Shale Member (Hoover, 1960; Schwietering, 1979). The Ohio Shale was deposited during the Late Devonian Period on top of the Olentangy Shale, and is overlain (Figure 1.7) by the Bedford Shale (Hoover, 1960). The deposition of black-shale-forming

[1] Note that U.S. standard dimensions (ft, acres) are used because they are the native units for data available in the project.

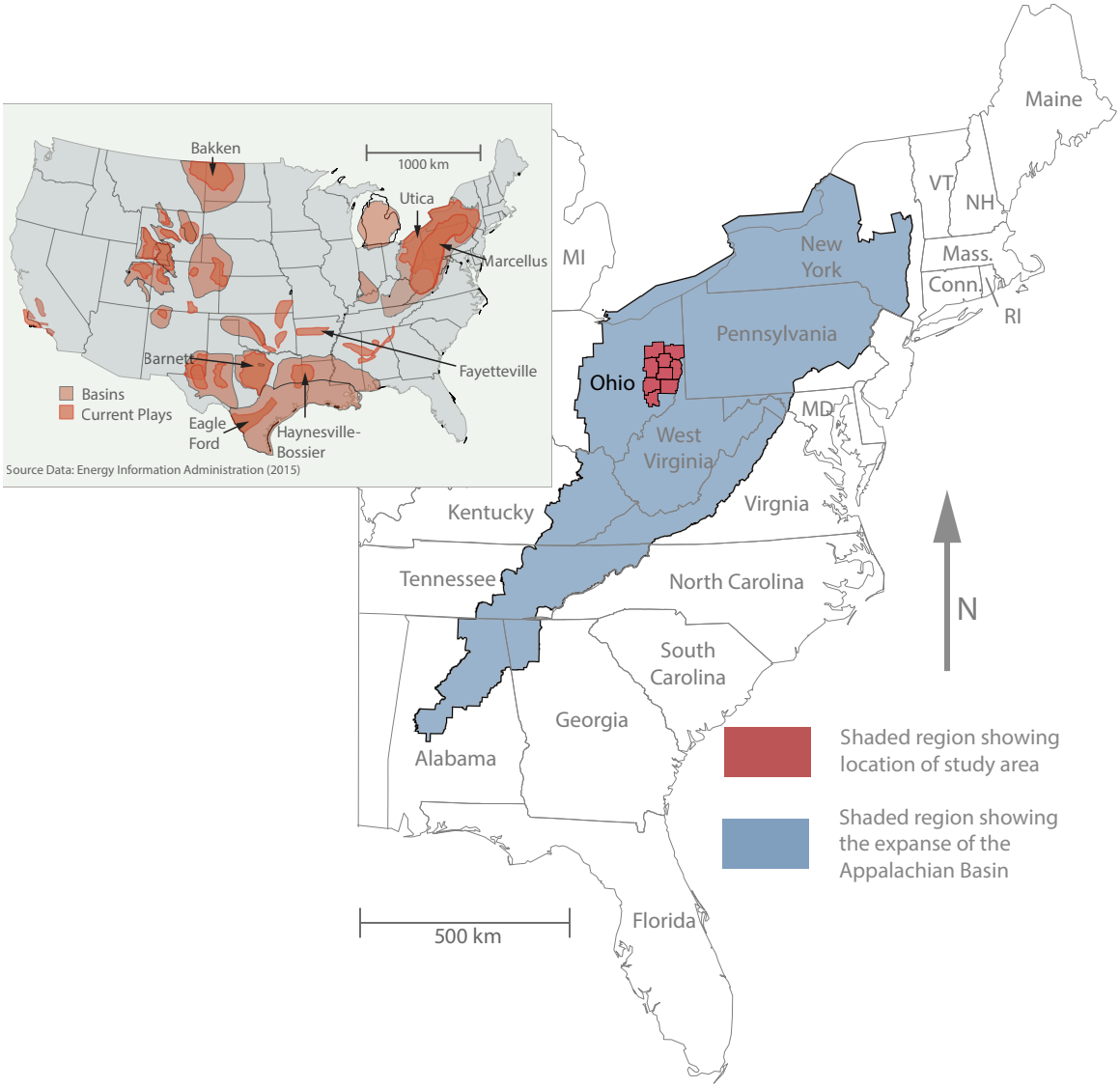

Figure 1.6. Map showing location of the study area within the Appalachian Basin compared to the locations of major current hydrocarbon plays and the basins in which they reside across the United States. Sources: Energy Information Association (2015); USGS (2002).

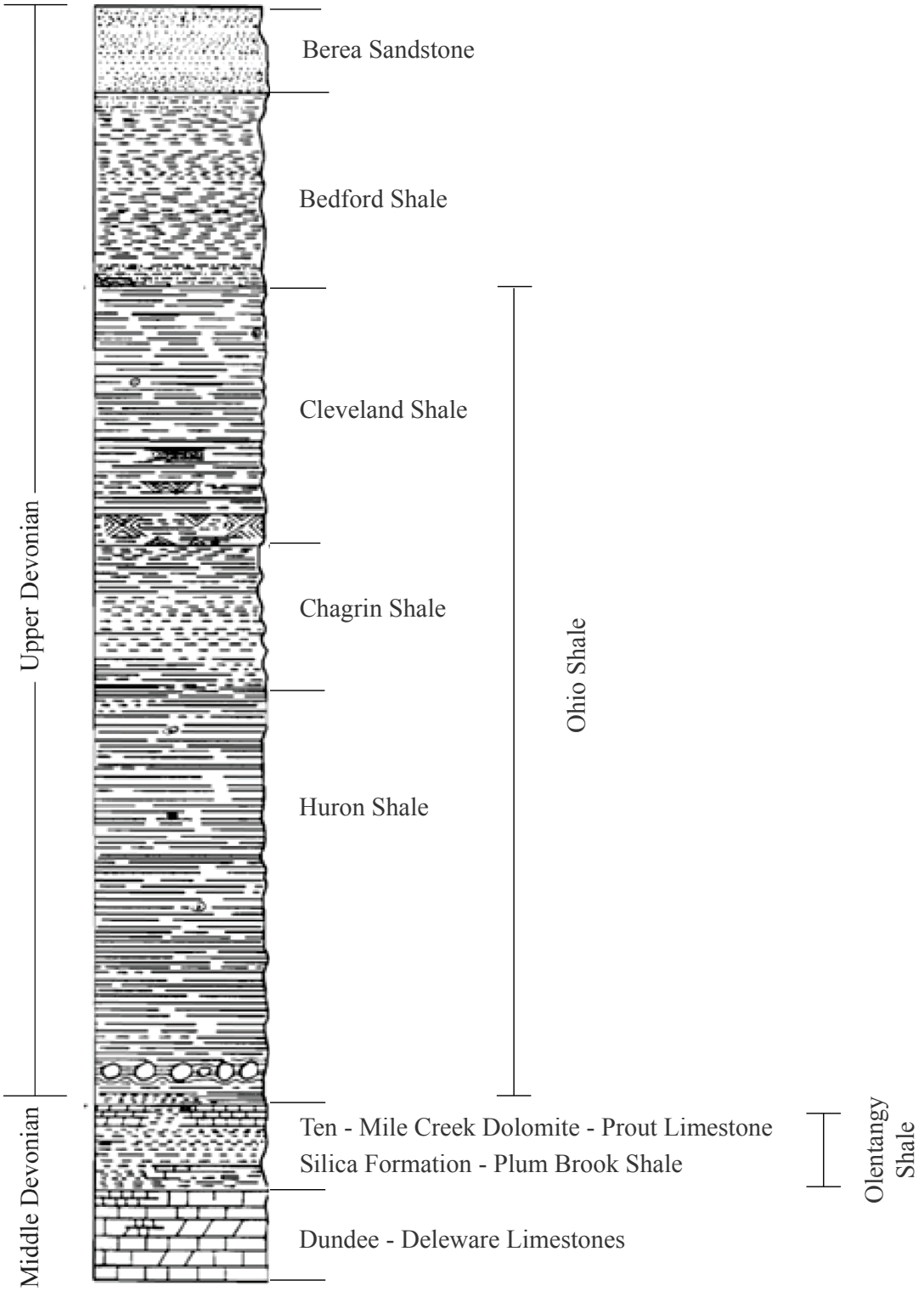

Figure 1.7. Stratigraphic section showing Middle Devonian to Upper Devonian shale sequences (Hoover, 1960). This figure has been modified to include the Bedford Shale and Berea Sandstone in the Upper Devonian, rather than the Mississippian (Figure from Slucher et al., 2006).

sediments primarily occurred in deep anoxic water within the basin (Figure 1.8), while interbedded greenish-grey shale formed in slightly shallower shelf conditions from turbidity currents (Potter et al., 1980). This change in depositional setting is seen within the Huron Shale Member, which contains black shales associated with transgressive seas interbedded with a greenish-grey deposit characterized by a regressive phase (Broadhead et al., 1982). Studies of paleocurrent indicators (Potter et al., 1980), give evidence of sediment originating from the orogenic belt to the east (Figure 1.9). Rowan (2006), using average heat flow in the area and paleothermometer evaluation, studied the burial history of the Appalachian Basin. From these calculations, a model was produced to simulate sediment accumulation, compaction, uplift, and erosion (Rowan, 2006). The results show maximum burial depth occurring ~270 Ma, with depths amounting to ~2500 ft in the west and reaching ~12,500 ft in the east. Current conditions have the Ohio Shale outcropping in western Ohio and reaching a maximum depth of ~5000 ft in the east.

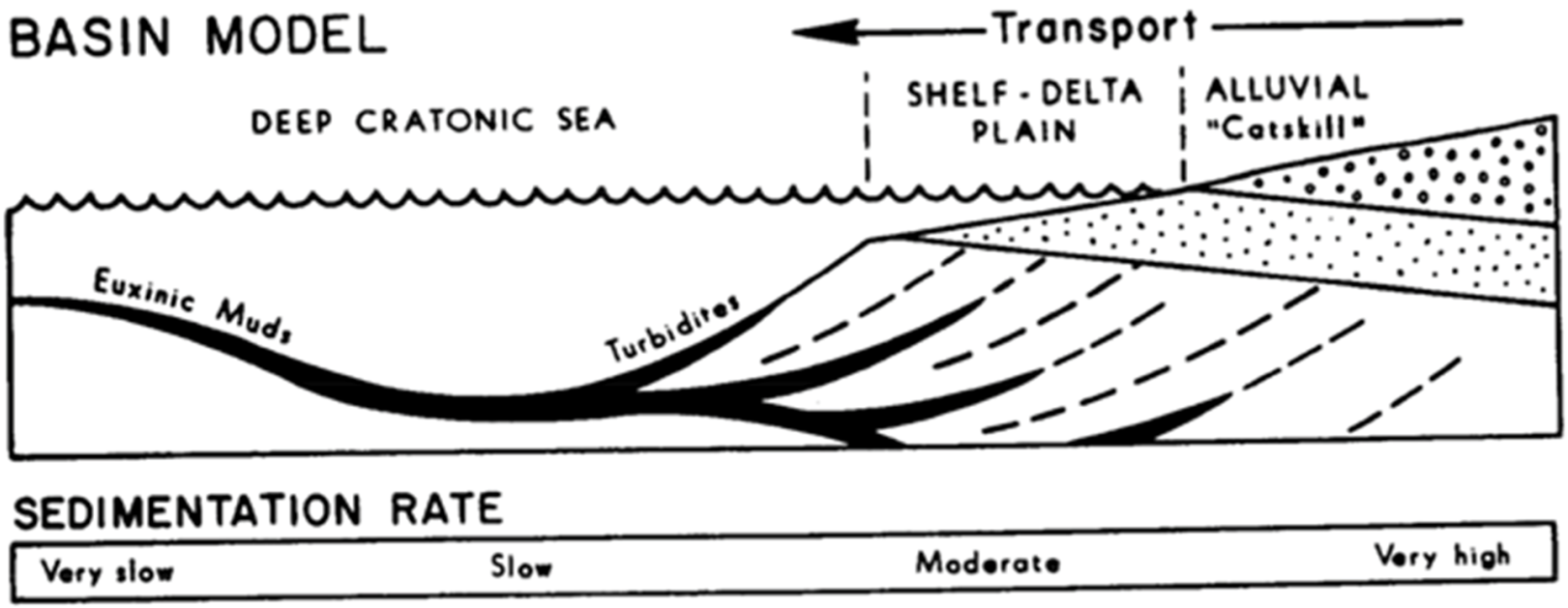

Figure 1.8. Diagrammatic cross section illustrating the depositional environment of the Upper Devonian Shale sequence in the Appalachian Basin (Figure from Potter et al., 1980).

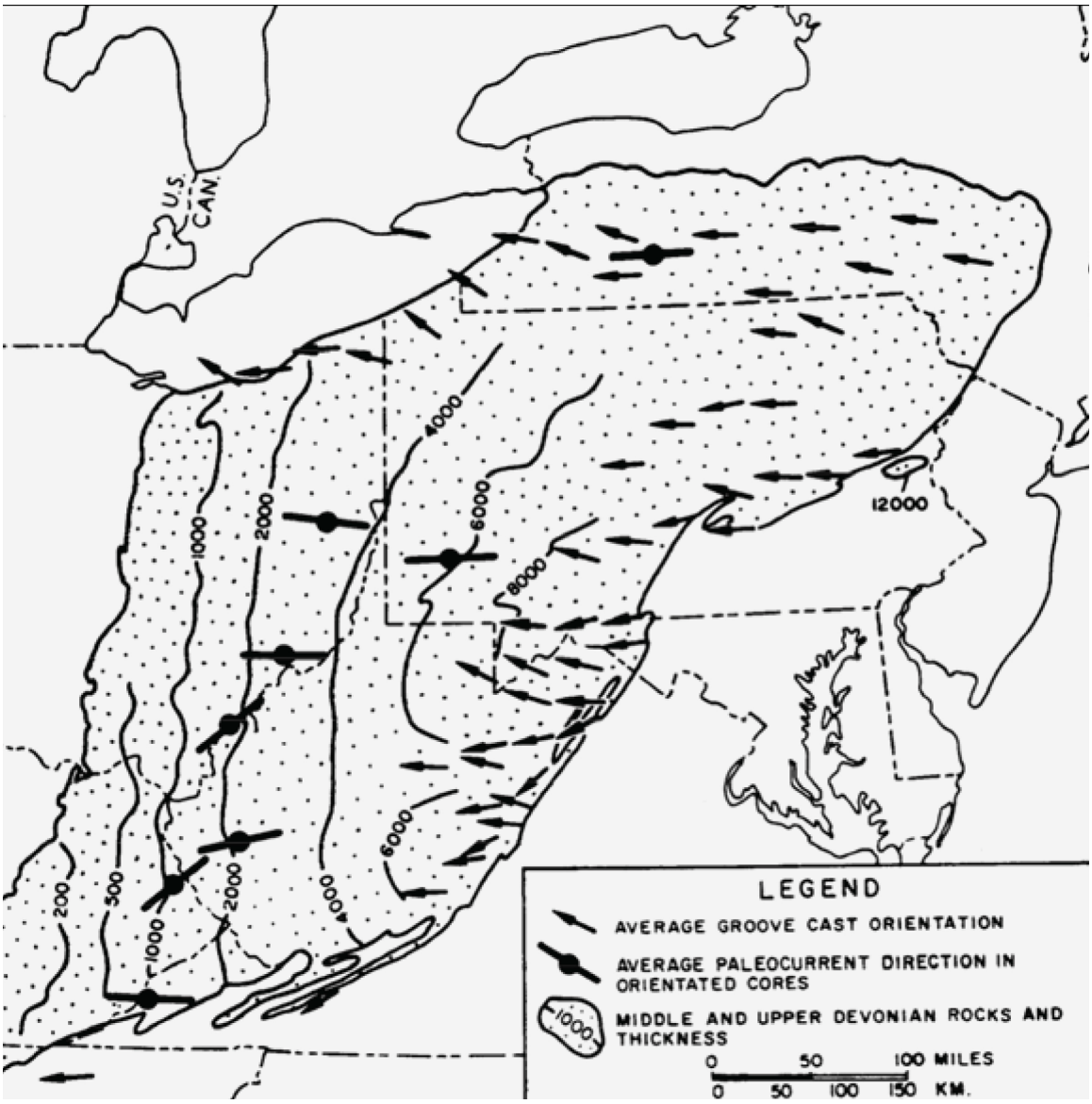

Figure 1.9. Map of paleocurrents to show sediment transportation directions during the Devonian period (Figure from Potter et al., 1980).

CHAPTER II

METHODS

2.1 Well Selection

The counties of interest for this project were those that are currently undergoing increased hydrocarbon drilling and exploration, including Stark, Columbiana, Tuscarawas, Carroll, Jefferson, Harrison, Guernsey, and Belmont counties. Samples of the Upper Devonian strata from the Ohio Shale were taken from wells drilled across these counties in order to adequately represent changes in thermal maturity across the basin. Wells were chosen by carefully examining the Ohio Department of Natural Resources (ODNR) well database and identifying viable wells based on the depth intervals sampled and the availability of digital geophysical logs (ODNR, 2014). Logs were needed in order to identify desired sampling positions in the formation. The geophysical log of primary concern was the gamma ray log, however some wells also included neutron porosity, density porosity, and caliper logs, which aided in the identification of targeted intervals. Preliminarily selected wells were visualized using the GIS software Global Mapper 16 to evaluate the spatial distribution across the counties of interest. Final wells chosen for sampling in the study were selected to allow for the most complete coverage within the area of interest.

2.2 Sample Selection

Three samples, including one each from the top of the Chagrin Shale Member, the center of the Chagrin Shale Member, and the center of the Huron Shale Member, were sought from three to four wells per county. In multiple cases, sample intervals listed as being present in the ODNR core lab database were incorrect, missing, or simply did not exist, thereby precluding sampling from those intervals. If it was discovered that a selected well was missing a desired sampling interval, then any remaining available desired intervals present were sampled and included in the study. If no desired sampling intervals for a well were obtainable, the well was removed from the study and replaced with another well containing the desired sampling intervals. Well logs provided by the Ohio Department of Natural Resources were studied to insure that sampling occurred at the top and center of the Chagrin Shale Member and the center of the Huron Shale Member. Using figure 2.1 as a guide (Broadhead, 1982), geophysical logs were carefully examined to identify the tops of formation members (Figure 2.2), which are most easily seen from observing changes in intensity of natural gamma radiation measured within the borehole.The top of the Chagrin Shale Member was taken as the first large increase in measured gamma radiation below the Berea Sandstone. The Berea Sandstone was identified by very low measured gamma radiation and high porosity. The top of the Huron Shale Member was identified by the next deeper large increase in measured natural gamma radiation. When available, gamma-gamma and neutron porosity curves were also used to help identify formation tops. Multiple wells initially selected for the study lacked geophysical logs or, in some cases, the supplied logs were of too low quality or missing too much information to use. To compensate for this missing information, desired sampling depths were projected to wells without logs using a calculated dip (explained below) between them and a well in which sampling depths were identified by geophysical

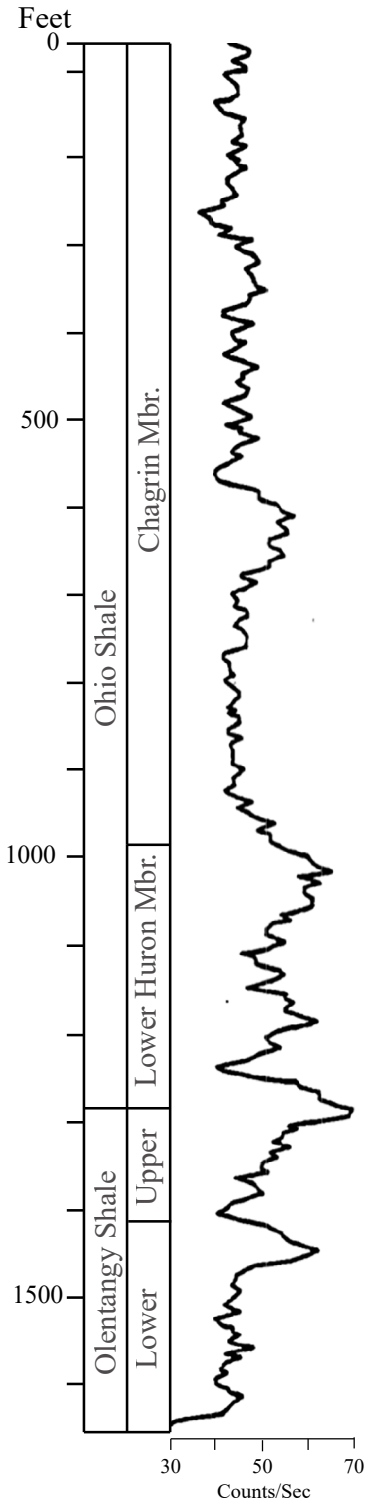

Figure 2.1. Illustration showing the changes in natural gamma radiation that occur with both the Chagrin Shale Member and Huron Shale Member (Figure from Broadhead, 1982). The Upper Huron Shale Member is not included in this profile to due its transition to the Chagrin Shale Member in the study area.

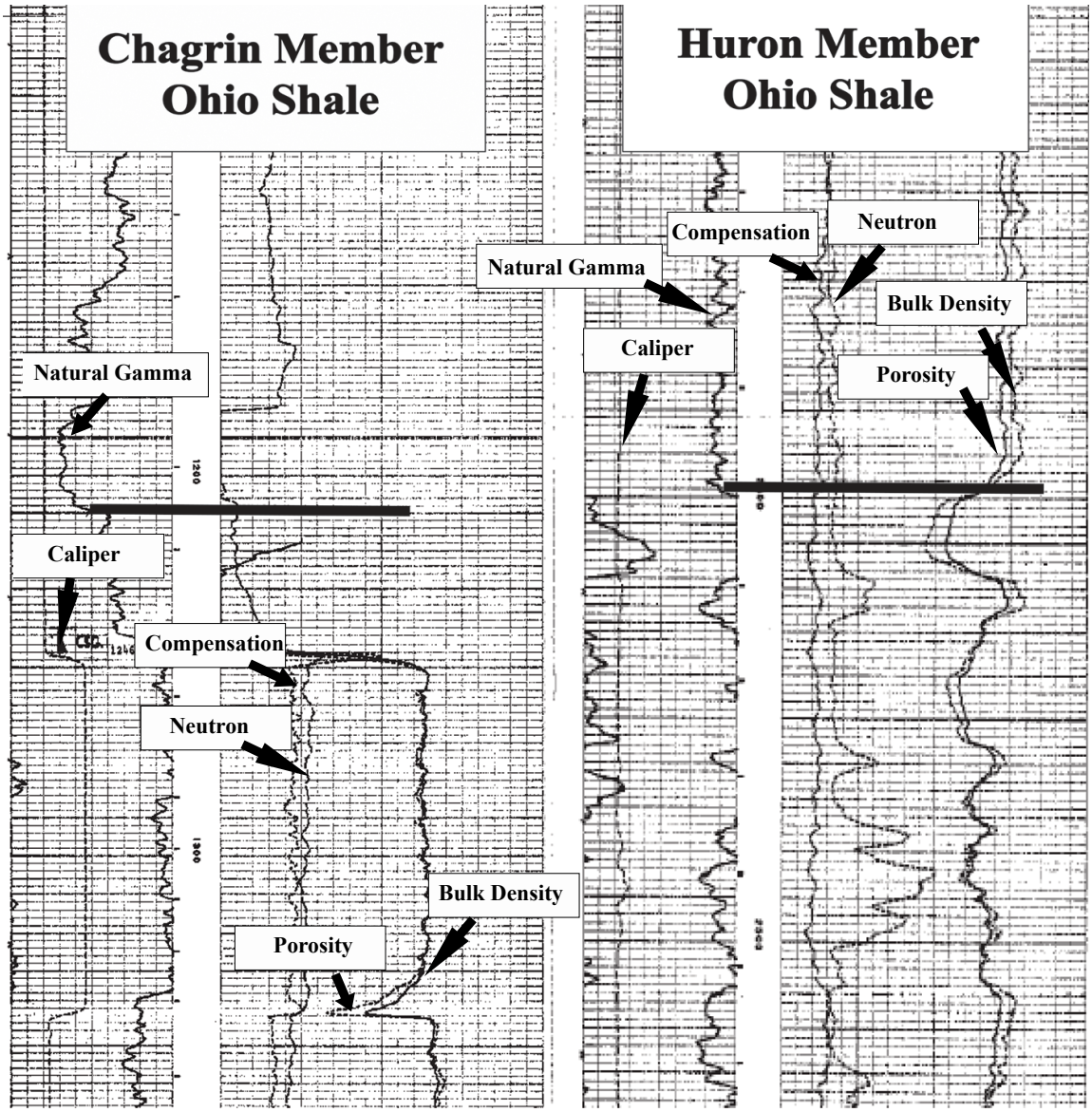

Figure 2.2. Example wireline log showing the tops of the Chagrin Shale Member and Huron Shale Member were chosen. The tops of these horizons (noted by the thick black horizontal lines) were chosen by observation of changes in the intensity of natural gamma that are characteristic to each member. Log from well API 34157247190000, Tuscarawas County.

log interpretation. The top of the Berea Sandstone was chosen to calculate dip between wells due to the lack of an overlying unconformity and the calculated offset was then trigonometrically applied to the boundaries identified in logs (Figure 2.3). Distances between wells with log-interpreted sampling depths and the wells for which sampling depth was calculated averaged 11.5 miles and ranged between 5.2 and 23.2 miles. Data for the depth projection calculations are listed in Appendix A.

Samples were named using the last four digits of the American Petroleum Institute (API) number followed by either a -1, -2, or a -3. The last number stands for the horizon from which the sample was taken, with the 1 standing for the top of the Chagrin Shale Member, 2 for the center of the Chagrin Shale Member, and 3 for the center of the Huron Shale Member.

2.3 Sample Acquisition

In total, 84 samples, each approximately 12 grams in mass, were obtained from the H.R. Collins Core and Sample Repository. The H.R. Collins laboratory is located at Alum Creek State Park in Delaware County, Ohio and is owned and operated by the Ohio Department of Natural Resources, Division of Geological Survey. Sample boxes for each well were pulled from storage prior to my arrival and placed in a processing room containing scales for the weighing and collection of samples. At least three well locations containing samples from all three targeted depths were collected per county (Figure 2.4). The only exception is Carroll County, where an entire well, API 34019208350000, was missing from the core lab and no replacement well was available. Samples in the Collins Lab are associated with accurate latitude and longitude, formation top, and formation thickness for the target formation, which was useful when comparing different areas of

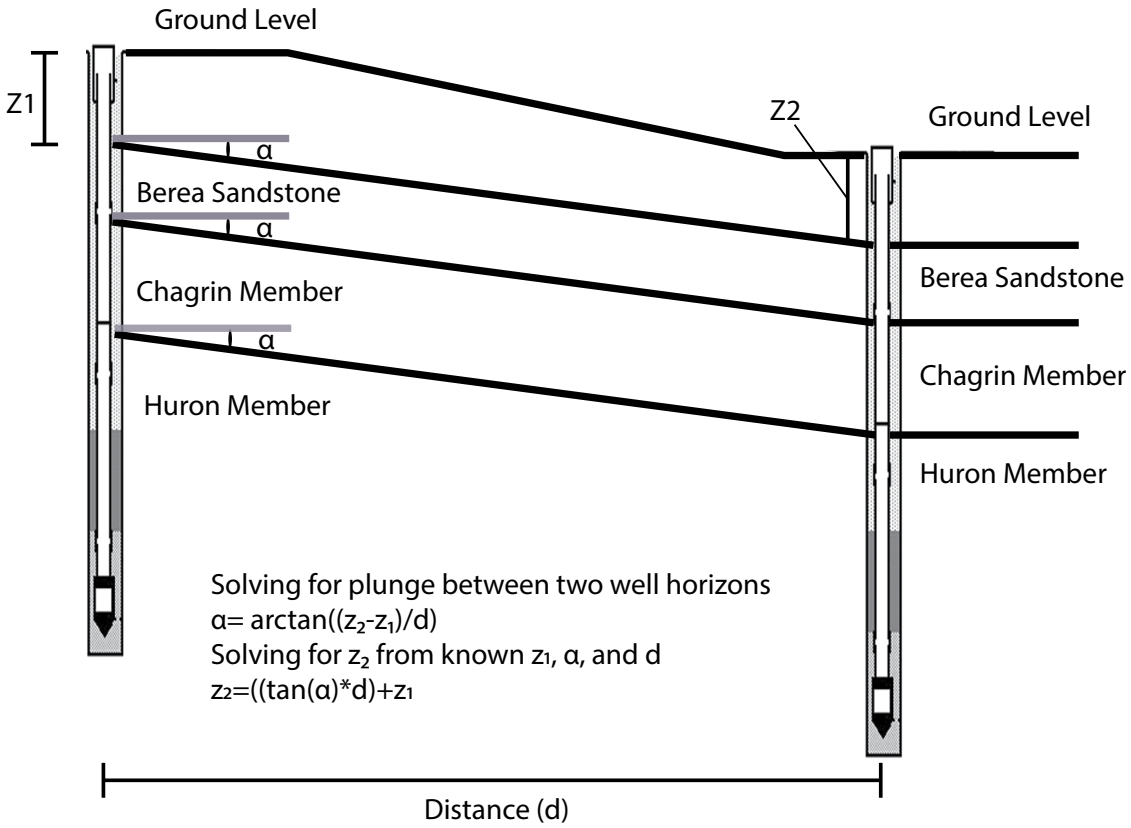

Figure 2.3. Illustration showing the method used to calculate the desired sampling depth of wells lacking wireline log data. See Appendix A for detailed description.

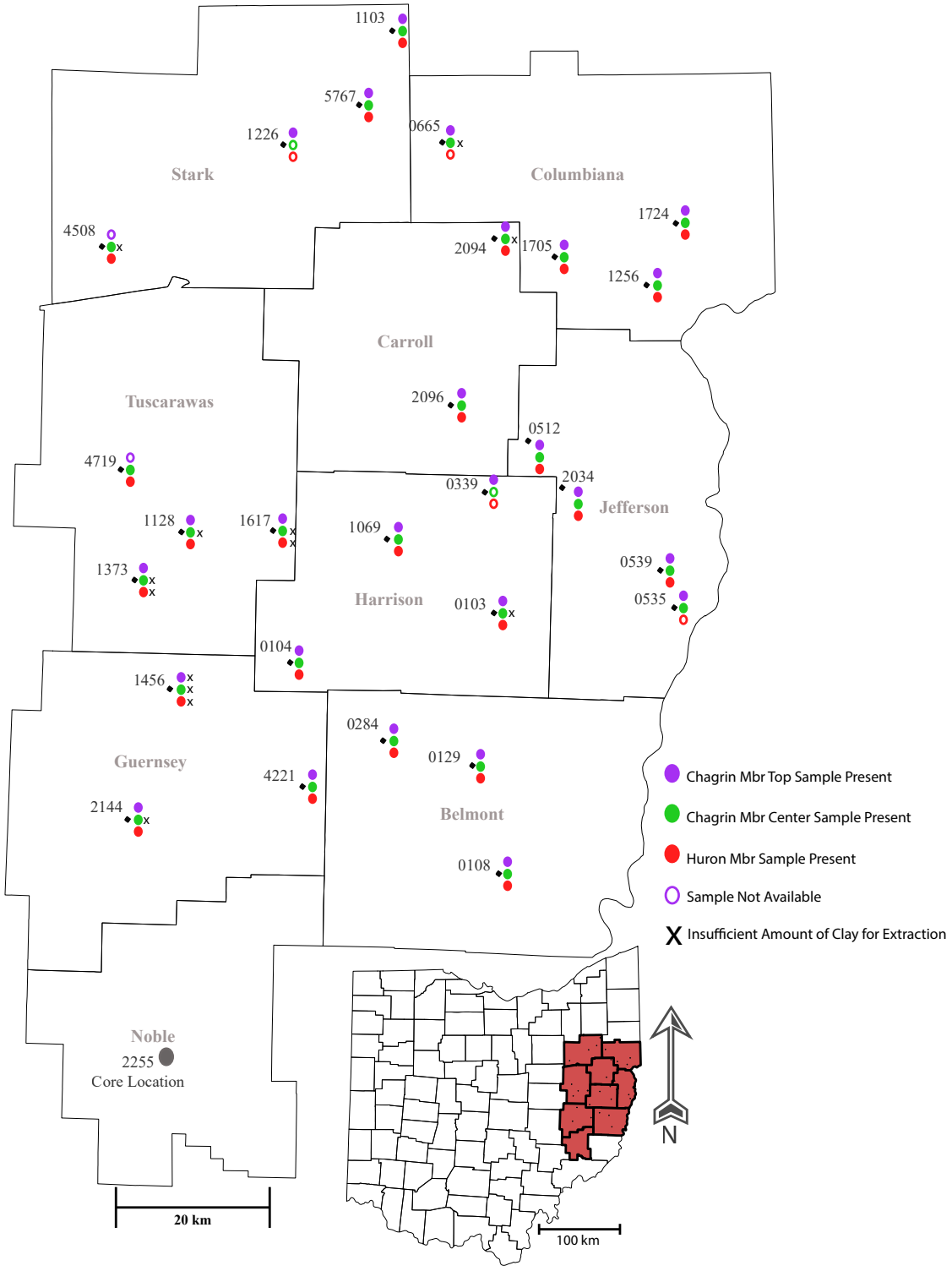

Figure 2.4. Map of study area and well locations.

the basin. The full list of samples with location, desired sampling depth, and sampling depth received is located in Appendix B.

2.4 Sample Preparation

Some of the laboratory techniques used, including X-ray diffraction (XRD), total carbon measurement (TOC), and total inorganic carbon measurement (TIC) using a CO_2 analyzing Coulometer, required samples to be in powder form. The environmental scanning electron microscope (ESEM) required raw sample. To this latter issue, a portion of raw sample was separated from the bulk sample before being pulverized. Samples to be pulverized were placed into a tungsten lined aluminum canister containing two tungsten-carbide balls and an end cap on each side equipped with a cork gasket to prevent the escape of finely powdered sample. The canister was then secured in a SPEX rock mill powered by an Emerson Electric S60AAW-6118 1/3 horsepower motor operating at 1725 revolutions per minute (Figure 2.5). Samples were processed for ten minutes and then stored in re-sealable plastic bags upon removal. Cleaning of the canister following the removal of the sample was performed using hot tap water and a brush to remove all remaining powder. Acetone was then added to the canister to ensure the complete removal of water before inserting the next sample.

2.5 X-ray Diffraction

X-ray powder diffraction unveils important information about the samples, such as rock mineral composition, types of clays present, and their proportional content within the sample (Jiang, 2012). Bulk sample X-ray diffraction was performed on each

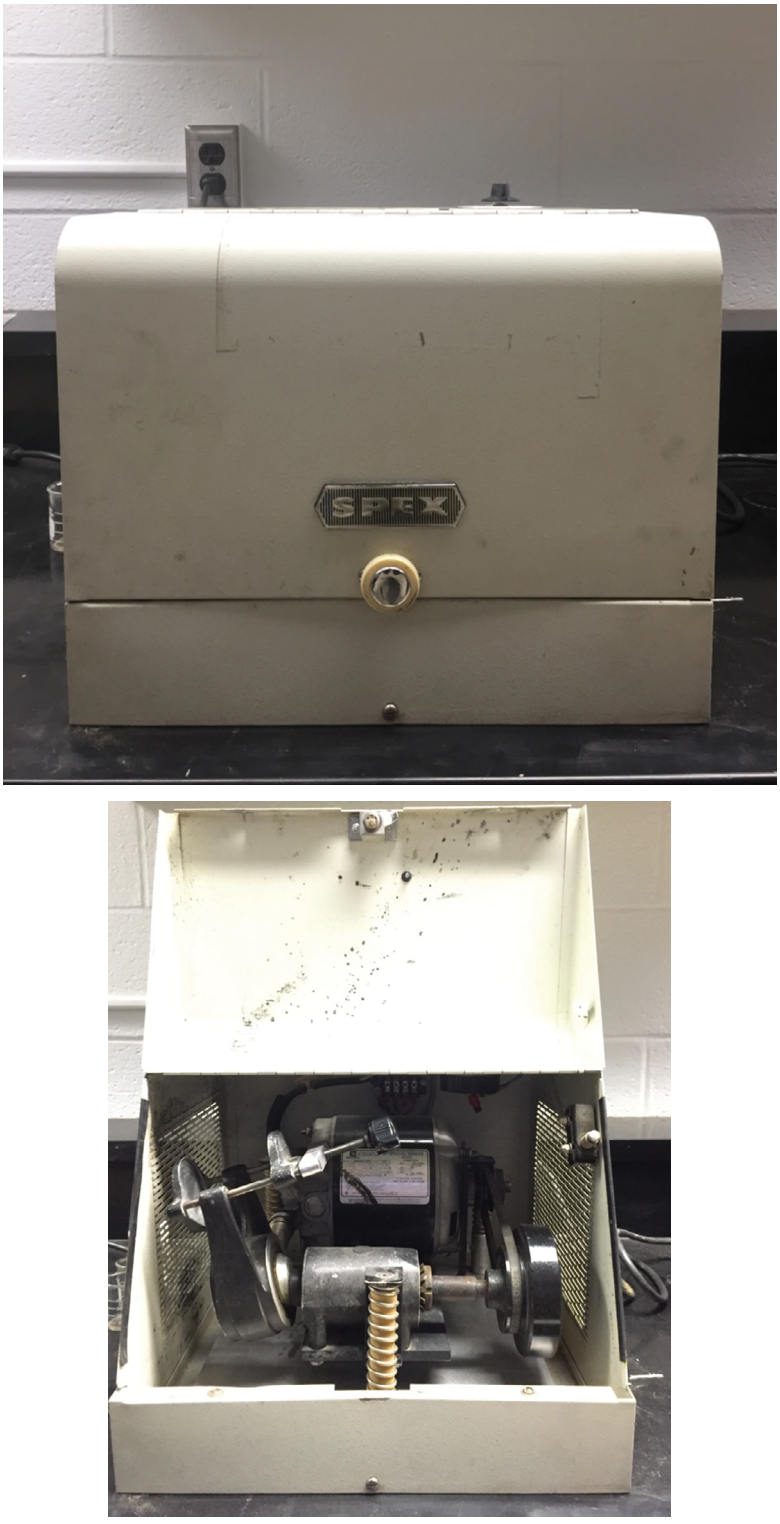

Figure 2.5. Photograph of the Spex ball-mill used for pulverizing samples.

sample prior to the separation of clay minerals to gain insight on mineralogical and compositional changes of the formations across the basin and with respect to depth. Pulverized samples were packed into Rigaku 900005 X-ray slides with a 2.0 mm indent (Figure 2.6b) and analyzed using a Rigaku Ultima IV X-Ray Diffractometer (Figure 2.6a) utilizing CuKα radiation with a scan speed of 1 minute per degree, a sample width of 0.04 mm, and a slit size of 0.3 mm.

Washing and disaggregation of clay materials were performed using the methods of Burtner and Warner (1986). The <2 μm clay fraction was separated via centrifugation at 2000 RPM for 70 seconds (Figure 2.7a). Settling to glass slides (Figure 2.6c) was accomplished following the vacuum and filter method shown in figure 2.7b. (Moore and Reynolds, 1997). After the drying of clay particles to be examined, the sample was examined via XRD. Ethylene glycolation (EG) of the sample was then performed by letting the sample sit in a fumigator containing ethylene glycol (Figure 2.8) overnight followed by another XRD. This was done to help differentiate between expandable clays (smectite), which expand upon glycol treatment, and illitic non-expandable clays (Mosser-Ruck et al., 2005). Samples were then heated at 550 degrees Celsius for at least 30 minutes to collapse all expandable minerals present to 10 Å and to verify by XRD the presence of chlorite by an increase in intensity of its (001) reflection at 14.2 Å.

MacDiff 4.2.6 software was used to interpret diffraction patterns and record the integrated peak areas of the 17 Å smectite peak at 5.2° 2θ and the 10 Å illite peak at 8.9° 2θ in the glycolated state; the 7 and 3.54 Å chlorite peaks at 12.5° 2θ and 25.1° 2θ in the air-dried state, and the 7 and 3.57 Å kaolinite peaks at 12.5° 2θ and 24.9° 2θ in the air-dried state. Representative diffraction patterns of the air-dried, ethylene glycol treated, and heat-treated samples can be seen in figure 2.9. Since both 7 Å kaolinite (001) and chlorite (002) reflections occur at 12.5° 2θ, the presence of kaolinite (Figure 2.10) is determined based on the occurrence or absence of a 3.57 Å peak at 24.9° 2θ (Iacoviello

A)

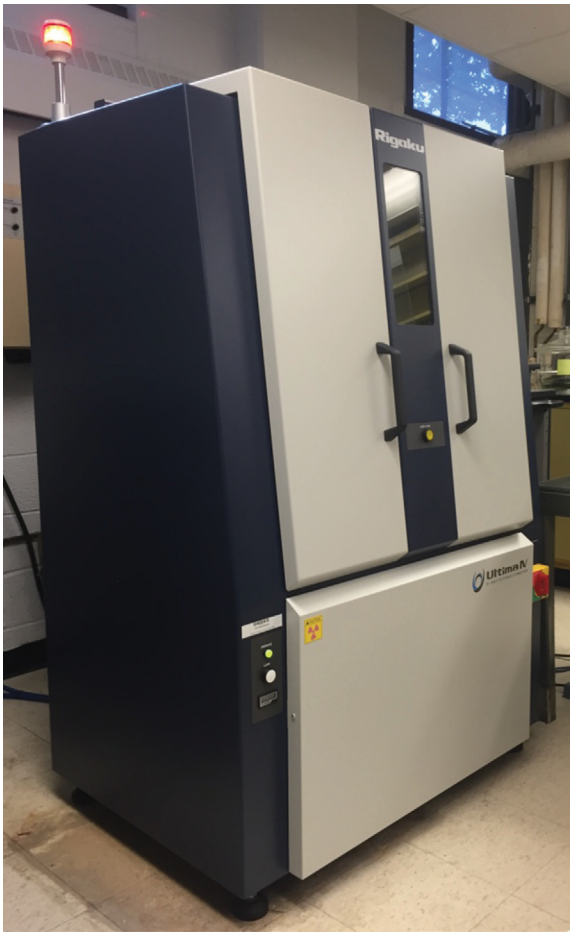

B)

C)

Figure 2.6. Photographs of X-ray Diffraction instrument and supplies. A) XRD instrument used for sample analysis. B) Sample holder for bulk XRD measurements. B) Glass slides used for mounting the clay fraction.

A) B)

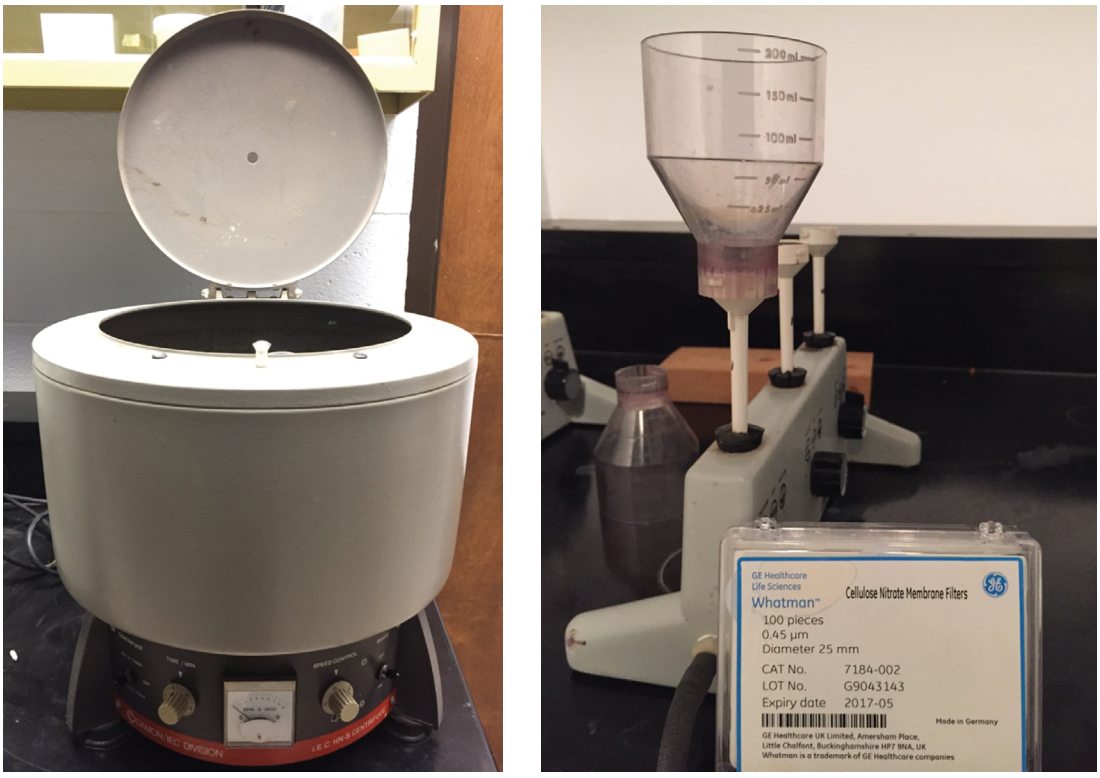

Figure 2.7. Photograph of equipment used for extraction of the clay sized fraction. (A) Centrifuge used for separating the <2 µm fraction and (B) the equipment used to vacuum the clay minerals onto the cellulose filters.

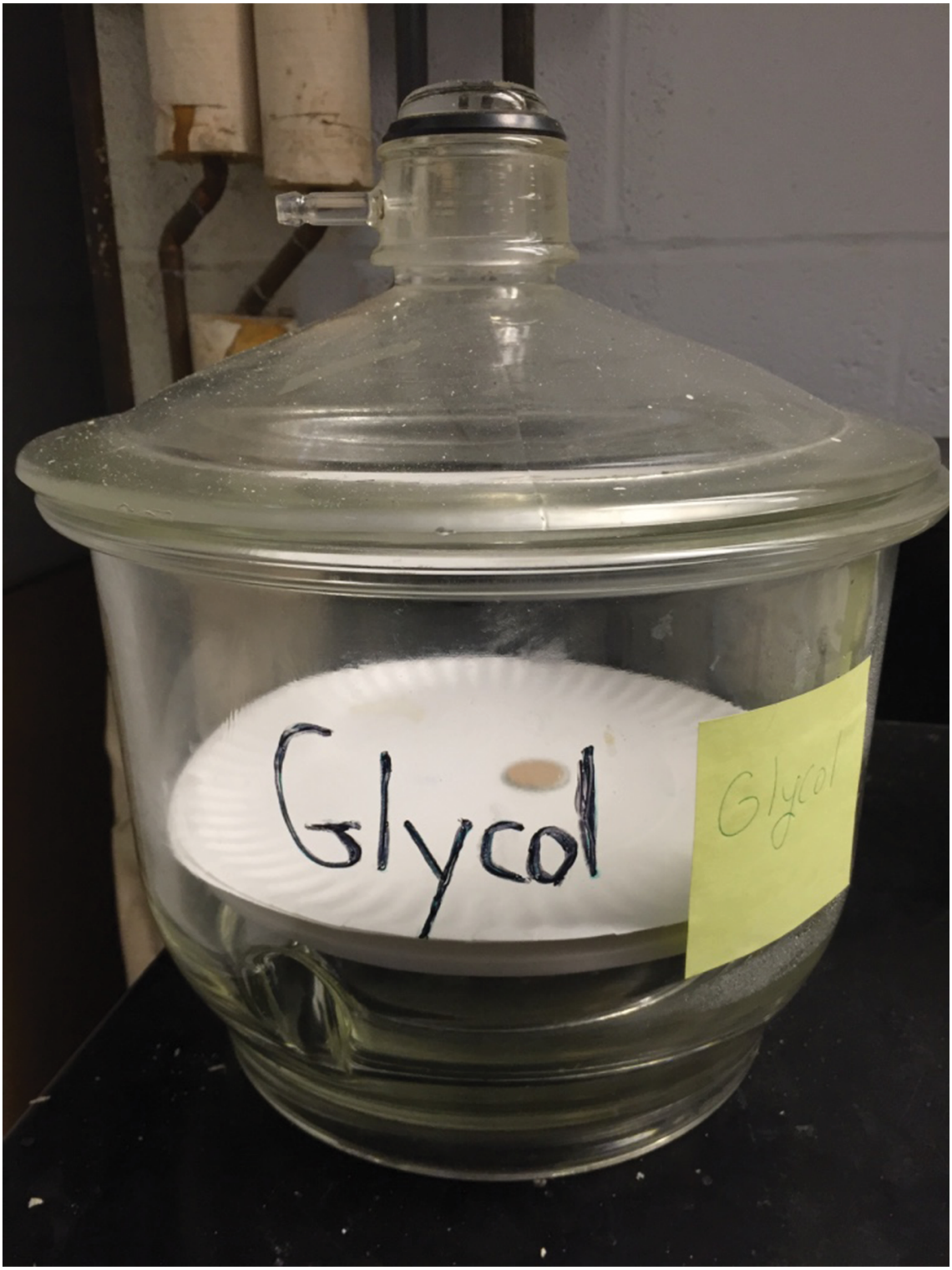

Figure 2.8. Photograph of ethylene glycol fumigator for expansion of clay minerals.

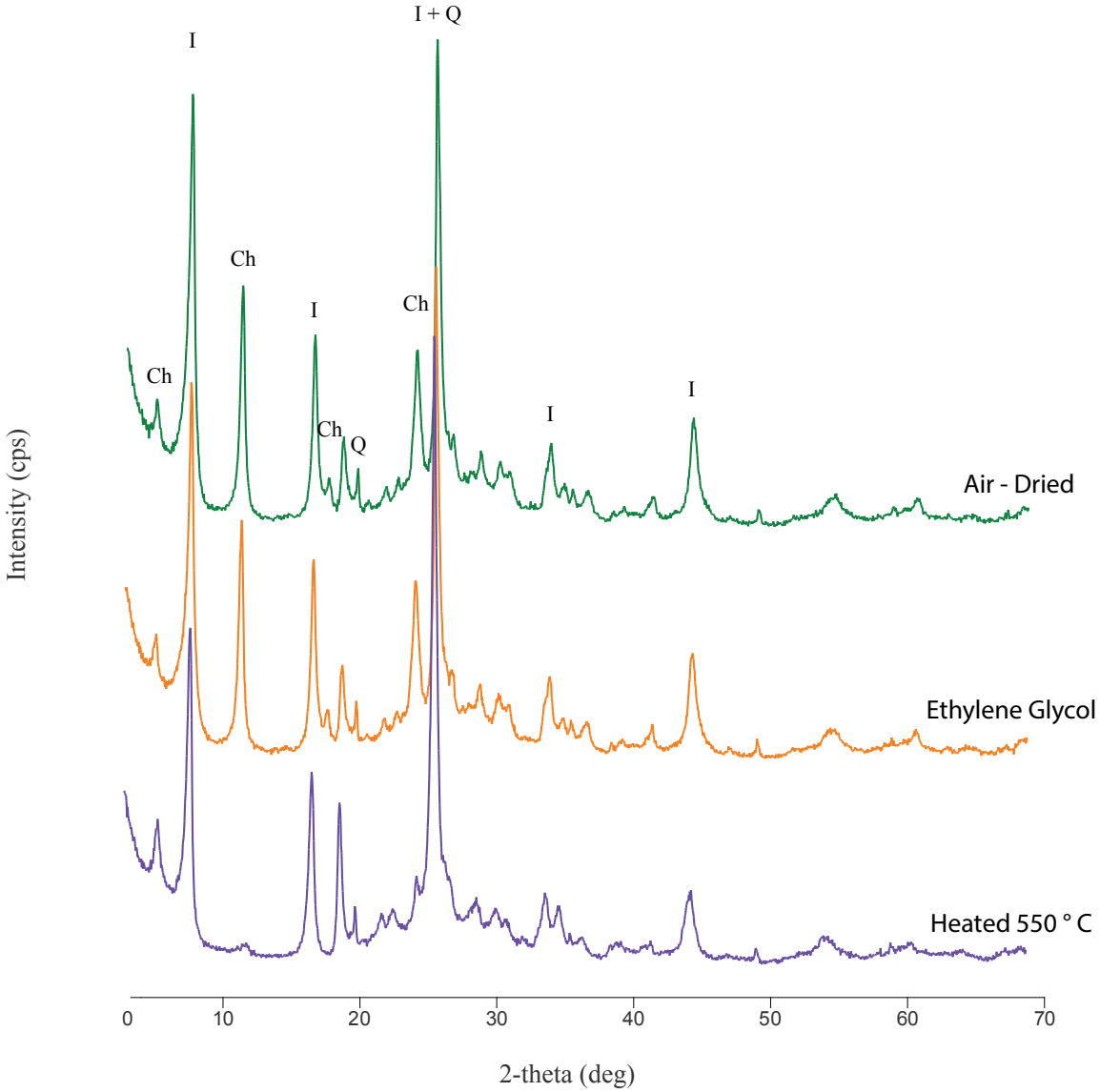

Figure 2.9. Illustration of diffraction patterns in the air-dried, ethylene glycol, and heat-treated states to show the common clay minerals identified in this study. (Ch) = Chlorite, (I) = Illite, (Q) = Quartz.

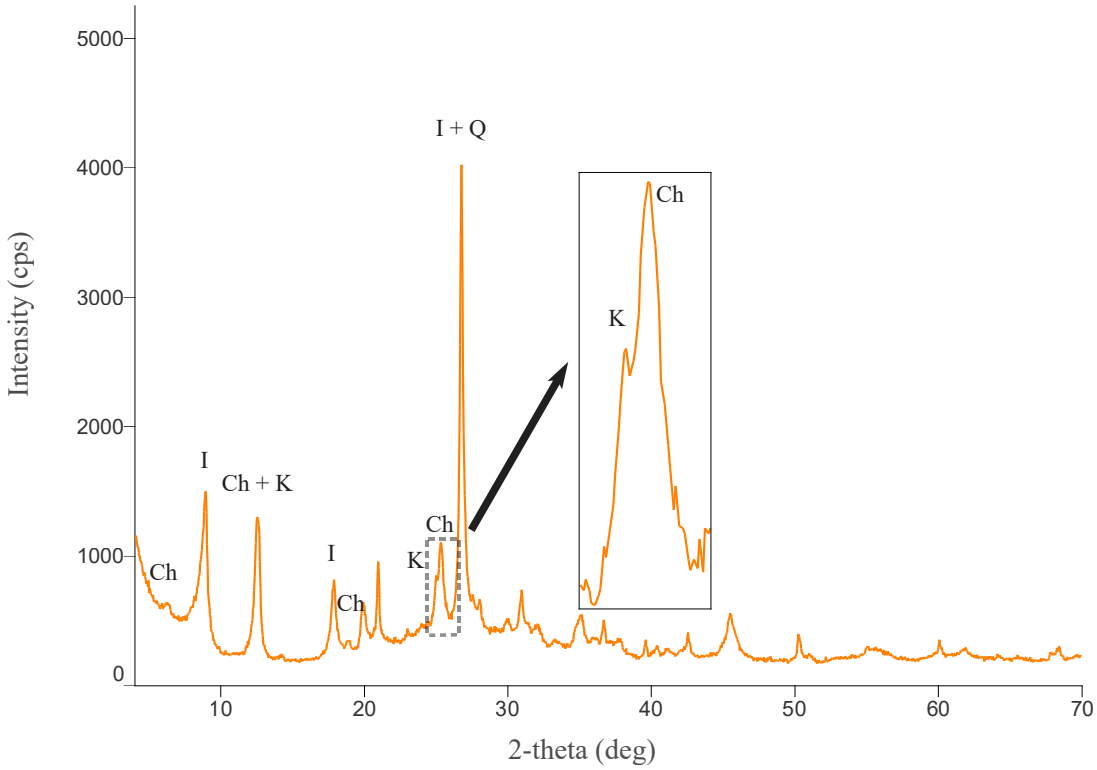

Figure 2.10. Diffractogram of the top of the Chagrin Member from sample 0339-1 showing the clear differentiation between the kaolinite (002) and chlorite (003) peaks at 24.9° 2θ and 25.1° 2θ, respectively.

et al., 2012). The MacDiff software was useful in this aspect, because it implements deconvolution techniques to separate the 3.57 Å kaolinite and 3.45 Å chlorite peaks that nearly overlap at at 24.9° 2θ and 25.1° 2θ, respectively. Percentages of each clay were calculated using the measured peak areas and standard weighting factors calculated from the integrated areas of the pure mineral reflections (Biscaye, 1965; Iacoviello et al., 2012).

Two alternate programs, Rigaku's PDXL-2 software and a new program named ClayStrat +, were also tested for use in the project, but did not prove suitable for the required analyses. Clay percentages calculated using the relative intensity ratio (RIR) method within the Rigaku software did not present reasonable values compared to previous studies (Hosterman and Whitlow, 1981; Leventhal and Hosterman, 1982), and the ClayStrat + program did not calculate background sufficiently.

Two standards, Bentonite and SWy-1 Montmorillonite from the Clay Mineral Society, were analyzed to confirm that the laboratory procedures could extract expandable clays and did not inhibit expansion of those clays after ethylene glycol treatment (Figure 2.11). The Kübler index is the measure of the full width of the illite peak at half maximum intensity (Abad, 2007), is related to illite crystallinity, and was recorded for each sample analyzed. The value of illite crystallinity relates to thermal maturity, with decreasing peak breadths resulting from thermal maturation (Abad, 2007).

2.6 Petrographic Analysis

SEM microscopy for petrographic analysis is a useful supplement to XRD techniques of identifying clay minerals. Samples were analyzed to help differentiate between authigenic and detrital grains (Pollastro, 1993). Petrological analysis not only gives

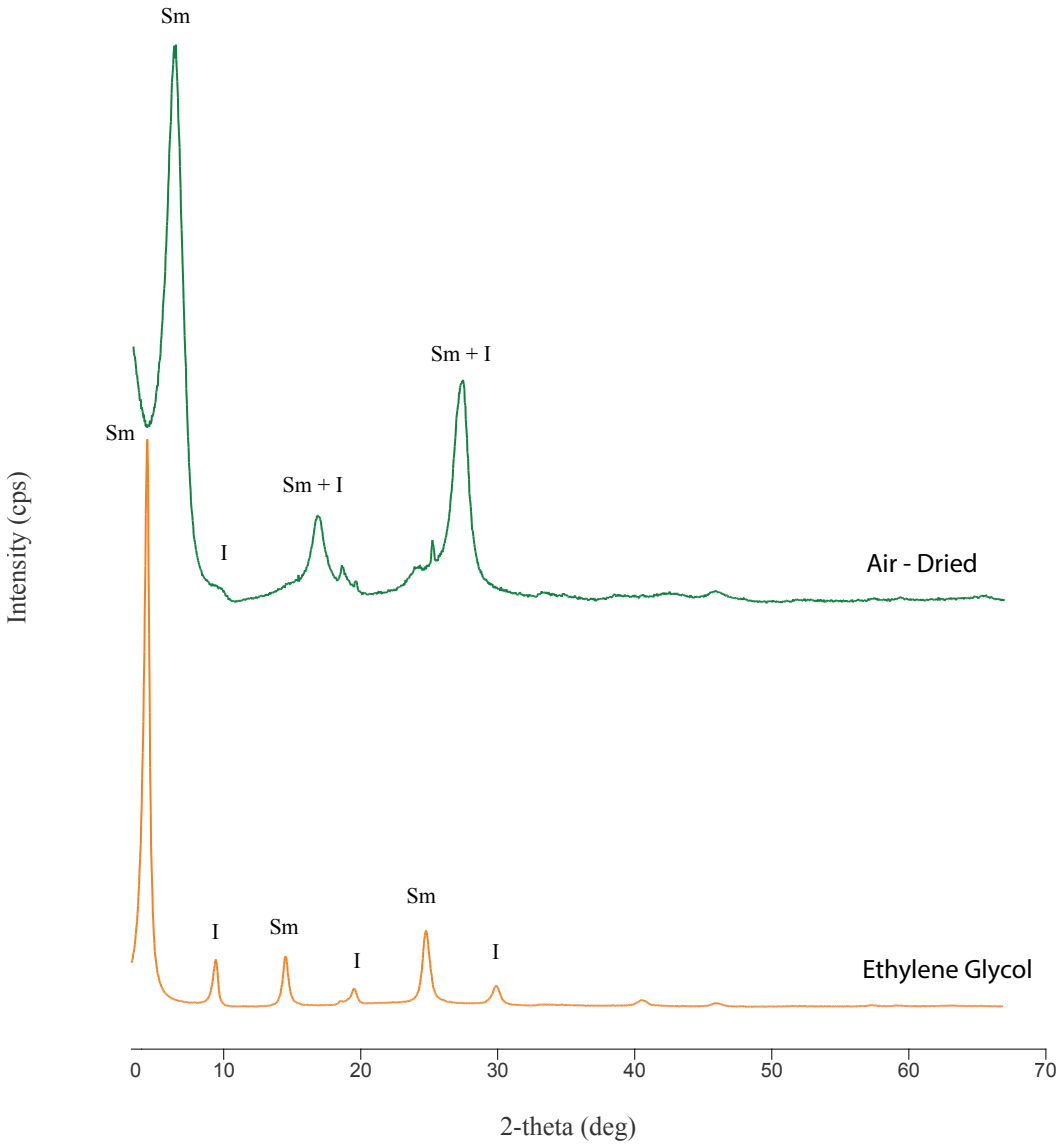

Figure 2.11. Illustration showing expansion of smectite after ethylene glycol treatment of the standard Swy-1 Montmorillonite. This confirms the effectiveness of the clay fraction preparation procedure used. (I) = Illite, (Sm) = Smectite.

information about crystal structure, but can also be used to identify possible alterations to the crystal structure that resulted from certain geologic events.

SEM microscopy was performed on the raw samples from each well using an FEI Quanta 200 Environmental Scanning Electron Microscope (Figure 2.12a) operating in low vacuum (.6 Torr) at 30 kV energy. Since the samples used were primarily from well cuttings, the size of grains varied from sample to sample. For samples that contained large grains, attempts were made to carefully break apart the grains and mount the fresh surface facing upwards to the sample post using double-sided carbon tape. Samples that contained grains too small for this procedure were simply mounted by applying the carbon tape to the sample post and pressing the post (Figure 2.12b) into the sample. At least 3 images were taken from each sample at 76x magnification to show an overview of the entire grain, 1,136x magnification to get a large view of the grain's surface, and 4,734x magnification to show the individual clay mineral growth. Along with imaging, Energy Dispersive X-ray (EDX) spectroscopy was performed using an EDAX Inc. EDX instrument operating with a 35 degree take off angle. EDAX Inc.'s standardless quantification mode was utilized, so no calibration had to be completed. The EDX analysis gives a quantitative weight percent for the elements present in the sample, which can be used to check the accuracy of the identified minerals from XRD analysis.

2.7 Total Organic Carbon

The total organic carbon (TOC) was quantified for each sample to help gain a better understanding of variables within the sample that could potentially alter diagenesis. This measurement required the use of two laboratory techniques; CHN analyzer to measure the total amount of carbon (TC) in the sample via elemental combustion, and the Coulometer to measure the inorganic portion (TIC). Between 1.5 mg and 2.5 mg of each sample was

A)

B)

Figure 2.12. Photographs of the ESEM and supplies. A) ESEM. B) Sample holders and adhesive used to mount samples.

weighed using a Mettler Toledo MX5 microbalance, held in Perkin Elmer 5 x 8 mm pre-cleaned tin capsules, and run using a Perkin Elmer 2400 Series II CHN analyzer (Figure 2.13). Between 35 mg and 45 mg of pulverized sample was weighed and added into plastic capsules to be analyzed using a UIC Coulometrics Inc. CO_2 Coulometer equipped with a CM5130 Acidification Module (Figure 2.14). For both laboratory techniques, a MESS 3 marine sediment standard was run at least every 11 samples to evaluate quality control. 20% of samples were also duplicated and compared for accuracy using standard deviation values for quality assurance. Quality assurance (QA) values for TIC analysis are as follows: MESS 3 (n = 15, avg = 0.62 ± 0.05); Duplicate samples (n = 18, ± 0.00 to ± 0.03). For the CHN, duplicates were also analyzed between runs on separate days to ensure machine consistency. QA values for CHN analysis are as follows: MESS 3 (n = 37, avg = 2.10 ± 0.08); Duplicate samples (n = 40, ± 0.00 to ± 0.09). TOC was then calculated by subtracting the amount of inorganic carbon measured in the Coulometer from the total carbon measured via CHN analysis. MESS 3 TOC values averaged 1.48 % ± 0.09, and duplicate samples (n = 6) showed standard deviations ranging between 0.0 and 0.01.

2.8 Core Description

Since all of the samples acquired for this project were of drill cuttings, a thorough examination of the Ohio Shale was completed on core samples from API 34121222550000 (Noble County) in order to generate detailed descriptions of the interbedded clays, shales, black shales, and turbidites. No full cores of the interval of interest were available for wells in the 8 county study area, therefore I used the Noble County core as an alternative. Although Noble County is not included as part of my

Figure 2.13. Photographs of CHN analyzer, supplies, and preparation. Top left photo taken by Annie Hartwell.

Figure 2.14. Photographs of the Coulometer and supplies used to measure inorganic carbon.

study area, the geology of the Ohio Shale is consistent throughout much of the targeted area.

All major lithologic changes were noted, sampled, and analyzed using the same laboratory techniques employed to analyze the rest of the samples in the project. This detailed description is helpful in understanding changes in depositional environments throughout the Upper Devonian and can be correlated to the data received from other analyses.

CHAPTER III

RESULTS

3.1 Bulk Powder XRD

All samples analyzed using the Rigaku PDXL-2 software contained quartz, illite, and some type of plagioclase mineral. Data are listed in Appendix C. The most common plagioclase mineral present in all three sampling horizons was albite and albite containing < 10% of calcium in its sodium-dominated chemical formula. However, the plagioclase minerals analbite, anorthite, orthoclase, and anorthoclase were identified in several samples throughout all horizons in the study. Most samples are shown to contain chlorite and kaolinite, however, due to the difficulty of clay mineral identification in bulk powder, the presence or absence of specific clays was preliminary until confirmed by separate analysis of the clay fraction, as explained in the next section. The less common non-clay minerals encountered include pyrite, calcite, dolomite, siderite, gypsum, and enstatite, the latter of which was only identified in one sample from Jefferson County. Pyrite was rarely identified in samples from the top of the Chagrin Shale Member, but became increasingly prevalent through the center of the Chagrin Shale Member. Nearly all samples from the Huron Shale Member contained pyrite, which is consistent with the anoxic burial conditions associated with organic-rich shale. Dolomite was most prevalent in the samples from the Chagrin top, while calcite was more common in samples from the Huron Shale Member. No gypsum was found in any samples from the top of the

Chagrin Shale Member, but it was identified in several samples from both the center of the Chagrin and Huron Shale Members.

3.2 Clay Fraction XRD

Illite was the major constituent of all clay fraction samples analyzed, ranging between 50 and 86%, averaging 71% for the top of the Chagrin Shale Member, 75% in the center of the Chagrin Shale Member, and 81% in the Huron Shale Member of the Ohio Shale (Appendix D). The highest illite content recorded came from the deepest sample of the Noble County core, totaling 89%. Illite percentages from the top of the Chagrin Shale Member per country in decreasing order are as follows; Harrison = Belmont = Carroll > Guernsey = Stark > Tuscarawas > Columbiana. For the center of the Chagrin Member, nearly all counties average between 74 and 77%, except for Tuscarawas at 68%. For the Huron Member, average illite concentrations per county fall between 80 and 84%, except Jefferson County with an average of 78%.

Chlorite was the next most abundant mineral, and was present in all samples throughout the study area. The average percent of chlorite present across all counties for the top of the Chagrin Shale Member, the center of the Chagrin Shale Member, and the Huron Shale Member are 25, 21, and 15%, respectively. Almost all counties in the study area have an average chlorite concentration ranging between 19 and 26% for the top of the Chagrin Shale Member, except for Columbiana with 35% and Belmont County and 16%. The chlorite concentrations for the center of the Chagrin Member per county range between 20 and 25%, except for Guernsey and Columbiana Counties with 17 and 18%, respectively. The Huron Shale Member concentrations range between 10 and 16%, except in Columbiana with 18%, and Jefferson with 20%. Expandable clay was only clearly identified in three samples, including 1373-1 in Tuscarawas County (Figure 3.1), and

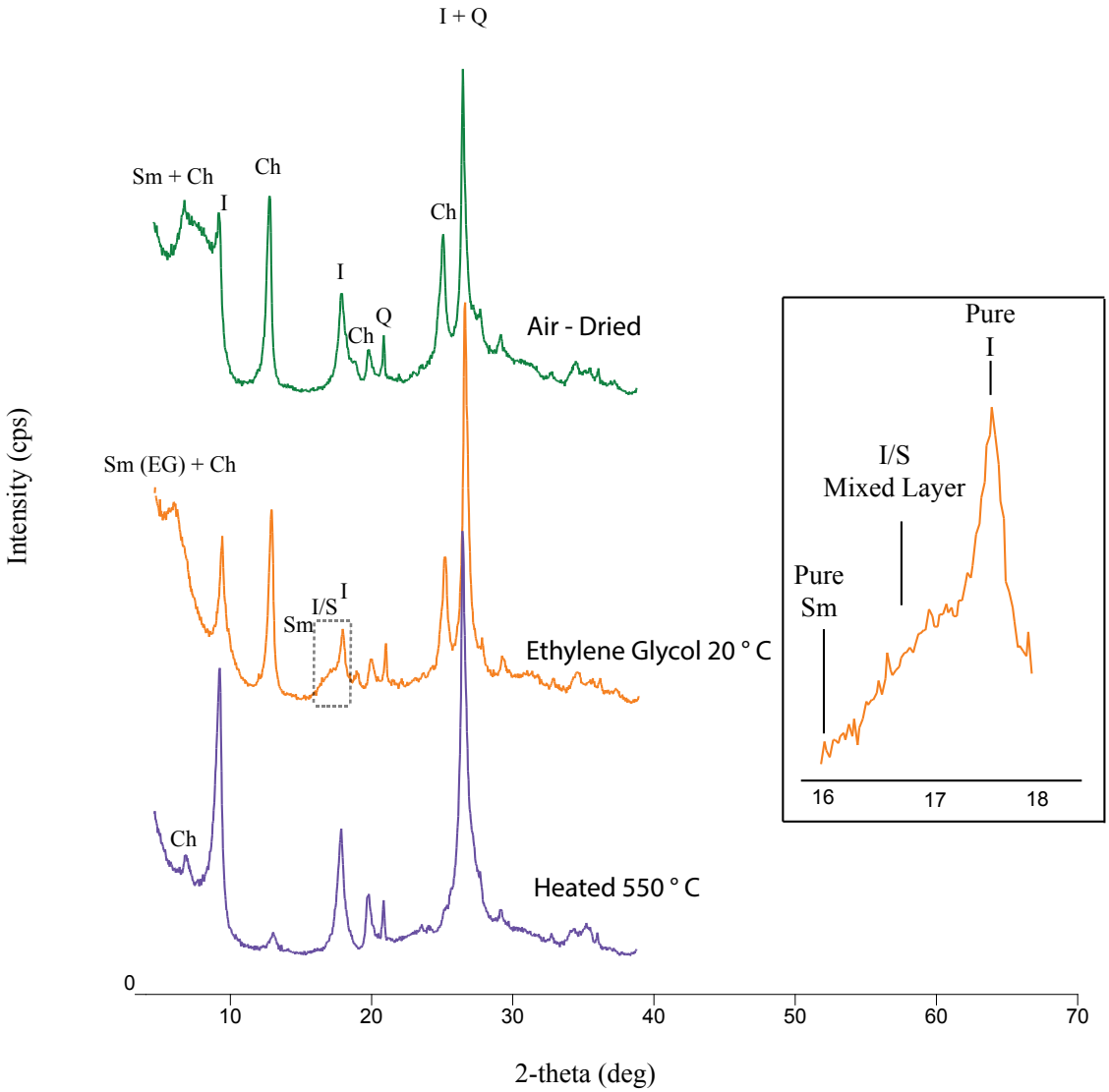

Figure 3.1. Example of the low angle shoulder seen on diffractogram between 15 and 18 degrees 2Θ formed by the existence of a mixed layer clay mineral from sample 1373 -1. The shoulder results from the input of the smectite (003) and illite (002) reflections. Using the Δdegrees 2ɵ method of Moore and Reynolds (1997), the material is estimated to be between 75 and 80% illite. (Ch) = Chlorite, (I) = Illite, (Q) = Quartz, (Sm) = Smectite

0102-1 and 0129-3 (Figure 3.2) in Belmont County. Figure 3.3 illustrates the average clay mineral concentrations for each member sampled. Evidence of mixed layer clays can be seen by a slight decrease in peak breadth between glycolated and heat-treated diffraction patterns (Figure 3.4), which would remain constant if the material was purely illite. This change in preak breadth leads to the possibility of a small percent (< 10%) of mixed layer clay being present in the sample. However, of that 10% of mixed layer clay, 90% or more of the layers are illite due to failure of peak migration after glycolation. Kaolinite was also present in some samples across the study area, usually occurring in trace amounts (< 5%), though as high as 16% in sample 1128-1 from the top of the Chagrin Shale Member. Illite concentrations usually increased with depth (Figure 3.5), whereas chlorite concentrations typically decreased with depth (Figure 3.6). Kaolinite, when identified, was usually in the shallowest samples of each well, and either decreased to trace levels with depth or completely disappeared (Figure 3.7). The Kübler indices recorded for all the samples in the study ranged between ~ 0.4 to ~ 0.65, with two outliers above 0.65 (Figure 3.8). The full list of values is given in Appendix E.

3.3 Petrographic Analysis

Both authigenic and detrital quartz, feldspar, and clay minerals were observed in all the samples (Figure 3.9) based on comparison of crystal morphology to a petrographic mineral identification atlas (Welton, 2003). Clay minerals are identified in SEM imaging by their unique morphologies, which are frail and unable to hold up against the compaction of burial (Iacoviello et al., 2012). Since shales and mudstones are primarily composed of detrital material (Figure 3.10), it was difficult to visually identify individual clay minerals. Therefore, minerals were identified as authigenic based on shape and presence of structures too frail to survive compaction (Iacoviello et al., 2012).

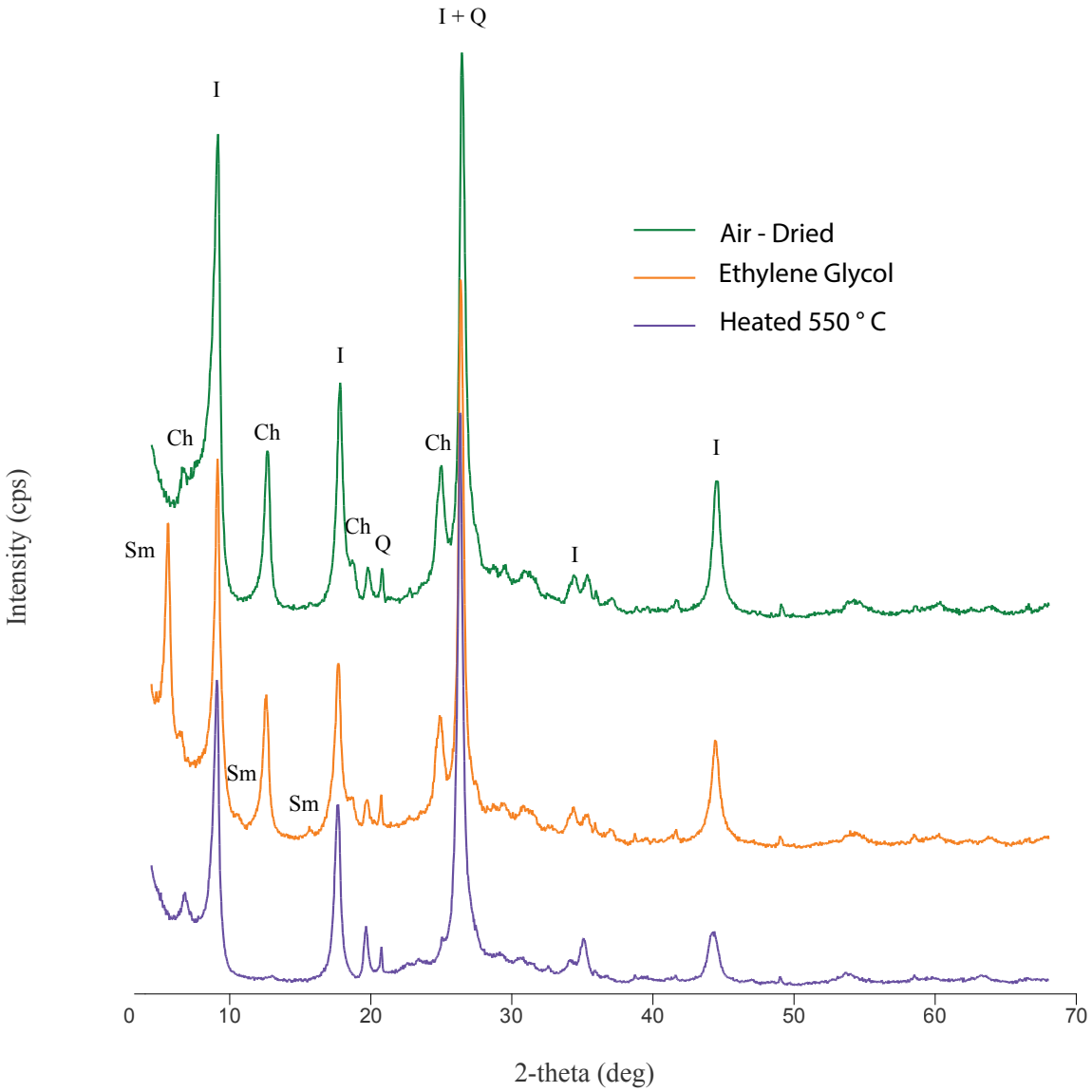

Figure 3.2. Example of a diffractogram showing a small amount of expandable clay from the Huron Shale Member from sample 0129-3. The presence of expandable clay is identified by the peak that migrates from ~ 7º 2Θ in the air-dried state to ~ 5º 2Θ after ethylene glycol treatment. (Ch) = Chlorite, (I) = Illite, (Q) = Quartz, (Sm) = Smectite.

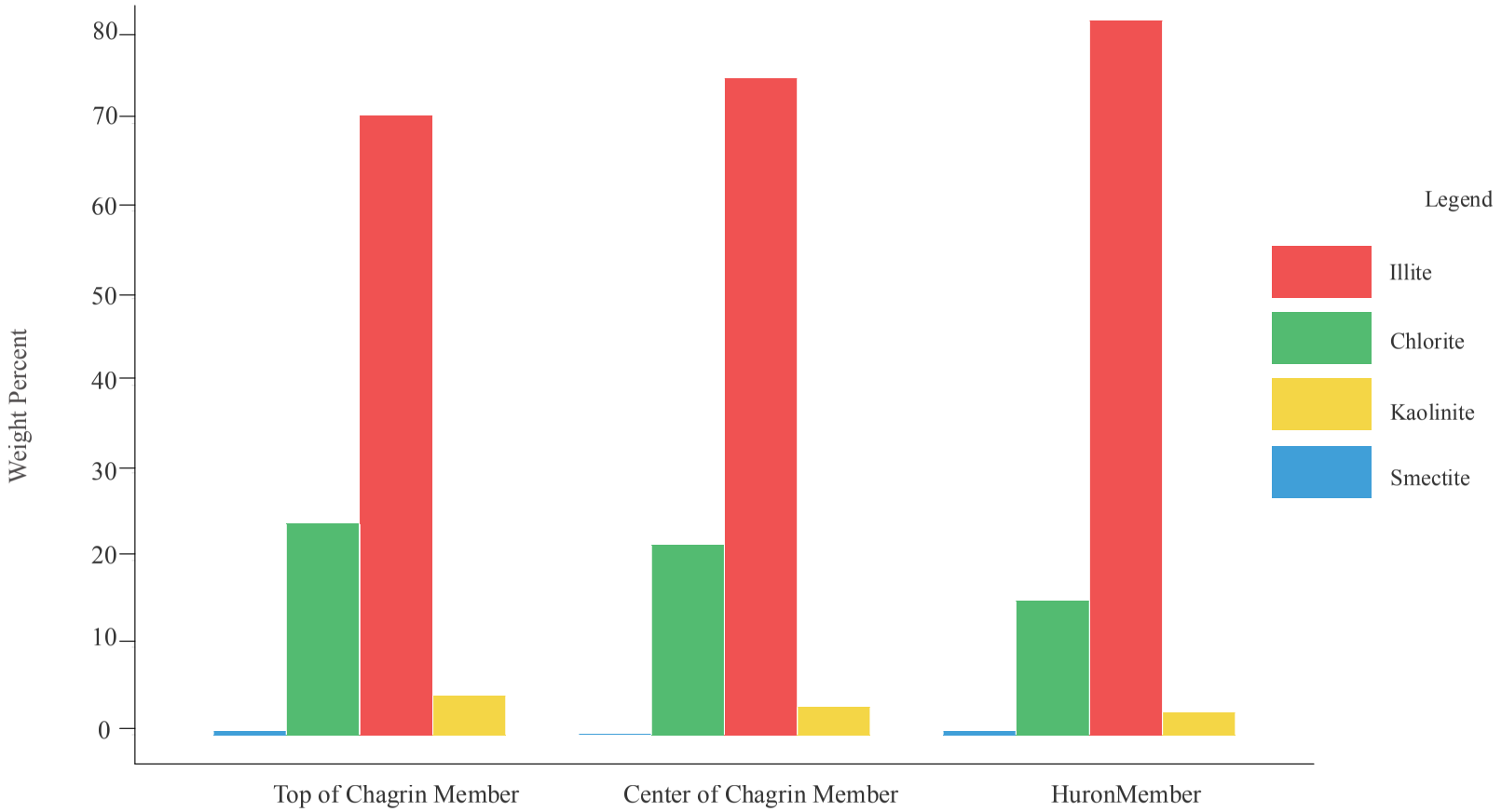

Figure 3.3. Histogram showing average clay mineral abundances from each of the sampling horizons in the study.

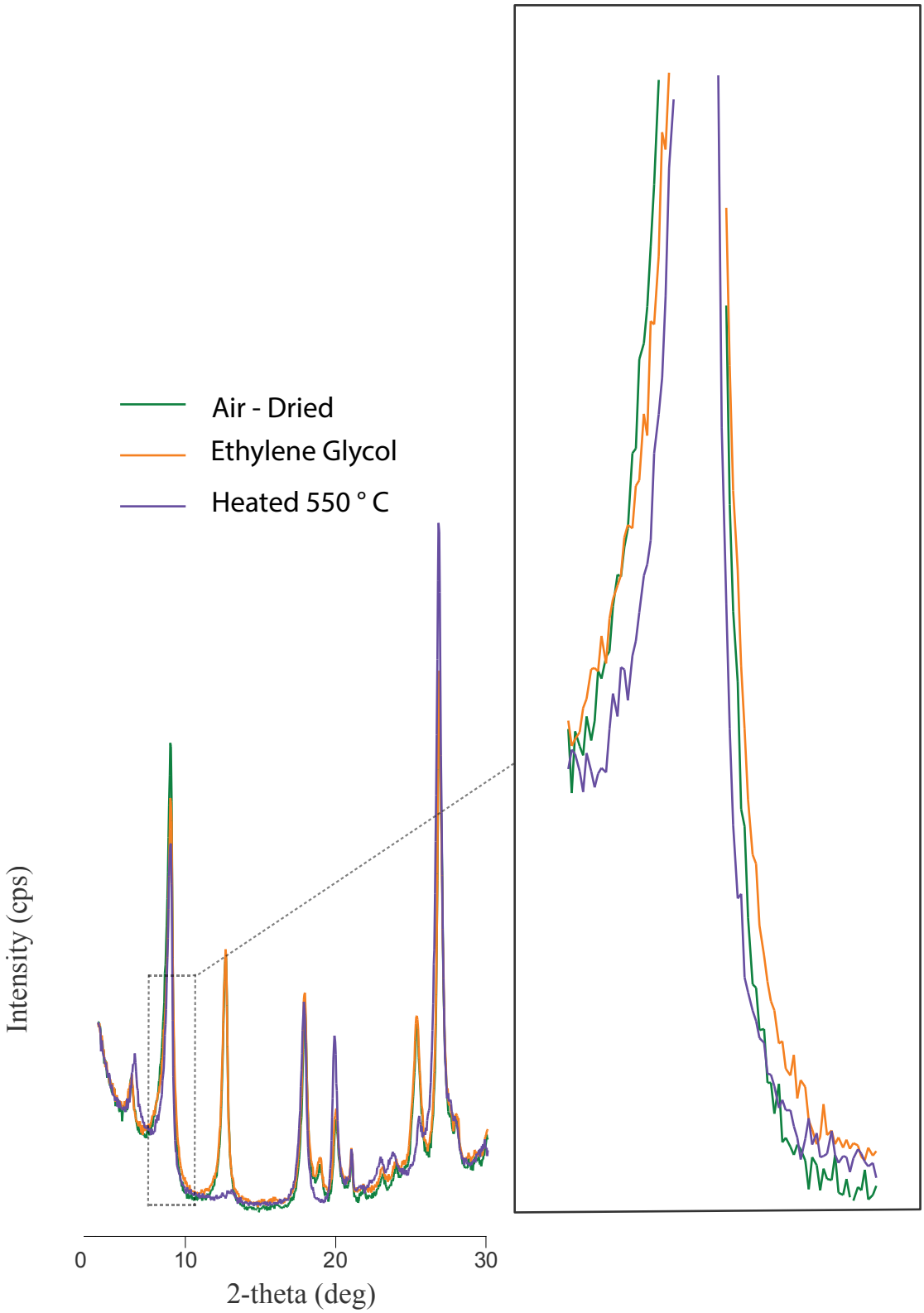

Figure 3.4. Illustration showing an example of small change in peak breadth between air-dried, ethylene glycol treated, and heat-treated patterns.

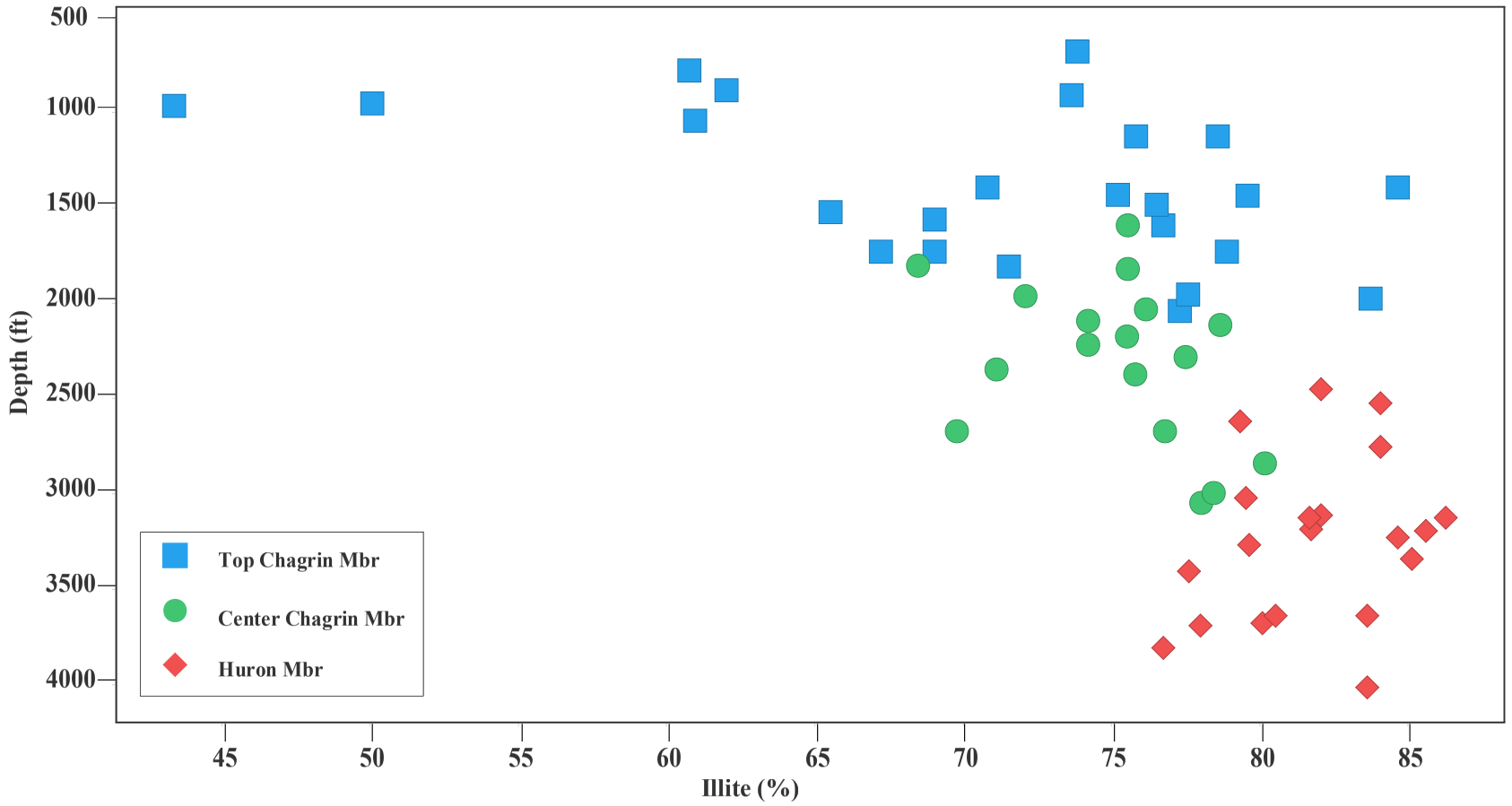

Figure 3.5. Abundance of illite plotted vs. depth for all wells in the study.

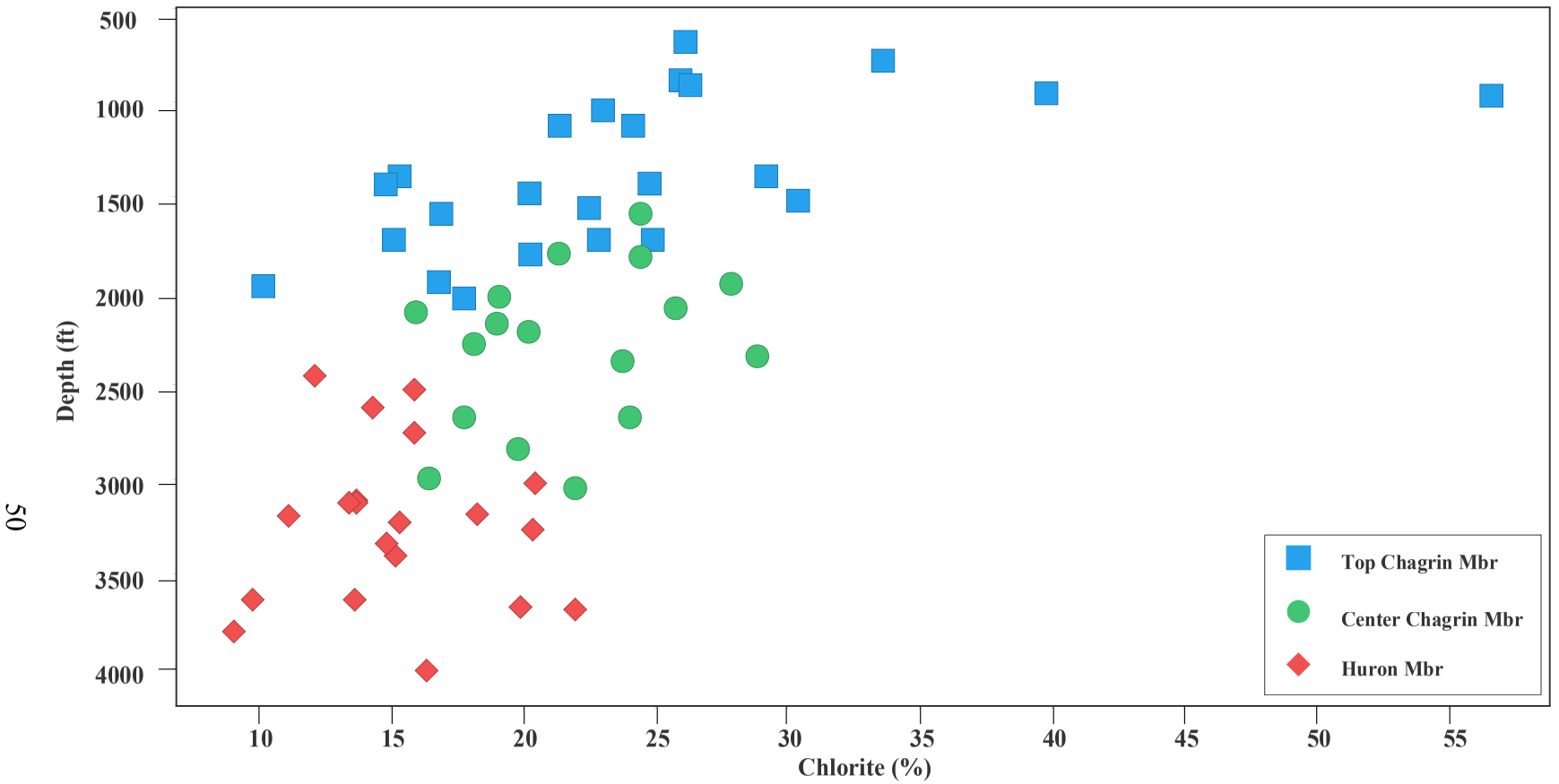

Figure 3.6. Abundance of chlorite plotted vs. depth for all wells in the study.

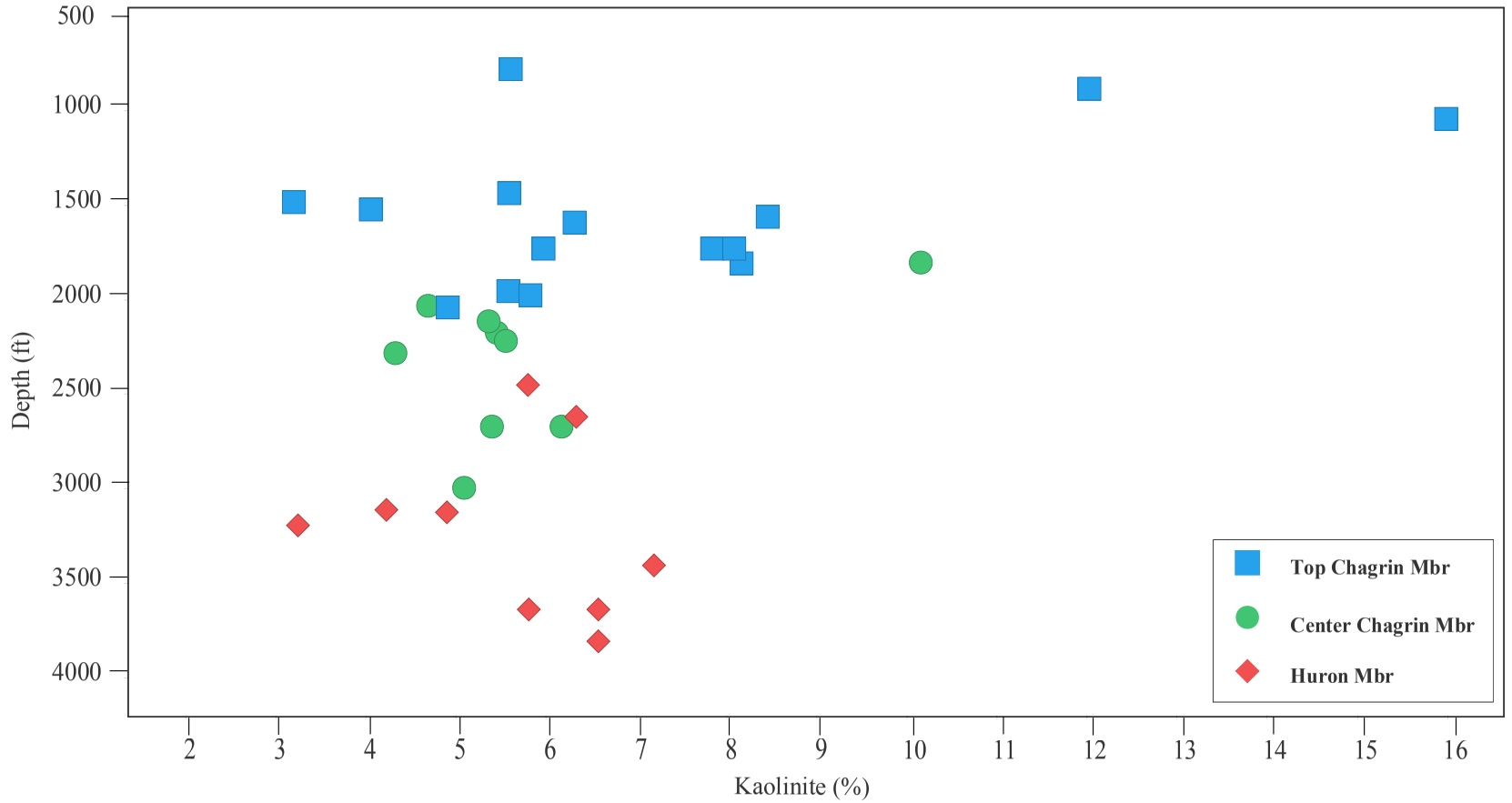

Figure 3.7. Abundance of kaolinite plotted vs. depth for all well in the study.

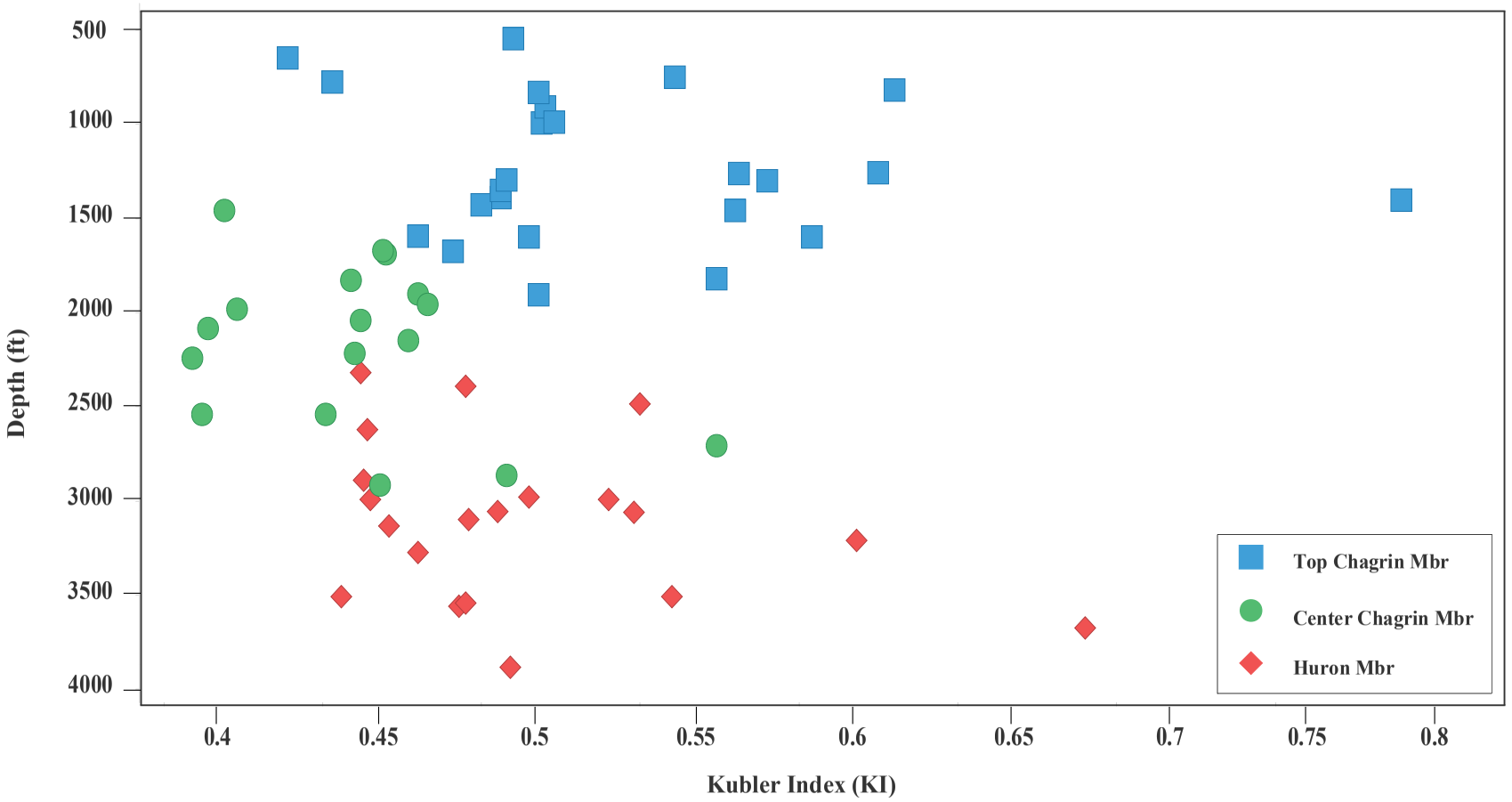

Figure 3.8. Kübler Indices plotted vs. depth for all wells in the study.

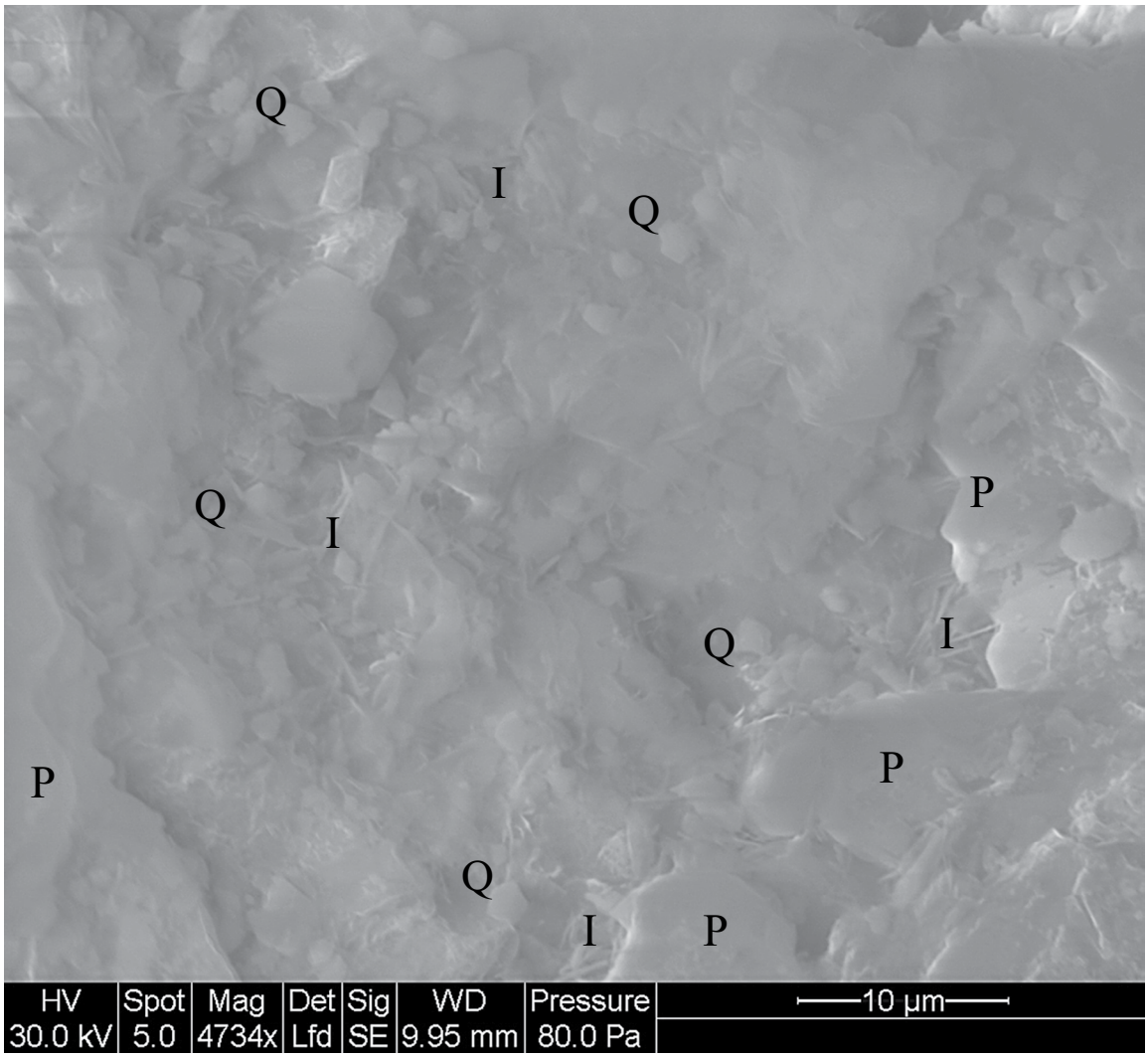

Figure 3.9. ESEM micrograph showing identification of minerals from a 4,734x magnified image, sample 1724-1 in Columbiana County, Ohio. P = Plagioclase, Q = Quartz, I = Illite.

A)

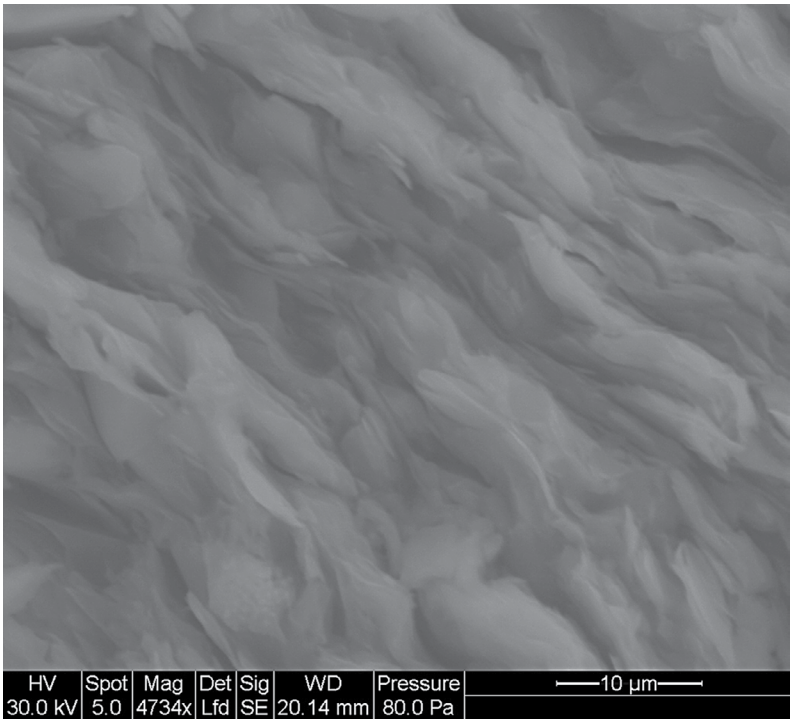

B)

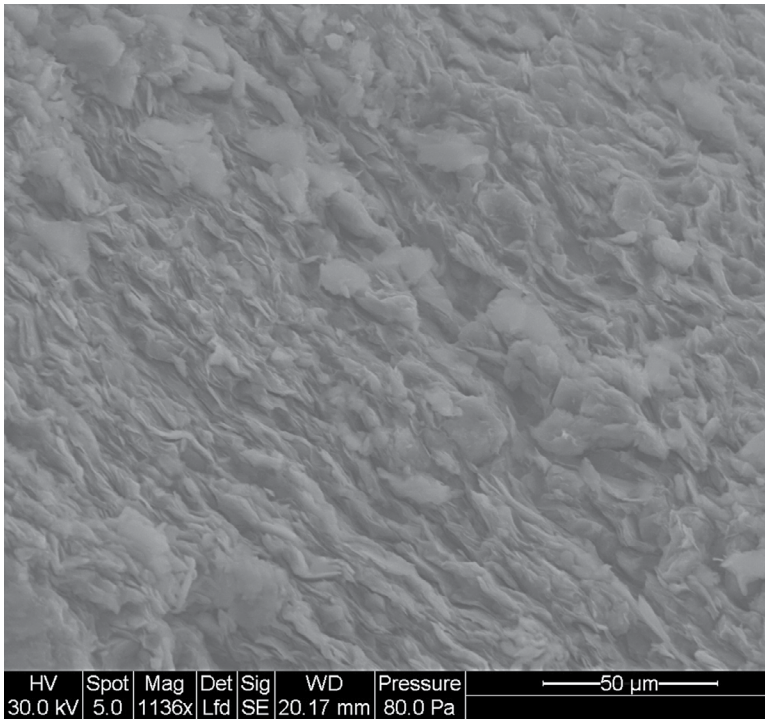

Figure 3.10. ESEM images of detrital clays from sample 1069-2 in Harrison County, Ohio. A) 4,734x magnification. B) 1136x magnification.

In all samples analyzed, an increase in the abundance of authigenic clay minerals can be identified with increased depth (Figure 3.11). The authigenic clays are seen by the increase in wispy, hair like structures between massive detrital grains and also rimming both authigenic and detrital grains. Authigenic quartz also seemed to generally increase with depth, as seen by the increase in smaller anhedral shaped grains forming in clusters. EDX values were not included in the results of this study due to two reasons; 1) The operator manual for chemical quantification calls for a flat polished surface, which was not feasible with samples obtained in this study, and 2) the difficulty in pinpointing authigenic clays for elemental analysis.

3.4 Total Organic Carbon (TOC)

The TOC content calculated from the total carbon (TC) and total inorganic carbon (TIC) analyses are presented in Appendix F, and summarized in table 3.1 The TOC values from the top of the Chagrin Shale Member range between .09% and 1.46% across all counties in the project area, with an average of 0.3%. The magnitude of the counties' average TOC values for the top of the Chagrin Shale Member are in the order of Belmont > Columbiana > Tuscarawas > Guernsey = Harrison > Jefferson > Carroll > Stark. The TOC values for the center of the Chagrin Shale Member range between 0.17% and 0.95% across all counties, with an average of 0.4%. The magnitude of the counties' average TOC values for the center of the Chagrin Shale Member are in the order of Tuscarawas > Stark > Guernsey > Columbiana > Jefferson > Carroll > Belmont > Harrison. Lastly, the TOC values for the Huron Shale Member across all counties of interest range from 0.51% to 2.82%, with an average of 0.95%. The magnitude of the counties' average TOC values for Huron Shale Member are in the order of Stark > Guernsey > Tuscarawas > Harrison > Columbiana > Belmont > Carroll > Jefferson. On average, TOC values increased with

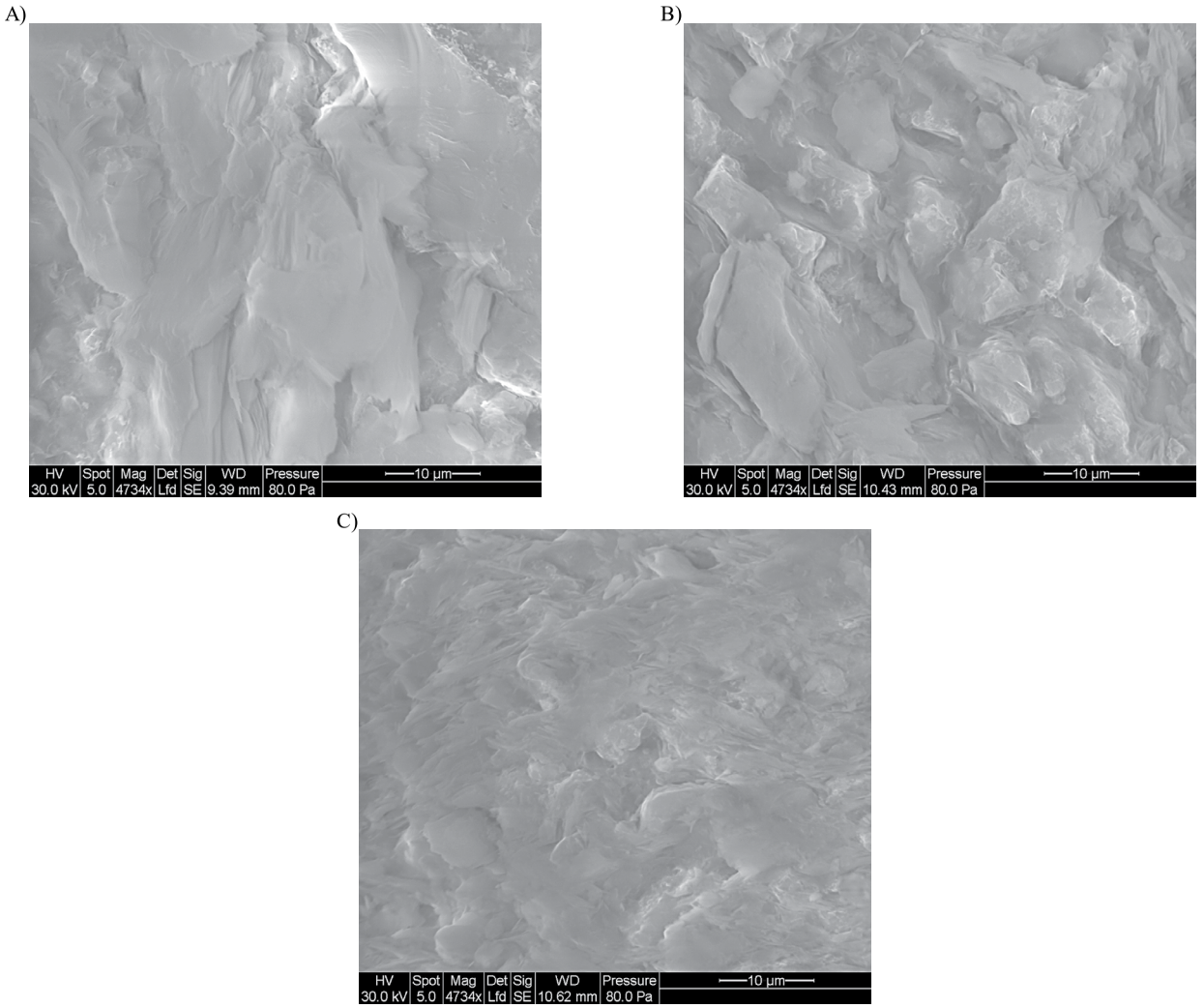

Figure 3.11. ESEM images showing increase in frail crystal structures with depth from well 2094 in Carroll County, Ohio. A) 2094-1. B) 2094-2. C) 2094-3. All images captured at 4,734x magnification.

Table 3.1 Average %TOC values

	Chagrin Shale Member Top	Chagrin Shale Member Center	Huron Shale Member
All Counties	0.30	0.40	0.95
Stark	0.17	0.61	1.78
Columbiana	0.32	0.33	0.89
Carroll	0.19	0.28	0.48
Tuscarawas	0.30	0.62	1.02
Guernsey	0.29	0.49	1.32
Belmont	0.63	0.26	0.65
Jefferson	0.23	0.31	0.46
Harrison	0.29	0.25	0.94

depth within each well (Figure 3.12), but did not show any trend in variance from west to east across the study area (Figure 3.13).

3.5 Core Description

The length of core from well 34121222550000 in Noble County, Ohio was examined and described to gain insight on the sampling intervals in an undisturbed state. This analysis of core is important to help understand differences in depositional environment at different sampling intervals. The intervals available for viewing included from 1,750 feet to 2,084 feet, 3,285 feet to 3,446 feet, and 3,456 feet to 3,464 feet, which includes both the Chagrin and Huron Shale Members of the Ohio Shale. The interval from 2,084 feet to 3,285 feet was missing for an unknown reason. The small missing interval from 3,446 feet to 3,456 feet was located within part of the Huron Member high in organic matter, as could be seen by the gamma ray log. It was reportedly taken by a private company to perform reservoir analyses.

The majority of the core through the Ohio Shale ranged between Munsell Color values of medium gray (N4 to N5) to light gray (N6 to N7). Well-sorted, fine grains dominated the entire length of the core, with darker colors usually being composed of slightly finer sized grains. Bedding ranged from massive in some areas to < 1 inch and fissile in others. Bioturbation was clearly identifiable in several intervals by the vertical swirling of light and darker gray sediments, and some sort of fossilized material or carbonate deposits that reacted to dilute hydrochloric acid was usually identified in these areas.

Much darker, very fine-grained sediments dominated the interval of core available through the Huron Member. No fossils, sedimentary structures, or bedding were able to be seen throughout this interval. Colors ranged from Olive Grey (N4, 5Y 4/1) to nearly

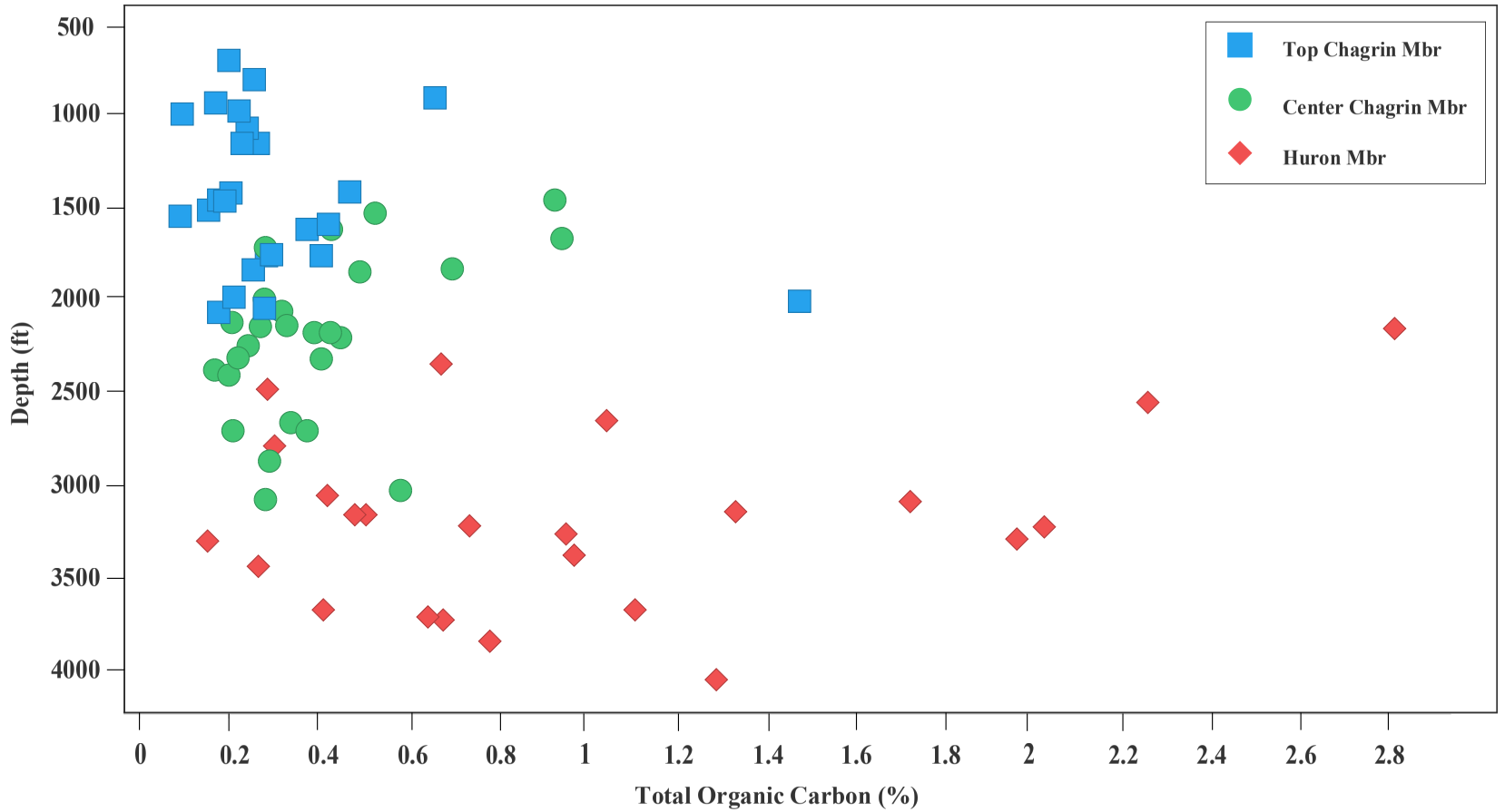

Figure 3.12. Total organic carbon (%) plotted vs. depth for all wells in the study.

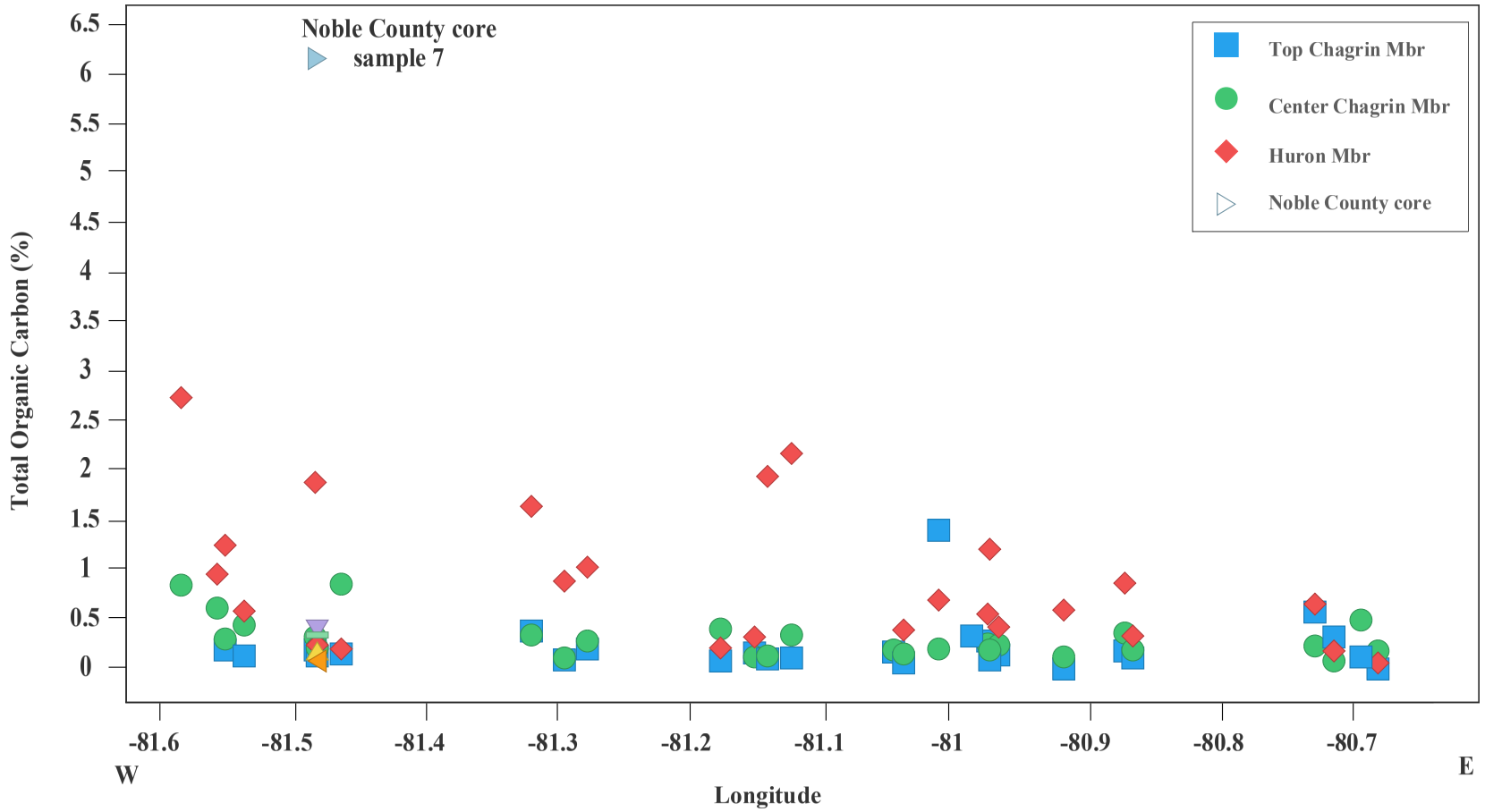

Figure 3.13. Total organic carbon (%) plotted vs. longitude to show variation across the study area.

purely black (N1) in the interval from 3,285’ to 3,463’, but returned to light grey (N5-N6) at 3,464’ through the remainder of the available sample. A graphic description is provided in Appendix G.

CHAPTER IV

DISCUSSION

Illite was the dominant clay mineral in all of the samples analyzed for all of the sampled formation members. This was followed by chlorite and kaolinite (Figure 3.3). Smectite was identified in three of the samples analyzed, including 1373-1 in Tuscarawas County, and 0102-1 and 0129-3 in Belmont County. The high illitic content compared to other minerals present could be influenced partially by each of two factors.

The first factor could be the original sediment source. Biscaye (1965) studied clay mineral assemblages in recent sediments from multiple ocean basins in order to identify trends in sediment source and clay mineral abundance. Illite is widespread in micaceous continental rock types of eastern North America, is present in many soils and glacial tills, and is resistant to chemical weathering (Biscaye, 1965). This phenomenon led to the observation of high illite abundances and low variance in areas with mid latitude continental sediment sources compared to tropical sources.

The second factor affecting the abundance of illite in the sample is the thermal maturation of the unit. Expandable clays (smectite) undergo diagenesis and are converted to illitic non-expandable clays (Jiang, 2012; Pollastro, 1993; Burtner and Warner, 1986) with increasing pressure (P) and temperature (T). The following reaction by Lynch et al., (1997) explains this diagenesis: 10.93 I/S (20%I) + 0.91 discrete illite + 2.75 kaolinite + 0.86 potassium feldspar + 1.46 plagioclase feldspar + 2.11 Al_2O_3 + 2.66 K_2O → 12.59 I/S (85%I) + 0.27 chlorite + 3.16 quartz + 1.98 albite + 4.70 SiO_2. The average increase of illite with depth gives evidence that, although most of the variance in illite may be from

detrital inputs, there is a correlation with increased illite abundances with increased P and T.

Supporting evidence for authigenic illite growth is seen in ESEM imaging of the samples analyzed in the study by the increase in fragile, hair–like structures that are too frail to withstand the pressures of compaction (Figure 3.11). Specific clay mineral identification in shales via ESEM imaging is very difficult to accomplish due to the small size of authigenic clays in shales (Personal Communication, Mansour Rahmatian, Core Mineralogy Labs, 2015). Two main reasons for this morphology are the small pore sizes in shale, limiting clay mineral authigenesis to the bounds of the pore itself, and also the length of time the mineral is exposed to fluids containing the K^+ that illite needs to grow (Personal Communication, Mansour Rahmatian, Core Mineralogy Labs, 2015).Because of the extremely small pore spaces in shales, clay minerals are not permitted to grow as large as they do in sandstones exhibiting large pore spaces. In a sandstone, clays can stay saturated in these fluids during compaction due to the larger pore spaces, while almost any compression on a shale leads to a more rapid expulsion of the fluids and ceases authigenesis (Personal Communication, Mansour Rahmatian, Core Mineralogy Labs, 2015). These factors explain the extremely small illite crystals imaged in this study.

Milici and Swezey (2006) analyzed the total petroleum system comprising the Ohio Shale, and noted that oil occurs west of the $\%R_0$ 0.6 boundary line (Figure 4.1) from dispersed vitrinite reflectance values. They postulate that the 0.6 line boundary could be moved 20 to 30 miles west, which is supported by comparison of the Milici and Swezey (2006) map to observed I/S ratios' in this study (Figure 4.1). As can be easily seen, the vast majority of the study area lays to the west of the $\%R_0$ 0.6 boundary and contains I/S ratio values that correspond to the gas generation window, or contain > 75% illite layers. Typically, the oil generation window is thought to occur at $\%R_0$ values between 0.6 and 2, and the gas window between $\%R_0$ values 2 and 3 (Abad, 2007). In terms of I/S

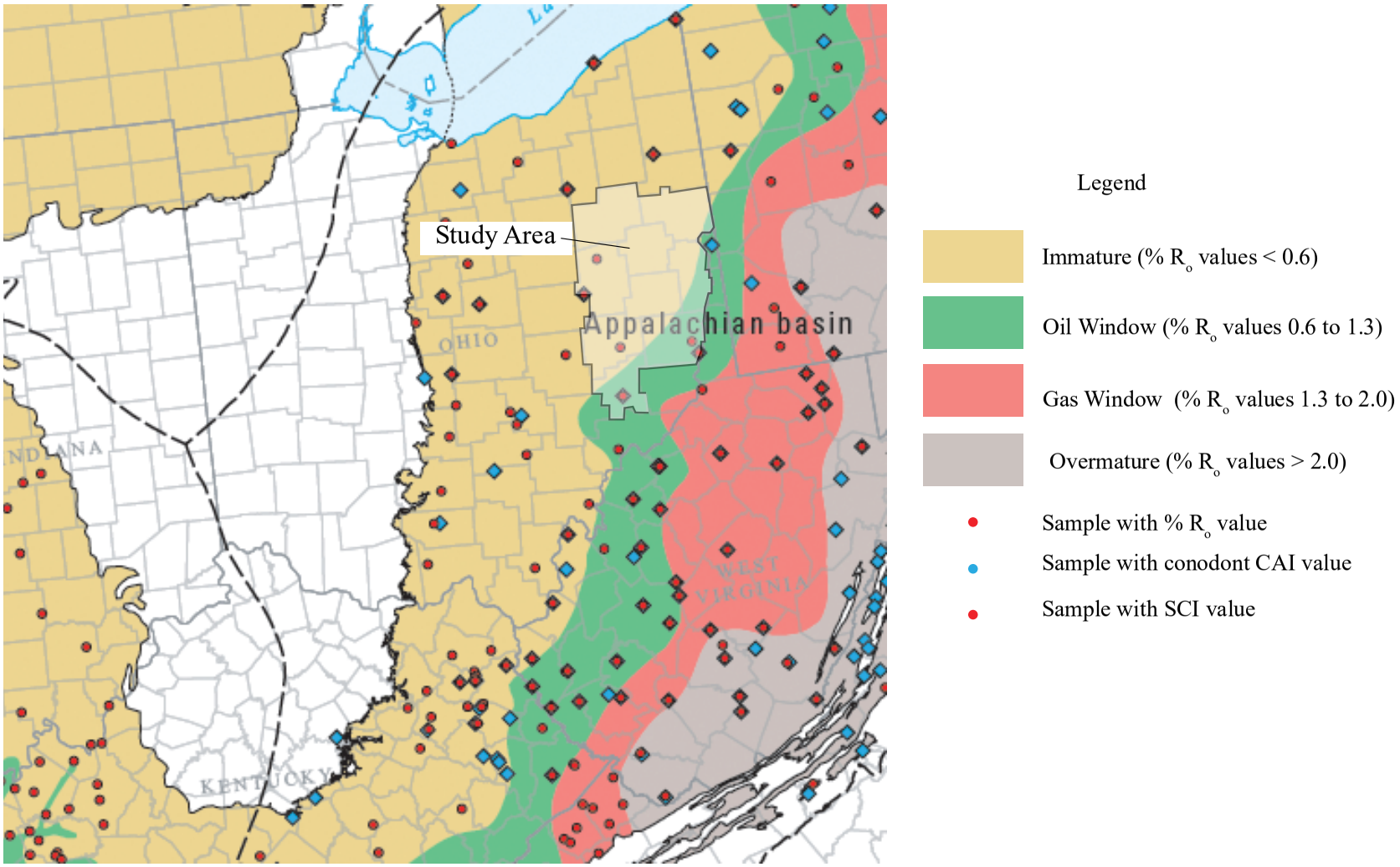

Figure 4.1. Map comparing the location of the study area to source rock maturity estimations interpreted from % R_o values, conodont coloration index (CAI) values, and spore coloration index (SCI) values (Milici and Swezey, 2006). It is recommended that the immature/oil window boundary be moved west to include the study area.

expandability, however, the oil generation window is thought to begin where I/S minerals transition from R=0 to R=1, or a change from ~50 % expandable material to 80 % non - expandable material (Pollastro, 1993). Furthermore, the transition from the oil window to the gas window is thought to occur near the change from R=2 to R=3, or when illite constitutes > 75 % of the layers within the mixed layer I/S material (Pollastro, 1993).

Vitrinite reflectance ($\%R_0$) is one of the most commonly used parameters for estimating thermal maturity of shales and other sedimentary rocks containing organic matter (Milici and Swezey, 2006). The reader should be aware that although the two systems use a similar abbreviation, vitrinite reflectance ($\%R_0$) and Reichweite Notation (R) represent different measurements. Several studies (Laughrey 2012; Raymond and Murchison, 1991; Milici and Swezey, 2006) noticed anomalously low $\%R_0$ values for Devonian black shale units and other similar age shale plays across the globe. These low $\%R_0$ values are caused by increased concentration of alginite, which suppresses the reflection of vitrinite and leads to low $\%R_0$ values (Lo, 1993; Raymond and Murchison, 1991). While it was previously thought that the Upper Devonian Shales of Ohio were immature with respect to generation of natural gas (Milici and Swezey, 2006), the clay mineral composition and Kübler indices' results from the present study suggest that the entire section of Upper Devonian Ohio Shale strata were previously heated into the gas window. The only data inconsistent with this interpretation are the three samples exhibiting detectable amounts of mixed layer clay (sample #'s 1373-1, 0102-1, 0102-3). However, all three of those samples exhibited R1 to R2 ordering, which places them somewhere in the oil window. Further evidence supporting this level of thermal maturity for the Ohio Shale can be seen in the Kübler index values measured in º 2Ɵ on the illite peak in the air-dried state (Appendix E). The range of crystallinity values between ~ 0.4 and 0.6 relate to temperatures above 100 degrees Celsius, vitrinite reflectance values greater than ~ 0.6% R0, and illite percentages of I/S minerals greater than 80% (Figure

Metapelitic zone (depth, km)	Temperature (°C)	KI (Δ°2Θ)	% illite in I/S	TEM mean illite crystallite thickness (Å)	Illite-muscovite polytype	Typical pelitic lithologies	Characteristic microfabrics	Metamorphic facies	Fluid zone	Maturation stages	Vitrinite reflectance Rr%	Conodont alteration index (CAI)
Shallow diagenetic zone										Diagenesis		1
3.5-4	~100	~1.00	60-80		$1M_d$ (1M?)	shale/ mudstone		zeolite	HHC		0.50	
Deep diagenetic zone							bedding-parallel (S_0)			Catagenesis	1.35	2 3
6.5-8	~200	0.42	~90	200							2.00	
Low anchizone					$2M_1$ (3T)		crenulated (S_0)					4
		0.30	95	400		slate	slaty	prehnite-pumpellyte	CH_4	Metagenesis	3.00	
High anchizone							cleavage (S_1)					5
10-12	~300	0.25	>99	500							4.00	5.5
Epizone					$2M_1$ (3T)	slate (phyllite)	(S_{1+})	greenschist	H_2O			

Figure 4.2. Kübler indices compared to other common forms of thermal maturity indicators. Included is the relation of illite crystallinity to % illite and to kerogen maturation (Figure from Abad 2007). Red lines indicate the range in which samples from this study are located.

4.2). A future study investigating changes in clay mineralogy at more closely spaced intervals over a greater range of depth to include overlying strata that are less thermally mature would be advantageous. The completion of this more detailed well profile would potentially characterize the transition from expandable to more non-expandable mixed layer clays with inreased burial depth in the study area, rather than only identifying the presence of already matured, mostly non-expandable mixed layer clays.

TOC and illite abundance generally increased with depth (Figure 4.3), but each for different reasons. The increase in TOC with depth is influenced by the conditions present at the time of deposition rather than by diagenetic changes in clay minerals with depth. The grey shales and siltstones of the Chagrin Shale Member were deposited on the western slope of the Catskill Delta as turbidites, whereas the Huron Shale Member is thought to have been deposited in nearly 700 ft of water, experiencing anoxic to near anoxic bottom waters which aids in the preservation of organic material (Broadhead et al., 1982).

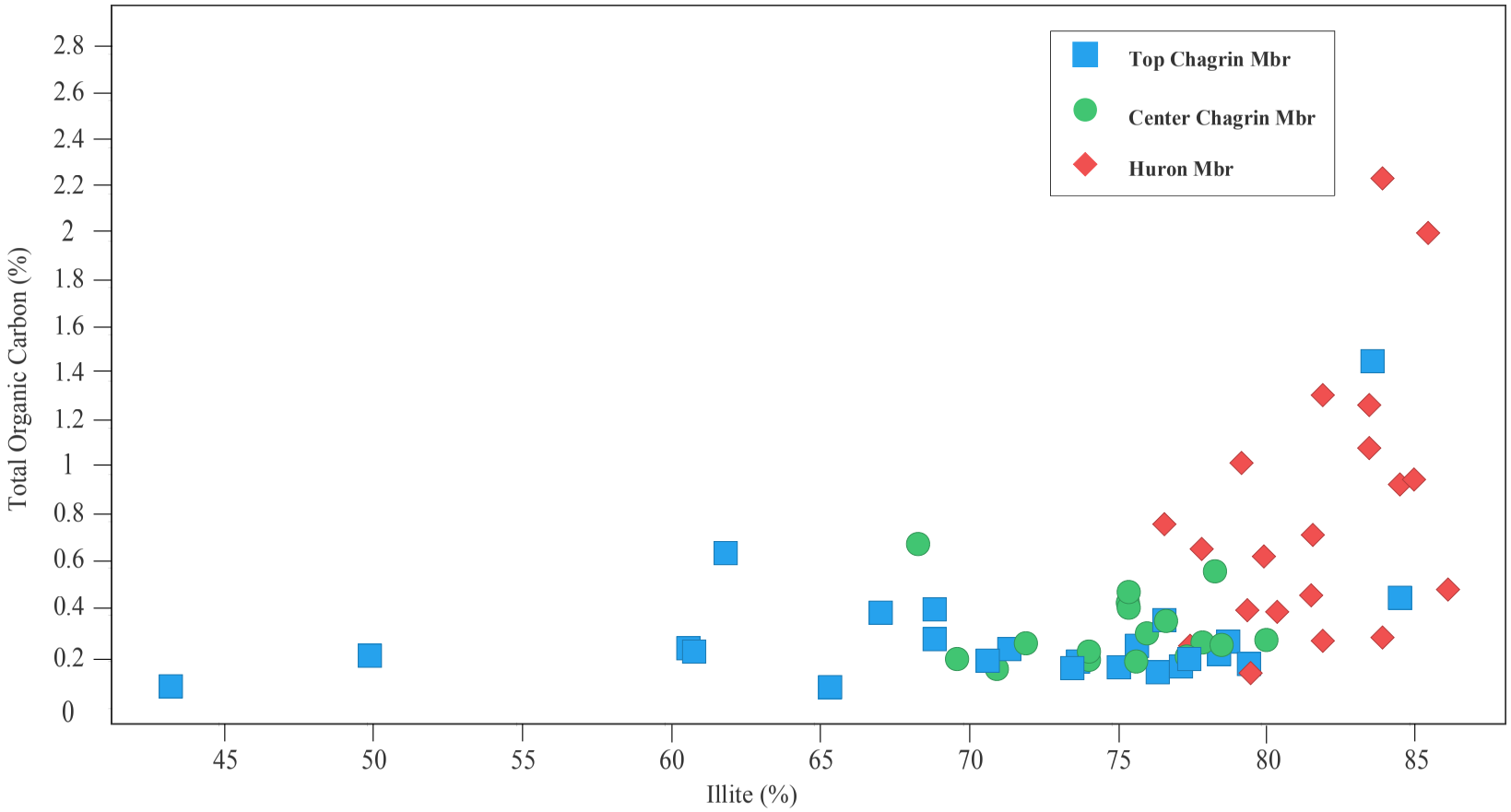

Figure 4.3. Total organic carbon (%) plotted vs. the abundance of illite for all wells in the study.

CHAPTER V

CONCLUSIONS

Total organic carbon, bulk mineralogy, clay fraction mineralogy, and Kübler indices measurements were made on samples from 3 different horizons over an eight-county study area in an attempt to characterize the thermal maturity of Upper Devonian shales in Ohio. The results from this study do not support the current placement of the immature/ mature line with respect to oil generation from previous studies (Milici and Swezey, 2006; Rowan, 2006) which are based on vitrinite reflectance values ($\%R_0$). Milici and Swezey (2006) state that hydrocarbons sourced from Upper Devonian strata are found west of the supposed boundary between immature and mature source rocks with respect to hydrocarbon generation. The occurences of oil west of the boundary (Milici and Swezey, 2006) support the findings in this study, which indicate that the thermal maturity of Upper Devonian black and grey shales and siltstones within the Appalachian Basin in Ohio are more accurately characterized by the analysis of clay mineralogy rather than by vitrinite reflectance. It is recommended that the boundary be moved far enough west to at least include the study area investigated. From the data and findings presented in this study, the following conclusions can also be made:

- Illite was the most dominant clay mineral in all of the samples analyzed, followed by chlorite (Figure 3.3). Kaolinite was present in low abundances in some wells and not present in others, while expandable clays were only detected in three samples. The majority of illite present is detrital in origin, although authigenesis is thought to have occurred in minor amounts. This interpretation is supported by

the low abundance of authigenic clay minerals compared to the amount of detrital material identified by ESEM imaging (Figures 3.9, 3.10, 3.11) and is explained by the highly illitic sediment source (Biscaye, 1965).

- Illite content increased with depth, while chlorite content decreased with depth. If kaolinite was present in a well column, the abundance decreased with depth, and usually disappeared in the Huron Shale Member.
- Variations in TOC values are controlled by depositional conditions and are not related to clay mineral diagenesis. The Huron Shale Member was deposited in deeper, more anoxic water than the Chagrin Shale Member, which aids in the preservation of organic carbon (Broadhead et al., 1982). The Chagrin Shale Member was deposited in more shallow water closer to the sediment source and was prone to turbidite flows, resulting in the mixing of the water column and addition of oxygen back into bottom waters (Broadhead et al., 1982).
- Of the trace of I/S that is seen to be present by changes in peak breadth (Figure 3.4), all instances are R3 and contain > ~ 90 % illite layers.
- The Upper Devonian black and grey shales and siltstones of the Chagrin and Huron Shale Members of the Ohio Shale have experienced thermal conditions placing them in the hydrocarbon generation window, as opposed to previous estimates made by dispersed vitrinite reflectance values ($\%R_0$). This conclusion is evidenced by the lack of widespread expandable I/S minerals and by the Kübler index values recorded, which both indicate thermally mature conditions with respect to the oil and gas window.

REFERENCES

Abad, I., 2007, Physical meaning and applications of the illite Kübler index: measuring reaction progress in low-grade metamorphism: Diagenesis and Low-Temperature Metamorphism, Theory, Methods and Regional Aspects, Seminarios.Sociedad Espanola: Sociedad Espanola Mineralogia, p. 53-64.

Altaner, S.P., and Bethke, C.M., 1988, Interlayer order in illite/smectite: American Mineralogist, v. 73, p. 766-774.

Altaner, S.P., and Ylagan, R.F., 1997, Comparison of structural models of mixed-layer illite/smectite and reaction mechanisms of smectite illitization: Clays and Clay Minerals, v. 45, p. 517-533.

Bethke, C.M., and Altaner, S., 1986, Layer-by-layer mechanism of smectite illitization and application to a new rate law: Clays and Clay Minerals, v. 34, p. 136.

Biscaye, P.E., 1965, Mineralogy and sedimentation of recent deep-sea clay in the Atlantic Ocean and adjacent seas and oceans: Geological Society of America Bulletin, v. 76, p. 803-832.

Broadhead, R.F., Kepferle, R.C., and Potter, P.E., 1982, Stratigraphic and sedimentologic controls of gas in shale--example from Upper Devonian of northern Ohio: AAPG Bulletin, v. 66, p. 10-27.

Burtner, R.L., and Warner, M.A., 1986, Relationship between illite/smectite diagenesis and hydrocarbon generation in Lower Cretaceous Mowry and Skull Creek shales of the northern Rocky Mountain area: Clays and Clay Minerals, v. 34, p. 390-402.

Chengzao, J., Zheng, M., and Zhang, Y., 2012, Unconventional hydrocarbon resources in China and the prospect of exploration and development: Petroleum Exploration and Development, v. 39, p. 139-146.

Dewing, K., and Sanei, H., 2009, Analysis of large thermal maturity datasets: examples from the Canadian Arctic Islands: International Journal of Coal Geology, v. 77, p. 436-448.

Faill, R.T., 1997, A geologic history of the north-central Appalachians; Part 1, Orogenesis from the Mesoproterozoic through the Taconic Orogeny: American Journal of Science, v. 297, p. 551-619.

Foscolos, A., Powell, T., and Gunther, P., 1976, The use of clay minerals and inorganic and organic geochemical indicators for evaluating the degree of diagenesis and oil generating potential of shales: Geochimica Et Cosmochimica Acta, v. 40, p. 953-966.

Gray, J., Struble, R., Carlton, R., Hodges, D., Honeycutt, F., Kingsbury, R., Knapp, N., Majchszak, F., and Stith, D., 1982, An integrated study of the Devonian-age black shales in eastern Ohio: US Department of Energy: Special Publication.

Hoover, K.V., 1960, Devonian-Mississippian shale sequence in Ohio: United States: Department of Natural Resources,Columbus, OH.

Hosterman, J.W., and Whitlow, S., 1981, Clay mineralogy of Devonian shales in the Appalachian Basin: U.S. Geological Survey Professional Paper 1298, v. 81, p 30.

Huang, W., Longo, J.M., and Pevear, D.R., 1993, An experimentally derived kinetic model for smectite-to-illite conversion and its use as a geothermometer: Clays and Clay Minerals, v. 41, p. 162-162.

Iacoviello, F., Giorgetti, G., Nieto, F., and Memmi, I.T., 2012, Evolution with depth from detrital to authigenic smectites in sediments from AND-2A drill core (McMurdo Sound, Antarctica): Clay Minerals, v. 47, p. 481-498.

Jiang, S., 2012, Clay Minerals from the Perspective of Oil and Gas Exploration: Clay Minerals in Nature - Their Characterization, Modification, and Application, Chapter 2.

Johns, W.D., 1979, Clay mineral catalysis and petroleum generation: Annual Review of Earth and Planetary Sciences, v. 7, p. 183.

Kargbo, D.M., Wilhelm, R.G., and Campbell, D.J., 2010, Natural gas plays in the Marcellus shale: Challenges and potential opportunities: Environmental Science & Technology, v. 44, p. 5679-5684.

Kuuskraa, V.A., Koperna, G., Schmoker, J.W., and Quinn, J.C., 1998, Barnett Shale rising star in Fort Worth basin: Oil and Gas Journal, v. 96, p. 67-76.

Lash, G.G., and Engelder, T., 2011, Thickness trends and sequence stratigraphy of the Middle Devonian Marcellus Formation, Appalachian Basin: Implications for Acadian foreland basin evolution: AAPG Bulletin, v. 95, p. 61-103.

Laughrey, C.D., 2012, Thermal maturity of Devonian black shale-gas reservoirs, northwestern Pennsylvania–evidence from organic petrology, geochemistry, and mineralogy, in Abstracts with Programs, AAPG Annual Eastern Conf., Pittsburgh, PA.

Leventhal, J.S., and Hosterman, J.W., 1982, Chemical and mineralogical analysis of Devonian black-shale samples from Martin County, Kentucky; Carroll and Washington counties, Ohio; Wise County, Virginia; and Overton County, Tennessee, USA: Chemical Geology, v. 37, p. 239-264.

Lynch, F.L., Mack, L.E., and Land, L.S., 1997, Burial diagenesis of illite/smectite in shales and the origins of authigenic quartz and secondary porosity in sandstones: Geochimica Et Cosmochimica Acta, v. 61, p. 1995-2006.

Lo, H., 1993, Correction criteria for the suppression of vitrinite reflectance in hydrogen-rich kerogens: preliminary guidelines: Organic Geochemistry, v. 20, p. 653-657.

Milici, R.C., and Swezey, C., 2006, Assessment of Appalachian basin oil and gas resources: Devonian shale-middle and upper paleozoic total petroleum system: US Department of the Interior, US Geological Survey, Open-File Rreport Series 2006-1237.

Moore, D. M., and Reynolds, R.C., 1997, X-Ray Diffraction and the Identification and Analysis of Clay Minerals: New York, Oxford University Press, Second Edidtion, 378 p.

Mosser-Ruck, R., Devineau, K., Charpentier, D., and Cathelineau, M., 2005, Effects of ethylene glycol saturation protocols on XRD patterns: a critical review and discussion: Clays and Clay Minerals, v. 53, p. 631-638.

Pollastro, R.M., 1993, Considerations and applications of the illite/smectite geothermometer in hydrocarbon-bearing rocks of Miocene to Mississippian age: Clays and Clay Minerals, v. 41, p. 119-119.

Potter, P.E., Maynard, J.B., and Pryor, W.A., 1980, Final Report of Special Geological, Geochemical, and Petrological Studies of the Devonian Shales in the Appalachian Basin, University of Cincinnati.

Quinlan, G.M., and Beaumont, C., 1984, Appalachian thrusting, lithospheric flexure, and the Paleozoic stratigraphy of the eastern interior of North America: Canadian Journal of Earth Sciences, v. 21, p. 973-996.

Raymond, A.C., and Murchison, D.G., 1991, Influence of exinitic macerals on the reflectance of vitrinite in Carboniferous sediments of the Midland Valley of Scotland: Fuel, v. 70, p. 155-161.

Rowan, E.L., 2006, Burial and thermal history of the central Appalachian basin, based on three 2-D models of Ohio, Pennsylvania, and West Virginia: US Department of the Interior, US Geological Survey, Open-File Report Series 2006-1019.

Schwietering, J., 1979, Devonian Shales of Ohio and their Eastern and Southern Equivalents: Morgantown Energy Technology Center, US Department of Energy.

Slucher, E.R., Swinford, E.M., Larsen, G.E., and others, with GIS production and cartography by Powers, D.M., 2006. Bedrock geologic map of Ohio. Ohio Division of Geological Survey Map BG-1, version 6.0, scale 1:500,000.

Welton, J.E., 2003, SEM petrology Atlas: Methods in Exploration Series, 237 pp.

APPENDICES

APPENDIX A

SAMPLING DEPTH CALCULATION

Data used to calculate sampling depths for wells without geophysical logs is listed below. White rows indicate wells that had logs; Grey rows immediately following represent wells which sampling depths were calculated for.

API	Lat	Long	Berea Top	Distance between	Distance	Plunge to Well	Chagrin Top	Chagrin Sample	Huron Sample
			ft amsl	km	ft	degrees	ft amsl	ft amsl	ft amsl
34151245080000	40.70314	-81.57188	324				165	-356	-1052
34151212260000	40.82256	-81.2863	407	27.47	90124.6748	0.000920946	248	-273	-969
34029206650000	40.82309	-81.03695	505				386	-524	-1459
34151211030000	40.95671	-81.11329	489	16.18	53083.9912	-0.000301409	370	-540	-1475
34157216170000	40.36312	-81.30865	-107				-237	-992	-1902
34019220960000	40.50996	-81.02925	-54	28.74	94291.3416	0.000562088	-184	-939	-1849
34067201040000	40.20575	-81.28404	-203				-303	-1248	-2216
34059214560000	40.17564	-81.47139	-187	16.26	53346.4584	0.000299926	-287	-1232	-2200
34067201040000	40.20575	-81.28404	-203				-303	-1248	-2216
34059242210000	40.05787	-81.26694	-429	16.51	54166.6684	-0.004172283	-529	-1474	-2442
34067201040000	40.20575	-81.28404	-203				-303	-1248	-2216
34013202840000	40.11145	-81.14108	-511	16.05	52657.482	-0.005849055	-611	-1556	-2524
34059216690000	39.88778	-81.64371	-439				-784	-1349	-2014
34059214560000	40.17564	-81.47139	-187	35.21	115518.3764	0.002181468	-532	-1097	-1762
34059216690000	39.88778	-81.64371	-439				-784	-1349	-2014
34059242210000	40.05787	-81.26694	-429	37.26	122244.0984	8.18035E-05	-774	-1339	-2004
34067201030000	40.26184	-80.96628	-283				-463	-1504	-2549
34081205350000	40.26476	-80.68574	-609	23.81	78116.8004	-0.004173214	-789	-1830	-2875
34067203390000	40.40572	-80.97788	-197				-290	-860	-1920
34081205120000	40.46614	-80.90922	-170	8.883	29143.70172	0.000926443	-263	-833	-1893
34067203390000	40.40572	-80.97788	-197				-290	-860	-1920
34081203400000	40.40984	-80.85727	-152	10.22	33530.1848	0.001342074	-245	-815	-1875
34151211030000	40.95671	-81.11329	489				370	-540	-1475
34151257670100	40.86885	-81.16673	436	10.75	35269.03	-0.001502734	317	-593	-1528
34157247190000	40.43735	-81.54497	60				1	-594.5	-1408
34157211280000	40.36246	-81.45131	-7	11.5	37729.66	-0.001775789	-66	-661.5	-1475
34157247190000	40.43735	-81.54497	60				1	-594.5	-1408
34157213730000	40.30574	-81.5248	-30	14.73	48326.7732	-0.00186232	-89	-684.5	-1498
34157216170000	40.36312	-81.30865	-107				-237	-992	-1902
34067210690000	40.35149	-81.13134	-182	15.08	49475.0672	-0.001515914	-312	-1067	-1977
34081203400000	40.40984	-80.85727	-152				-245	-815	-1875
34081205390000	40.30955	-80.70643	-525	16.96	55643.0464	-0.006703343	-618	-1188	-2248
34059214560000	40.17564	-81.47139	-187				-287	-1232	-2200
34059214400000	40.0206	-81.53858	-293	18.16	59580.0544	-0.001779117	-393	-1338	-2306
34013202840000	40.11145	-81.14108	-511				-691	-1556	-2524
34013201290000	40.0805	-81.00309	-562	12.23	40124.6732	-0.001271038	-742	-1607	-2575
34013202840000	40.11145	-81.14108	-511				-691	-1556	-2524
34013201080000	39.95128	-80.96452	-826	23.31	76476.3804	-0.004118895	-863	-1871	-2839
34067201030000	40.26184	-80.96628	-283				-463	-1504	-2549
34081205390000	40.30955	-80.70643	-525	22.67	74376.6428	-0.003253698	-705	-1746	-2791
34019210940000	40.70768	-80.9576	221				110	-873	-1891
34029217050000	40.68486	-80.86348	194	8.331	27332.67804	-0.000987828	83	-900	-1918

APPENDIX B

LIST OF SAMPLES

Full list of samples received from the H.R. Collins Lab. Both the target sampling depth and depth of samples taken are listed for each shale member in the study.

County	API	Missing Intervals	ODNR Sample Number	Chagrin Top (1)	Sample Taken	Chagrin Center (2)	Sample Taken	Lower Huron (3)	Sample Taken 2
		ft		ft	ft	ft	ft	ft	ft
Stark	34151211030000	-	1911	679	680-690	1589	1580-1610	2524	2510-2540
	34151245080000	0-1030	3951	908	-	1429	1400-1430	2125	2120-2150
	34151257670100	-	5432	909	910	1819	1820	2670	2660
	34151212260000	1000-3100	2049	839	830-840	1360	-	2056	-
Columbiana	34029206650000	2300-TD	2580	780	770-780	1690	1680-1690	2625	-
	34029217050000	-	5413	1125	1100-1150	2122.5	2150	3229	3200
	34029217240000	-	5487	966	960-990	2114	2100-2130	3266	3250-3300
	34029212560000	-	4362	882	880-900	2032	2030-2040	3187	3180-3190
Tuscarawas	34157211280000	-	2309	1042	1040-1045	1637.5	1635-45	2451	2450-65
	34157213730000	-	2527	950	960-970 (visual lag noted)	1502.5	1500-1510	2316	2310-2320
	34157247190000	-	3959	1209	-	1805.5	1790-1820	2616	2600-2630
	34157216170000	-	2774	1390	1380-1390	2145	2140-2150	3055	3050-3060
Carroll	34019220960000	-	5410	1484	1500	2216	2200	3126	3100-3150
	34019210940000	-	3472	1124	1120-1130	2107	2103-2134	3125	3119-3148
Harrison	34067201040000	-	2389	1430	1420-1418	2375	2410-2440	3343	3340-3370
	34067210690000	-	5443	1435	1400-1450	2283	2250-2300	3193	3150-3200
	34067203390000	2510-4010	3547	1560	1550-1570	2605	-	3665	-
	34067201030000	-	2287	1590	1610-1620	2631	2620-2630, 2630-2640	3676	3660-3690
Jefferson	34081205120000	-	5387	1521	1500-1550	2091	2050-2100	3691	3650-3700
	34081203400000	-	1060	1393	1390-1400	1963	1960-1970	3023	3020-3030
	34081205390000	-	5519	1731	1720-1750	2347	2350	3407	3400
	34081205350000	3700-4041	5474	1955	1950-2000	2996	2950-3000	4041	-
Guernsey	34059214400000	-	2571	1300	1290-1300	2144	2170-2180	3112	3110-3120
	34059214560000	-	2549	2017	2010-2020	2287	2280-2290	3255	3250-3260
	34059242210000	-	5558	1728	1730	2673	2660-2690	3641	3620-3650
Belmont	34013202840000	-	5573	1807	1780-1810 composit	2672	2680	3640	3640
	34013201290000	-	166	1975	1975-1980	2840	2840-2850	3808	3800-3810
	34013201080000	-	40	2039	2027-2042	3047	3042-3059	4015	4005-4020

Depths listed represent depth to sample below the Kelly Bushing

APPENDIX C

BULK XRD DATA

Data used to understand changes in bulk mineralogy between samples. “1” indicates the presence of that mineral in the respective sample. “-” indicates the absence of the mineral in that respective sample.

County	Sample Name	Quartz	Illite	Chlorite	Kaolinite	Albite	Albite, Calcian	Analbite	Anorthite	Anorthite, Sodian	Anorthite (Mn)	Orthoclase	Anorthoclase	Dolomite	Calcite	Pyrite	Arsenopyrite	Marcastie	Siderite	Gypsum	Enstatite
Belmont	0284-1	1	1	1	1	1	-	-	-	-	-	-	-	-	-	-	-	-	-	-	-
Belmont	0284-2	1	1	1	1	1	-	-	-	-	-	-	-	-	-	-	-	-	-	-	-
Belmont	0284-3	1	1	1	1	1	-	-	-	-	-	-	-	-	-	1	-	-	-	-	-
Belmont	0284-22	1	1	1	-	-	1	-	-	-	-	-	-	-	-	-	-	-	-	-	-
Belmont	0108-1	1	1	1	1	1	-	-	-	-	-	-	-	-	-	-	-	-	-	-	-
Belmont	0108-2	1	1	1	1	1	-	-	-	-	-	-	-	-	-	-	-	-	-	-	-
Belmont	0108-3	1	1	1	1	1	-	-	-	-	-	-	-	-	-	1	-	-	-	-	-
Belmont	0108-32	1	1	1	1	1	-	-	-	-	-	-	-	1	-	1	-	-	-	-	-
Belmont	0129-1	1	1	-	1	-	-	-	-	-	-	-	-	-	1	-	-	-	-	-	-
Belmont	0129-2	1	1	1	1	1	-	-	-	-	-	-	-	-	-	1	-	-	-	-	-
Belmont	0129-3	1	1	1	1	1	-	-	-	-	-	-	-	-	1	1	-	-	-	-	-
Belmont	0129-22	1	1	1	1	1	-	-	-	-	-	-	-	-	1	1	-	-	-	-	-
Carroll	2094-1	1	1	-	1	-	1	-	-	-	-	-	1	-	-	-	-	-	-	-	-
Carroll	2094-2	1	1	1	1	1	-	1	-	-	-	-	-	-	-	1	-	-	-	-	-
Carroll	2094-3	1	1	1	1	1	-	1	-	-	-	-	-	-	-	1	-	-	-	-	-
Carroll	2094-22	1	1	1	1	-	-	1	1	-	-	-	-	-	-	-	-	-	-	-	-
Carroll	2096-1	1	1	1	1	1	-	-	-	-	-	-	-	-	-	-	-	-	-	-	-
Carroll	2096-2	1	1	1	1	1	-	-	-	-	-	-	-	-	-	1	-	-	-	-	-
Carroll	2096-3	1	1	1	1	-	-	-	-	1	-	-	-	-	-	-	-	-	-	-	-
Columbiana	1705-1	1	1	1	1	-	1	-	-	-	-	-	-	-	-	-	-	-	-	-	-
Columbiana	1705-2	1	1	1	1	-	1	-	-	-	-	-	-	-	-	1	-	-	-	-	-
Columbiana	1705-3	1	1	1	1	-	1	-	-	-	-	-	-	-	-	1	-	-	-	-	-
Columbiana	1705-22	1	1	1	1	-	1	-	-	-	-	-	-	-	-	1	-	-	-	-	-
Columbiana	1256-1	1	1	-	1	-	1	-	-	-	-	-	-	1	1	-	-	-	-	-	-
Columbiana	1256-2	1	1	1	1	-	1	-	-	-	-	-	-	-	-	1	-	-	-	-	-
Columbiana	1256-3	1	1	1	1	-	1	-	-	-	-	-	-	-	-	1	-	-	-	-	-
Columbiana	1256-22	1	1	1	1	1	-	1	-	-	-	-	-	-	-	1	-	-	-	-	-
Columbiana	0665-1	1	1	1	1	-	1	-	-	1	-	-	-	-	-	-	-	-	-	-	-
Columbiana	0665-2	1	1	1	1	-	1	-	-	-	-	-	-	-	-	1	-	-	-	-	-
Colmbiana	0665-22	1	1	1	1	-	1	-	-	-	-	-	-	-	-	-	-	-	-	-	-
Columbiana	1724-1	1	1	-	1	1	-	-	-	-	-	-	-	-	-	-	-	-	-	-	-
Columbiana	1724-2	1	1	1	1	-	1	-	-	-	-	-	-	-	-	-	-	-	-	-	-
Columbiana	1724-3	1	1	1	1	-	1	1	-	-	-	-	-	-	1	-	-	-	-	-	-
Guernsey	2144-1	1	1	1	1	-	-	-	-	1	-	-	-	-	-	-	-	-	-	-	-
Guernsey	2144-2	1	1	1	1	-	1	-	-	1	-	-	-	-	-	-	-	-	-	1	-
Guernsey	2144-3	1	1	1	1	1	-	-	-	-	-	-	-	-	1	1	-	-	-	-	-
Guernsey	4221-1	1	1	-	1	-	1	-	-	1	-	-	-	-	-	-	-	-	-	-	-
Guernsey	4221-2	1	1	1	1	-	-	-	-	-	-	1	-	-	-	1	-	-	-	-	-
Guernsey	4221-3	1	1	1	1	-	1	-	-	-	-	1	-	-	-	1	-	-	-	-	-
Guernsey	1456-1	1	1	1	1	-	-	1	-	1	-	-	-	-	1	1	-	-	-	-	-
Guernsey	1456-2	1	1	1	-	-	1	-	-	-	1	-	-	-	-	-	-	-	1	-	-
Guernsey	1456-3	1	1	1	1	1	-	-	-	1	-	-	-	-	1	1	-	-	-	1	-
Guernsey	1456-22	1	1	1	1	1	-	-	1	-	-	-	-	-	-	1	-	-	-	-	-
Harrison	0103-1	1	1	-	1	1	-	-	-	-	-	-	-	-	-	-	-	-	-	-	-
Harrison	0103-2	1	1	1	1	1	-	-	-	-	-	-	-	-	-	-	-	-	-	-	-
Harrison	0103-3	1	1	1	1	1	-	-	-	-	-	-	-	1	1	1	-	-	-	-	-
Harrison	0103-32	1	1	1	1	1	-	-	-	-	-	-	-	1	1	1	-	-	-	-	-
Harrison	0339-1	1	1	-	1	-	1	-	-	-	-	-	-	-	-	-	-	-	-	-	-
Harrison	0104-1	1	1	1	1	1	-	-	-	-	-	-	-	-	-	-	-	-	-	-	-
Harrison	0104-2	1	1	1	1	1	-	-	-	-	-	-	-	-	1	-	-	-	-	-	-
Harrison	0104-3	1	1	1	1	1	-	-	-	-	-	-	-	-	-	1	-	-	-	-	-
Harrison	1069-1	1	1	-	1	1	-	-	-	-	-	-	-	1	-	1	-	-	-	-	-
Harrison	1069-2	1	1	1	1	1	-	-	-	-	-	-	-	-	-	1	-	-	-	-	-
Harrison	1069-3	1	1	1	1	1	-	-	-	-	-	-	-	-	-	1	-	-	-	-	-
Harrison	1069-22	1	1	1	1	1	-	-	-	-	-	-	-	-	-	1	-	-	-	-	-
Jefferson	0512-1	1	1	-	1	-	1	-	-	-	1	-	-	-	-	-	-	-	-	-	-
Jefferson	0512-2	1	1	1	1	1	-	-	-	-	1	-	-	-	1	-	-	-	1	-	-
Jefferson	0512-3	1	1	1	-	-	1	-	-	-	1	-	-	-	-	1	-	-	-	-	-
Jefferson	0512-22	1	1	1	1	1	-	-	-	-	-	-	-	-	1	1	-	-	-	-	1
Jefferson	0539-1	1	1	-	1	1	-	-	-	-	-	-	-	-	-	-	-	-	-	-	-
Jefferson	0539-2	1	1	1	1	-	1	-	-	-	-	-	-	1	1	1	-	-	-	-	-
Jefferson	0539-3	1	1	1	1	-	1	-	-	-	-	-	-	-	1	1	-	-	-	-	-
Jefferson	2034-1	1	1	-	1	1	-	-	-	-	-	-	-	-	-	-	-	-	-	-	-
Jefferson	2034-2	1	1	1	1	1	-	-	-	-	-	-	-	-	-	1	-	-	-	-	-
Jefferson	2034-3	1	1	1	1	-	1	-	-	-	-	-	-	-	-	1	-	-	-	1	-
Jefferson	2034-32	1	1	1	1	-	1	-	-	-	-	-	-	-	-	1	-	-	-	1	-
Jefferson	0535-1	1	1	1	1	1	-	-	-	-	-	-	-	-	-	-	-	-	-	-	-
Jefferson	0535-2	1	1	1	1	1	-	-	-	-	-	-	-	-	-	1	-	-	-	-	-
Noble	2255-1	1	1	1	1	1	-	-	-	-	-	-	-	-	-	-	-	-	-	-	-
Noble	2255-2	1	1	1	1	-	-	-	-	-	1	-	-	-	-	-	-	-	-	-	-
Noble	2255-3	1	1	1	1	-	1	-	-	-	-	-	-	-	-	-	-	-	-	-	-
Noble	2255-4	1	1	1	1	-	1	-	-	-	-	-	-	-	-	-	-	-	-	-	-
Noble	2255-5	1	1	-	1	-	1	-	-	-	-	-	-	-	-	-	-	-	-	-	-
Noble	2255-6	1	1	1	1	-	1	-	-	-	-	-	-	-	1	-	-	-	-	-	-
Noble	2255-7	1	1	1	1	-	1	-	1	1	-	-	-	-	-	1	-	-	-	-	-
Noble	2255-8	1	1	1	1	-	1	-	-	-	-	-	1	-	-	-	-	-	-	-	-
Stark	2226-1	1	1	-	1	-	1	-	-	1	-	-	-	-	-	-	-	-	-	-	-
Stark	1103-1	1	1	-	1	1	-	-	-	-	-	-	-	-	1	-	-	-	-	-	-

Stark	1103-2	1	1	1	1	1	-	-	-	-	-	-	-	-	-	1	-	-	-	-	-
Stark	1103-3	1	1	1	1	1	-	1	-	-	-	-	-	-	-	1	-	-	-	-	-
Stark	1103-12	1	1	1	1	-	1	-	-	-	-	-	-	-	-	-	-	-	-	-	-
Stark	1103-32	1	1	1	1	1	-	1	-	-	-	-	-	-	-	1	-	-	-	-	-
Stark	4508-2	1	1	1	1	-	1	-	-	-	-	1	-	-	1		1	-	1	-	-
Stark	4508-3	1	1	1	1	-	1	-	-	-	-	1	-	-	-	-	-	-	1	-	-
Stark	4508-32	1	1	1	-	-	1	-	-	1	-	-	-	-	1	1	-	-	-	-	-
Stark	5767-1	1	1	1	1	-	1	-	-	-	-	-	-	1	-	-	-	-	-	-	-
Stark	5767-2	1	1	1	1	-	1	-	-	-	-	-	-	-	-	1	-	-	-	-	-
Stark	5767-3	1	1	1	1	-	1	-	-	-	1	-	-	-	-	-	-	-	-	-	-
Stark	5767-22	1	1	1	1	-	1	-	-	-	-	-	-	-	-	1	-	-	-	-	-
Tuscarawas	1128-1	1	1	-	1	-	1	-	-	-	-	1	-	-	1	-	-	-	-	-	-
Tuscarawas	1128-2	1	1	1	1	1	-	-	-	-	-	-	-	-	-	-	-	-	-	-	-
Tuscarawas	1128-3	1	1	1	1	1	-	-	-	-	-	-	-	-	1	1	-	-	-	-	-
Tuscarawas	1617-1	1	1	1	1	-	1	-	-	-	1	-	-	-	-	-	-	-	-	-	-
Tuscarawas	1617-2	1	1	1	1	-	-	-	-	-	-	-	1	-	1	-	-	-	-	-	-
Tuscarawas	1617-3	1	1	1	1	-	1	-	-	-	-	-	-	-	1	1	-	-	1	-	-
Tuscarawas	1373-1	1	1	-	1	1	-	-	-	-	-	-	-	1	-	-	-	-	-	-	-
Tuscarawas	1373-2	1	1	1	1	1	-	-	-	-	-	-	-	-	-	-	-	-	-	1	-
Tuscarawas	1373-3	1	1	1	1	1	-	-	-	-	-	-	-	-	-	1	-	-	-	-	-
Tuscarawas	4719-2	1	1	1	1	-	1	-	-	1	-	-	-	-	-	1	-	-	-	-	-
Tuscarawas	4719-3	1	1	1	1	-	1	-	-	1	-	-	-	-	-	1	-	-	-	-	-

"1" indicates the presence the mineral in the respective sample.
"-" indicates that mineral is NOT identified in that respective sample.

APPENDIX D

CLAY MINERAL XRD DATA

Data used for the quantification of clay minerals. Peak areas were calculated using MacDiff 4.2.6 software.

Sample Name	0103-1	0103-3	0104-1	0104-2
17 Angstrom Glycolated				
2 Theta	-	-	-	-
Area Value by MacDiff / DMD	-	-	-	-
Weight Factor	1	1	1	1
Weighted Area	N/A	N/A	N/A	N/A
10 Angstrom				
2 Theta	8.92	8.88	8.92	8.92
Area Value by MacDiff / DMD (Glycolated)	81368	92402	76148	84447
Weight Factor	4	4	4	4
Weighted Area	325472	369608	304592	337788
7 Angstrom Air-Dried				
2 Theta	12.28	12.6	12.56	12.56
Area Value by MacDiff / DMD	49277	45956	50175	53896
Weight Factor	2	2	2	2
Weighted Area	98554	91912	100350	107792
3.54 Angstrom Ch(004)				
2 Theta	25.32	25.28	25.32	25.25
Area Value by MacDiff / DMD	25318	28333	36046	37644
Weight Factor	1	1	1	1
Weighted Area	25318	28333	36046	37644
3.58 Angstrom K(002)				
2 Theta	25.027			24.9
Area Value by MacDiff / DMD	9433	0	0	667
Weight Factor	1	1	1	1
Weighted Area	9433	N/A	N/A	667
Sum of Weighted Areas(17A,10A,7A)	424026	461520	404942	445580
Smectite 17A	N/A	N/A	N/A	N/A
Chlorite (14/7/3.54)	16.93	19.92	24.78	23.77
Illite (10)	76.76	80.08	75.22	75.81
Kaolinite (7/3.58)	6.31	N/A	N/A	0.42
Total	100	100	100	100

0104-3	0108-1	0108-2	0108-3	0129-1	0129-2	0129-3
-	-	-	-	5.4	-	5.32
-	-	-	-	1386	-	43971
1	1	1	1	1	1	1
N/A	N/A	N/A	N/A	1386	N/A	43971
8.96	8.88	8.88	8.92	8.96	8.96	8.92
84939	69848	81791	75122	116199	116199	111194
4	4	4	4	4	4	4
339756	279392	327164	300488	464796	464796	444776
12.56	12.56	12.56	12.52	12.52	12.6	12.56
29662	41038	46086	29396	44409	57512	45384
2	2	2	2	2	2	2
59324	82076	92172	58792	88818	115024	90768
25.32	25.334	25.32	25.24	25.32	25.32	25.4
22392	23812	30019	19130	24361	47505	20913
1	1	1	1	1	1	1
22392	23812	30019	19130	24361	47505	20913
	24.987			24.9		25.13
0	6568			13921		15135
1	1	1	1	1	1	1
N/A	6568	N/A	N/A	13921	N/A	15135
399080	361468	419336	359280	555000	579820	579515
N/A	N/A	N/A	N/A	0.25	N/A	7.59
14.87	17.80	21.98	16.36	10.18	19.84	9.09
85.13	77.29	78.02	83.64	83.75	80.16	76.75
N/A	4.91	N/A	N/A	5.82	N/A	6.58
100	100	100	100	100	100	100

0284-1	0284-2	0284-3	0339-1	0512-1	0512-2	0512-3
-	-	-	-	-	-	-
-	-	-	-	-	-	-
1	1	1	1	1	1	1
N/A	N/A	N/A	N/A	N/A	N/A	N/A
8.92	8.92	8.92	8.92	8.92	8.92	8.92
66578	69976	84541	38356	44384	88079	74333
4	4	4	4	4	4	4
266312	279904	338164	153424	177536	352316	297332
12.6	12.56	12.52	12.56	12.6	12.64	12.6
52949	60605	40847	34419	46710	61167	41904
2	2	2	2	2	2	2
105898	121210	81694	68838	93420	122334	83808
25.3	25.2	25.2	25.3	25.3	25.36	25.3
24173	31072	20602	17513	24116	42735	27699
1	1	1	1	1	1	1
24173	31072	20602	17513	24116	42735	27699
25.6	25	24.9	25	25		
9736	7974	8751	6579	3212		
1	1	1	1	1	1	1
9736	7974	8751	6579	3212	N/A	N/A
372210	401114	419858	222262	270956	474650	381140
N/A	N/A	N/A	N/A	N/A	N/A	N/A
20.28	24.05	13.66	22.51	30.43	25.77	21.99
71.55	69.78	80.54	69.03	65.52	74.23	78.01
8.17	6.17	5.80	8.46	4.05	N/A	N/A
100	100	100	100	100	100	100

0535-1	0535-2	0539-1	0539-2	0539-3	0665-1	1069-1
-	-	-	-	-	-	-
-	-	-	-	-	-	-
1	1	1	1	1	1	1
N/A	N/A	N/A	N/A	N/A	N/A	N/A
8.96	8.92	8.96	8.96	8.96	8.92	8.92
79779	67704	50768	82646	86818	44744	98975
4	4	4	4	4	4	4
319116	270816	203072	330584	347272	178976	395900
12.6	12.5	12.6	12.6	12.5	12.6	12.5
46103	37180	49480	67077	50074	57765	50797
2	2	2	2	2	2	2
92206	74360	98960	134154	100148	115530	101594
25.3	25.3	25.3	25.3	25.3	25.3	25.3
26401	22586	22660	44295	23279	30188	23689
1	1	1	1	1	1	1
26401	22586	22660	44295	23279	30188	23689
25	25	25		25	25	25
8746	6988	7131		11036	5030	8921
1	1	1	1	1	1	1
8746	6988	7131	N/A	11036	5030	8921
411322	345176	302032	464738	447420	294506	497494
N/A	N/A	N/A	N/A	N/A	N/A	N/A
16.84	16.45	24.92	28.87	15.18	33.63	14.83
77.58	78.46	67.24	71.13	77.62	60.77	79.58
5.58	5.09	7.84	N/A	7.20	5.60	5.59
100	100	100	100	100	100	100

1069-2	1069-3	1128-1	1128-3	1256-1	1256-2	1256-3
-	-	-	-	-	-	-
-	-	-	-	-	-	-
1	1	1	1	1	1	1
N/A	N/A	N/A	N/A	N/A	N/A	N/A
8.92	8.92	8.92	8.92	8.96	8.96	8.96
116707	71170	36959	108819	46311	81227	89092
4	4	4	4	4	4	4
466828	284680	147836	435276	185244	324908	356368
12.56	12.56	12.56	12.5	12.56	12.5	12.5
67710	23932	47323	47559	56742	50799	39833
2	2	2	2	2	2	2
135420	47864	94646	95118	113484	101598	79666
25.28	25.3	25.3	25.3	25.3	25.3	25.28
35577	13504	20966	23474	25461	29163	28900
1	1	1	1	1	1	1
35577	13504	20966	23474	25461	29163	28900
25	25.2	24.9	24.9	24.9	25	
8482	3931	14541	11206	11793	7153	
1	1	1	1	1	1	1
8482	3931	14541	11206	11793	7153	N/A
602248	332544	242482	530394	298728	426506	436034
N/A	N/A	N/A	N/A	N/A	N/A	N/A
18.16	11.15	23.05	12.14	25.96	19.13	18.27
77.51	85.61	60.97	82.07	62.01	76.18	81.73
4.33	3.25	15.98	5.79	12.03	4.69	N/A
100	100	100	100	100	100	100

1373-1	1617-1	1705-1	1705-2	1705-3	1724-1	1724-2
5.52	-	-	-	-	-	-
25847	-	-	-	-	-	-
1	1	1	1	1	1	1
25847	N/A	N/A	N/A	N/A	N/A	N/A
8.96	8.92	8.96	9	8.96	8.92	8.92
32004	137491	77150	77216	94328	30720	105668
4	4	4	4	4	4	4
128016	549964	308600	308864	377312	122880	422672
12.6	12.56	12.6	12.56	12.6	12.6	12.56
50869	65769	49166	50029	34188	80158	57333
2	2	2	2	2	2	2
101738	131538	98332	100058	68376	160316	114666
25.3	25.3	25.3	25.3	25.3	25.32	25.3
35693	33581	35219	29576	24644	45142	29845
1	1	1	1	1	1	1
35693	33581	35219	29576	24644	45142	29845
	25.1		25			25
	13782		8479			10004
1	1	1	1	1	1	1
N/A	13782	N/A	8479	N/A	N/A	10004
255601	681502	406932	408922	445688	283196	537338
10.11	N/A	N/A	N/A	N/A	N/A	N/A
39.80	13.68	24.16	19.02	15.34	56.61	15.98
50.08	80.70	75.84	75.53	84.66	43.39	78.66
N/A	5.62	N/A	5.45	N/A	N/A	5.36
100	100	100	100	100	100	100

1724-3	2094-1	2094-3	2096-1	2096-2	2096-3	2144-1
-	-	-	-	-	-	-
-	-	-	-	-	-	-
1	1	1	1	1	1	1
N/A	N/A	N/A	N/A	N/A	N/A	N/A
8.92	8.92	8.92	8.92	8.92	8.92	8.92
122250	65988	107738	68239	75438	93964	83701
4	4	4	4	4	4	4
489000	263952	430952	272956	301752	375856	334804
12.56	12.56	12.56	12.56	12.56	12.56	12.56
62535	35946	34283	41837	52441	42172	44820
2	2	2	2	2	2	2
125070	71892	68566	83674	104882	84344	89640
25.3	25.3	25.3	25.3	25.3	25.3	25.3
39747	25702	23874	24471	25819	21920	20589
1	1	1	1	1	1	1
39747	25702	23874	24471	25819	21920	20589
			25	25	25	25
			3858	7082	7990	8113
1	1	1	1	1	1	1
N/A	N/A	N/A	3858	7082	7990	8113
614070	335844	499518	356630	406634	460200	424444
N/A	N/A	N/A	N/A	N/A	N/A	N/A
20.37	21.41	13.73	20.27	20.24	13.43	15.15
79.63	78.59	86.27	76.54	74.21	81.67	78.88
N/A	N/A	N/A	3.20	5.55	4.90	5.97
100	100	100	100	100	100	100

2144-3	2255-1	2255-2	2255-3	2255-4	2255-5	2255-6
-	-	-	-	-	-	-
-	-	-	-	-	-	-
1	1	1	1	1	1	1
N/A	N/A	N/A	N/A	N/A	N/A	N/A
8.96	8.92	8.92	8.92	8.96	8.92	8.92
111811	157432	111071	125955	151162	15463	19327
4	4	4	4	4	4	4
447244	629728	444284	503820	604648	61852	77308
12.6	12.5	12.4	12.5	12.4	12.5	12.56
48891	113037	57267	64839	74786	57438	30320
2	2	2	2	2	2	2
97782	226074	114534	129678	149572	114876	60640
25.3	25.4	25.3	25.3	25.3	25.3	25.3
24517	52114	25546	31573	35744	30972	14052
1	1	1	1	1	1	1
24517	52114	25546	31573	35744	30972	14052
25	24.9	25	25	25		24.9
7558	21471	15863	14557	16386		4309
1	1	1	1	1	1	1
7558	21471	15863	14557	16386	N/A	4309
545026	855802	558818	633498	754220	176728	137948
N/A	N/A	N/A	N/A	N/A	N/A	N/A
13.71	18.71	12.64	14.01	13.60	65.00	33.64
82.06	73.58	79.50	79.53	80.17	35.00	56.04
4.23	7.71	7.85	6.46	6.23	N/A	10.32
100	100	100	100	100	100	100

2255-7	2255-8	4221-1	4221-2	4221-3	5767-1	5767-2
-	-	-	-	-	-	-
-	-	-	-	-	-	-
1	1	1	1	1	1	1
N/A	N/A	N/A	N/A	N/A	N/A	N/A
8.92	8.92	8.92	8.92	8.96	8.92	8.92
35098	111867	52365	68644	74482	88383	77730
4	4	4	4	4	4	4
140392	447468	209460	274576	297928	353532	310920
12.56	12.56	12.6	12.6	12.6	12.6	12.6
10620	28083	46947	41473	29178	63198	50308
2	2	2	2	2	2	2
21240	56166	93894	82946	58356	126396	100616
25.5	25.2	25.3	25.4	25.4	25.3	25.3
6978	19166	26141	26642	14233	43813	36384
1	1	1	1	1	1	1
6978	19166	26141	26642	14233	43813	36384
25.2		25	25	25		
4401		9238	8079	9553		
1	1	1	1	1	1	1
4401	N/A	9238	8079	9553	N/A	N/A
161632	503634	303354	357522	356284	479928	411536
N/A	N/A	N/A	N/A	N/A	N/A	N/A
8.06	11.15	22.87	17.80	9.80	26.34	24.45
86.86	88.85	69.05	76.80	83.62	73.66	75.55
5.08	N/A	8.08	5.40	6.58	N/A	N/A
100	100	100	100	100	100	100

5767-3	1103-1	1103-2	1103-3	2034-1	2034-2	2034-3
-	-	-	-	-	-	-
-	-	-	-	-	-	-
1	1	1	1	1	1	1
N/A	N/A	N/A	N/A	N/A	N/A	N/A
8.92	8.92	8.92	8.92	8.95	8.96	8.96
81777	85463	84779	81780	80217	81782	87427
4	4	4	4	4	4	4
327108	341852	339116	327120	320868	327128	349708
12.5	12.6	12.5	12.6	12.5	12.6	12.6
30954	60512	54897	30957	66151	63258	44987
2	2	2	2	2	2	2
61908	121024	109794	61914	132302	126516	89974
25.3	25.3	25.3	25.3	25.4	25.3	25.3
22796	24658	23580	23678	23679	22590	20643
1	1	1	1	1	1	1
22796	24658	23580	23678	23679	22590	20643
1	1	1	1	1	1	1
N/A	N/A	N/A	N/A	N/A	N/A	N/A
389016	462876	448910	389034	453170	453644	439682
N/A	N/A	N/A	N/A	N/A	N/A	N/A
15.91	26.15	24.46	15.91	29.19	27.89	20.46
84.09	73.85	75.54	84.09	70.81	72.11	79.54
N/A	N/A	N/A	N/A	N/A	N/A	N/A
100	100	100	100	100	100	100

4719-2	4719-3
-	-
-	-
1	1
N/A	N/A
8.92	8.92
50862	86429
4	4
203448	345716
12.5	12.5
46834	44989
2	2
93668	89978
26.3	27.3
24578	25340
1	1
24578	25340
24.9	24.9
11674	11205
1	1
11674	11205
297116	435694
N/A	N/A
21.37	14.32
68.47	79.35
10.15	6.33
100	100

APPENDIX E

KÜBLER INDICIES

The Kübler indicies are listed for all the samples analyzed in the study. Data is presented in degrees 2-theta (º2Ɵ).

County	Sample Name	Kubler index (10 A air dried)
Columbiana	1705-1	0.519
Columbiana	1705-2	0.462
Columbiana	1705-3	0.496
Stark	1103-1	0.51
Stark	1103-2	0.419
Stark	1103-3	0.495
Guernsey	2144-1	0.604
Guernsey	2144-2	-
Guernsey	2144-3	0.515
Columbiana	1256-1	0.561
Columbiana	1256-2	0.48
Columbiana	1256-3	0.505
Jefferson	0512-1	0.506
Jefferson	0512-2	0.483
Jefferson	0512-3	0.493
Columbiana	0665-1	0.439
Columbiana	0665-2	-
Harrison	0103-1	0.58
Harrison	0103-2	-
Harrison	0103-3	0.495
Tuscarawas	1128-1	0.52
Tuscarawas	1128-2	-
Tuscarawas	1128-3	0.462
Carroll	2094-1	0.523
Carroll	2094-2	-
Carroll	2094-3	0.54
Harrison	0339-1	0.5
Jefferson	0539-1	0.515
Jefferson	0539-2	0.46
Jefferson	0539-3	0.48
Belmont	0284-1	0.491
Belmont	0284-2	0.412
Belmont	0284-3	0.56
Carroll	2096-1	0.506
Carroll	2096-2	0.414
Carroll	2096-3	0.465
Harrison	0104-1	0.508
Harrison	0104-2	0.409
Harrison	0104-3	0.618
Jefferson	2034-1	0.581
Jefferson	2034-2	0.459
Jefferson	2034-3	0.463
Guernsey	4221-1	0.48
Guernsey	4221-2	0.451
Guernsey	4221-3	0.456

County	Sample Name	Kubler index (10 A air dried)
Stark	4508-2	-
Stark	4508-3	-
Tuscarawas	1617-1	0.625
Tuscarawas	1617-2	-
Tuscarawas	1617-3	-
Stark	5767-1	0.453
Stark	5767-2	0.47
Stark	5767-3	0.464
Belmont	0108-1	0.518
Belmont	0108-2	0.468
Belmont	0108-3	0.509
Tuscarawas	1373-1	0.63
Tuscarawas	1373-2	-
Tuscarawas	1373-3	-
Harrison	1069-1	0.59
Harrison	1069-2	0.477
Harrison	1069-3	0.548
Tuscarawas	4719-2	0.469
Tuscarawas	4719-3	0.55
Columbiana	1724-1	0.518
Columbiana	1724-2	0.423
Columbiana	1724-3	0.471
Jefferson	0535-1	0.574
Jefferson	0535-2	0.508
Belmont	0129-1	0.77
Belmont	0129-2	0.574
Belmont	0129-3	0.69
Guernsey	1456-1	-
Guernsey	1456-2	-
Guernsey	1456-3	-
Noble	2255-1	0.512
Noble	2255-2	0.534
Noble	2255-3	0.545
Noble	2255-4	0.599
Noble	2255-5	0.47
Noble	2255-6	0.349
Noble	2255-7	0.499
Noble	2255-8	0.542

APPENDIX F

TOTAL ORGANIC CARBON DATA

All data used for the calculation of total organic carbon (TOC) from total inorganic carbon (TIC) and total carbon (TC) measurements is listed below.

Sample Name	Total Carbon	Std. Dev.	Total Inorganic Carbon	Std. Dev.2	Total Organic Carbon	Std. Dev.3
	%		%		%	
MESS3	2.10	0.08	0.62	0.05	1.48	0.09
STD100	-	-	11.85	0.14	-	-
2226-1	0.30	0.01	0.13	-	0.17	-
1705-1	0.57	0.03	0.31	-	0.27	-
1705-2	0.48	0.05	0.03	-	0.45	-
1705-3	1.22	-	0.27	-	0.96	-
1103-1	0.46	-	0.26	-	0.20	-
1103-2	0.54	0.02	0.10	-	0.43	-
1103-3	3.13	-	0.86	-	2.27	-
2144-1	0.49	0.06	0.21	-	0.29	-
2144-2	0.44	-	0.05	-	0.39	-
2144-3	1.74	0.02	0.40	-	1.34	-
1256-1	1.02	-	0.35	-	0.66	-
1256-2	0.38	0.01	0.06	-	0.32	-
1256-3	1.03	-	0.29	-	0.74	-
0512-1	0.22	0.01	0.13	-	0.09	-
0512-2	0.39	-	0.18	-	0.21	-
0512-3	0.89	0.02	0.21	-	0.68	-
0665-1	0.65	0.02	0.39	-	0.26	-
0665-2	0.39	0.03	0.11	-	0.28	-
0103-1	0.53	-	0.16	-	0.38	-
0103-2	0.42	0.03	0.08	-	0.34	-
0103-3	1.77	-	1.13	-	0.65	-
1128-1	1.11	0.01	0.87	-	0.24	-
1128-2	1.30	-	0.35	-	0.95	-
1128-3	1.14	0.02	0.85	-	0.29	-
2094-1	0.57	0.02	0.34	-	0.23	-
2094-2	0.37	0.01	0.04	-	0.33	-
2094-3	1.32	-	0.81	-	0.51	-
0339-1	0.89	-	0.47	-	0.42	-
0539-1	0.64	0.02	0.23	-	0.41	-
0539-2	0.30	0.02	0.13	-	0.17	-
0539-3	0.43	-	0.16	-	0.27	-
0284-1	0.49	0.00	0.23	-	0.26	-
0284-2	0.26	0.02	0.05	-	0.21	-
0284-3	0.51	0.02	0.10	0.00	0.41	0.02
2096-1	0.37	-	0.22	-	0.15	-
2096-2	0.47	0.04	0.22	-	0.24	-
2096-3	0.94	0.04	0.46	-	0.48	-
0104-1	0.46	0.03	0.28	-	0.18	-
0104-2	1.55	0.01	1.35	-	0.20	-
0104-3	1.00	-	0.03	-	0.98	-
2034-1	0.41	-	0.21	-	0.21	-
2034-2	0.32	-	0.04	-	0.28	-
2034-3	0.47	0.04	0.04	-	0.42	-
4221-1	0.54	-	0.24	-	0.30	-
4221-2	0.40	0.03	0.03	-	0.38	-
4221-3	1.26	0.04	0.15	0.00	1.11	0.04
4508-2	1.04	0.03	0.11	-	0.93	-
4508-3	3.24	-	0.41	-	2.82	-
1617-1	0.68	-	0.21	-	0.47	-
1617-2	0.44	0.09	0.02	-	0.43	-
1617-3	1.80	0.02	0.06	-	1.73	-
5767-1	1.21	0.05	1.04	-	0.17	-
5767-2	0.62	0.04	0.12	-	0.50	-
5767-3	1.82	0.06	1.52	-	0.30	-
0108-1	0.35	-	0.18	-	0.18	-
0108-2	0.42	0.02	0.14	0.01	0.28	0.02

0108-3	1.33	-	0.04	-	1.30	-
1373-1	0.73	0.09	0.51	0.03	0.22	0.09
1373-2	0.55	-	0.02	-	0.53	-
1373-3	0.83	-	0.15	-	0.68	-
1069-1	0.61	0.02	0.41	-	0.19	-
1069-2	0.33	-	0.11	-	0.22	-
1069-3	2.17	0.02	0.13	0.01	2.04	0.03
4719-2	0.78	0.04	0.08	0.01	0.70	0.04
4719-3	1.71	-	0.66	-	1.05	-
1724-1	0.23	-	0.13	-	0.10	-
1724-2	0.36	-	0.09	-	0.27	-
1724-3	0.56	0.04	0.41	-	0.15	-
0535-1	0.47	-	0.26	-	0.21	-
0535-2	0.62	0.06	0.03	0.02	0.59	0.07
0129-1	2.36	0.07	0.88	0.02	1.49	0.08
0129-2	0.45	-	0.16	-	0.29	-
0129-3	1.03	-	0.24	-	0.79	-
1456-1	0.44	-	0.16	-	0.28	-
1456-2	0.46	0.02	0.06	0.01	0.41	0.02
1456-3	2.36	0.03	0.38	-	1.97	-
2255-1	0.22	0.00	0.00	-	0.22	-
2255-2	0.30	0.02	0.00	-	0.30	-
2255-3	0.35	-	0.01	-	0.34	-
2255-4	0.36	0.01	0.09	-	0.27	-
2255-5	0.69	-	0.20	-	0.50	-
2255-6	0.74	0.03	0.58	-	0.17	-
2255-7	6.36	-	0.11	-	6.25	-
2255-8	0.43	-	0.00	-	0.43	-

Standard deviations listed for samples with duplicate runs

APPENDIX G

CORE SAMPLE DESCRIPTIONS

Core descriptions made on the length of core from well 34121222550000 in Noble County, Ohio are listed below.

Core Description
34121222550000
Noble County, Ohio

Chagrin

1750’

Chagrin Shale
Medium grey (N5-N6)
No apparent bedding
No fossils
Fine grained
Well sorted
No sign of carbonates



1752.7’

Brachiopods present
Medium grey (N5-N6)
Fine grained
Well sorted

1753.7’

Loss of fossils
Medium grey (N5-N6)
No carbonate
Slightly larger grain size

1855’

Fine grained
Medium grey (N5-N6)
No carbonate
Small red nodules


1863’

Slightly darker grey (N4-N5)
Interbedded N4-N5 and N5-N6
Smaller bedding (inches)
Darker material is finer grained/less crystalline

1877’

Darker grey (N4-N5)
Becomes fissile and shaley
Easily breaks into shards
No visible sedimentary structures

1914.3’

Light grey (N6-N7)
Interbedded with darker material
Small amounts of swirling bioturbation and carbonate shells

1919.5’-1920’

Increase in bioturbation and carbonate shell concentration
Approximately 1 inch carbonate layer at 1919.6’
Medium grey (N4-N5)

2018’

Interbedded light grey and dark grey becoming more fine (.25”-.5”)
Small amounts of bioturbation

2022

Heavy bioturbation
Medium grey (N5-N6)
Prominent carbonate layers (>1”)
Fully reactive to HCl
Contains brachiopods and other shelled remains

2026’-2061’

Repeated large scale interbedding of medium and light grey shales

2061'

Swirling bioturbation
Light (N5-N6) and darker grey (N4-N5) interbedding
Not fully reactive to HCl

***Break in core 2084'-3285'**

<u>Huron</u>

3285'

Very fine grain size
Olive grey (N4, 5Y 4/1)
No visible bedding
No apparent fossils
No visible sedimentary structures
Progressively darker with depth (N2-N3)
Periodic, small interbeds of light grey

***Missing 3446'-3456' (Gamma hot zone, completely missing for sampling)**

3463'

Very fine grained
Nearly black in color (N1)
No visible bedding
High gamma spike on geophysical log

3464'

Light grey shale (N5-N6)
Fine grained
No visible bedding
No apparent sedimentary structures